ANALYSIS OF WRINKLING IN DEEP DRAWING PROCESSES

A THESIS SUBMITTED TO
THE GRADUATE SCHOOL OF NATURAL AND APPLIED SCIENCES
OF
MIDDLE EAST TECHNICAL UNIVERSITY

BY

SANİYE RABİA DAL

IN PARTIAL FULFILLMENT OF THE REQUIREMENTS
FOR
THE DEGREE OF MASTER OF SCIENCE
IN
MECHANICAL ENGINEERING

SEPTEMBER 2019

Approval of the thesis:

ANALYSIS OF WRINKLING IN DEEP DRAWING PROCESSES

submitted by **SANİYE RABİA DAL** in partial fulfillment of the requirements for the degree of **Master of Science in Mechanical Engineering Department, Middle East Technical University** by,

Prof. Dr. Halil Kalıpçılar
Dean, Graduate School of **Natural and Applied Sciences** _____

Prof. Dr. M. A. Sahir Arıkan
Head of Department, **Mechanical Engineering** _____

Prof. Dr. Haluk Darendeliler
Supervisor, **Mechanical Engineering, METU** _____

Examining Committee Members:

Prof. Dr. Suha Oral
Mechanical Engineering, METU _____

Prof. Dr. Haluk Darendeliler
Mechanical Engineering, METU _____

Prof. Dr. F. Suat Kadıoğlu
Mechanical Engineering, METU _____

Prof. Dr. Can Çoğun
Mechatronics Engineering, Çankaya University _____

Assist. Prof. Dr. Orkun Özşahin
Mechanical Engineering, METU _____

Date:

I hereby declare that all information in this document has been obtained and presented in accordance with academic rules and ethical conduct. I also declare that, as required by these rules and conduct, I have fully cited and referenced all material and results that are not original to this work.

Name, Surname: Saniye Rabia Dal

Signature :

ABSTRACT

ANALYSIS OF WRINKLING IN DEEP DRAWING PROCESSES

Dal, Saniye Rabia
M.S., Department of Mechanical Engineering
Supervisor: Prof. Dr. Haluk Darendeliler

September 2019, 88 pages

Wrinkling, observed due to compressive instability, is one of the main failure modes in deep drawing processes. The prediction and prevention of wrinkles are critical for production of stamping parts which require good surface quality. In the current work, the occurrence of wrinkling in square and cylindrical cup deep drawing processes are investigated considering various constitutive models; formed by using CPB06ex2, Hill'48, BBC2008-8p, BBC2008-16p, and von Mises yield criterion with isotropic, kinematic and combined hardening. Numerical simulations were performed by implementing CPB06ex2, BBC2008-8p and BBC2008-16p models to a commercial finite element code through user subroutines. In the simulations, AA5042-H2 aluminum alloy with 1 mm thickness were employed. First a comparison is made between the predictions of the constitutive models and the experimental results of the previous works to evaluate the accuracy of the developed models. It was found that the predictions of all constitutive models for the number of wrinkles are in good agreement with experimental data. The CPB06ex2 model gives closer numerical results with experiments for the wrinkling profile and the punch force evolution comparing to the other models. Moreover, square cup drawing process needs higher

blank holding forces to prevent wrinkling than cylindrical cup drawing at the same punch travel.

Keywords: Wrinkling, Sheet Metal Forming, Deep drawing, Finite Element Method

ÖZ

DERİN ÇEKME İŞLEMLERİNDE KIRIŞMA ANALİZİ

Dal, Saniye Rabia
Yüksek Lisans, Makina Mühendisliği Bölümü
Tez Yöneticisi: Prof. Dr. Haluk Darendeliler

Eylül 2019 , 88 sayfa

Sıkıştırma kararsızlığının neden olduğu kırışma, sac metal şekillendirme işlemlerinde yaygın olarak görülen hatalardan biridir. İyi yüzey kalitesinin gerektiği parçaların derin çekme işlemi ile üretiminde kırışmanın öngörülmesi ve önlenmesi önemlidir. Bu çalışmada, kare ve silindirik derin çekme işlemlerinde görülen buruşma von Mises, CPB06ex2, BBC2008-8p, BBC2008-16p, Hill'48 akma kriterleri ve izotropik, kinematik ve birleşik pekleşme modelleri kullanılarak elde edilen bünye denklemleri ile incelenmiştir. Sayısal analizler, BBC2008-8p, BBC2008-16p ve CPB06ex2 modelleri bir ticari sonlu elemanlar yazılımına kullanıcı malzeme altprogramı eklenerek gerçekleştirilmiştir. Analizlerde sac metal olarak 1 mm kalınlığındaki AA5042-H2 alüminyum alaşımı kullanılmıştır. Ayrıca, geliştirilen modellerin doğruluklarını değerlendirebilmek için literatürden elde edilen deneysel sonuçlar ile karşılaştırılmıştır. Analizler sonucunda modellerce belirlenen kırışıklık sayılarının deneysel sonuçlarla uyumlu olduğu gözlenmiştir. CPB06ex2 modeli, kırışıklık profili ve zımba kuvveti tespitinde diğer modellere göre deneylere daha yakın sonuçlar vermiştir. Ek olarak, kare plakalarının kullanıldığı derin çekme işlemlerinde, silindirik kap derin çekme işlemlerine kıyasla kırışıklığı önlemek için daha fazla baskı plakası

kuvvetinin gerektiği görülmüştür.

Anahtar Kelimeler: Buruşma, Sac Metal Şekillendirme, Derin Çekme, Sonlu Elemanlar Metodu

To my lovely family

ACKNOWLEDGMENTS

First of all, I would like to present my special thanks to my supervisor Prof. Dr. Haluk DARENDELİLER for his generous advices throughout my thesis and sparing time whenever I approached him. It was an honor to work with him.

Also, I am profoundly grateful to my colleagues in ROKETSAN for their valuable support.

Most importantly, I wish to thank my loving and supportive husband Fırat DAL for his endless patience, understanding and faith. Every time I need some motivation and help, he is always there for me. My thesis would have not finished without his encouragement.

Finally, I am profoundly grateful to the biggest source of my strength, my family. I can not thank them enough for everything they have ever done for me. It means the world to me.

TABLE OF CONTENTS

LIST OF TABLES

TABLES

LIST OF FIGURES

FIGURES

CHAPTER 1

INTRODUCTION

1.1 Background

A material undergoes plastic deformation when the tensile, compressive, torsional or bending stresses occured due to applied loads exceed its yield strength and that causes the material to change its shape permanently. In metal forming processes, materials are plastically deformed intentionally by tools in order to obtain the desired shape.

In sheet metal forming process, a piece of sheet metal is deformed with a small change of thickness [1]. In recent years, sheet metal forming becomes a widely used process in the industry because of increasing demand for sheet metals with complex shapes and different properties. Deep drawing, which is one of the sheet metal forming processes, is applied especially in automotive, aerospace, marine industries and even in the production of cooking utensil and beverage cans. In the deep drawing process, the sheet metal is held by the blank holder and then the punch pushes the sheet metal plate into the die cavity to achieve the desired shape. During deep drawing process, sheet metal may fail when it is subjected to stretching, shearing or compression. Necking, excessive thinning, earing and tearing are some examples of failures.

Wrinkling is one of the ways to fail due to compressive instability in deep drawing operations. It is a kind of buckling which is developed due to compressive hoop stresses. It depends on several factors such as values of friction coefficient between tools and blank, blank holding force, tool geometry, mechanical properties of blank, blank thickness, lubrication etc.

Blank holding force can be used in order to eliminate excessive material draw-in

and apply restraining force to the blank. If the blank holding force is higher than necessary, tears may occur on the sheet plate. However, if it is less than required, wrinkling may be formed. For successful deep drawing process, adequate blank holding force should be determined. In addition, wrinkling tendency decreases with increasing sheet thickness, increasing strain hardening and decreasing flange length [2].

1.2 Motivation

In recent years, usage of high strength sheet metals with low thickness is excessively in industry and that increases the occurrence of wrinkling. Therefore, wrinkling becomes more prevalent than other failure modes. In stamping of automotive parts, eighty percent of the part failure is caused by wrinkling whereas twenty percent of the part failure is caused by excessive tearing. In spite of this ratio, tensile instabilities have been investigated more in the last two decades [3] .

Wrinkling is not desired in stamping parts because of its aesthetic and functional reasons. The part assembly and part operations, like sealing and welding can be severely affected due to wrinkling. Large wrinkles can damage dies and causes blank material to be out of usage [4]. Therefore, it is important to predict and prevent wrinkling in sheet metal forming processes.

Deep drawing is one of the expensive sheet metal forming processes due to high die costs. Therefore, preventing wrinkling will not only increase the quality and efficiency of the process, but also reduce the cost in the current competitive industry. For this purpose, numerical solution of the deep drawing process is a requirement. Finite element analysis is a cheap procedure that can be used to simulate the process, understanding of the factors that affect the formation and development of wrinkles and finally, designing optimal tools and process parameters. For finite element analysis, various constitutive models were proposed to predict behaviour of material under plastic deformation. Selection of suitable constitutive models is crucial for simulation and forecast of wrinkling at early stage. Consequently, researches on prediction and prevention of wrinkling occurrence and correspondingly, selection of

a proper constitutive model for wrinkling simulations should be carried out.

1.3 Objective and Scope of the Thesis

The main objective of this study is to demonstrate the capabilities of various constitutive models in simulation of wrinkling for different cup drawing processes. The amplitude of wrinkles at several blank holding forces for changing punch displacements are presented by employing these constitutive models.

This thesis describes numerical results concerning the wrinkle formation in cylindrical and square cup drawing processes. The effects of seven constitutive models namely; Hill'48, CPB06ex2, BBC2008-8p and BBC2008-16p yield criteria with isotropic hardening and von Mises yield criteria with kinematic, isotropic and combined hardening on simulation of wrinkling are found. AA5042-H2 aluminum alloy is selected as a sheet material with 1 mm thickness. Numerical simulations are done with a commercial finite element code. CPB06ex2, BBC2008-8p, BBC2008-16p yield criteria are implemented to the code by means of a developed user subroutine. Other constitutive models are used directly from the program's library. For the verification of codes, the predictions of the constitutive models for the wrinkling profile and punch load are compared with experimental data reported by Neto et al. [5].

1.4 Outline of the Thesis

This current work is divided into six chapters and references. Chapter 1 will provide a brief background, motivation and scope of the thesis.

In Chapter 2, a brief history of the past researches is explained. In the first part, previous researches about analytical and numerical approaches that were made to improve prediction of wrinkling are summarized. In the second part, previous studies about implementations of yield functions into a finite element software and verification of numerical results are included. Eventually, in the third part, studies about the effect of various parameters on failure modes of deep drawing simulation

are described.

In Chapter 3, theoretical formulations of yield criteria and hardening models used in this work are given.

In Chapter 4, details of the finite element method used in this study are described.

In Chapter 5, numerical results of the finite element analyses of the square and cylindrical cup deep drawing operations at various punch displacements by using different constitutive models and the comparison of the related models with experimental results of Numisheet 2014 benchmark 4 are given. The verification of the CPB06ex2 code is also presented.

Finally, in Chapter 6, conclusions of this thesis and suggestions for future work are discussed.

CHAPTER 2

LITERATURE SURVEY

This chapter is split into three sections. The first section presents studies in literature about analytical and numerical approaches to the prediction of wrinkling. Second section contains past studies about implementations of several yield functions into a finite element software. In the last section, past studies and papers about the effect of various parameters on simulation of cup drawing operations are explained.

2.1 Studies about Analytical and Numerical Approach to the Prediction of Wrinkling

There are many analytical and numerical methods to predict the occurrence of wrinkling in literature. Firstly, previous researches about energy method are summarized.

Wang et al. [4] introduced a modified energy approach so as to forecast the side-wall wrinkling in deep drawing processes. In this approach, firsly, the external work done by membrane forces and the bending energy is equated so that the critical buckling stress is calculated in terms of the in-plane stress ratio, thickness of sheet, geometry parameters, material properties. Secondly, the actual applied compressive stress is obtained from the FEM simulations. When the actual applied stress is higher than the calculated buckling stress, wrinkling can be observed. Also, the applied stress found from the FEM simulations was not compressive in all region. Therefore, the effective dimensions of the compressive area was introduced to decide the critical buckling state. Additionally, the comparison was made between experimental results of the conical cup forming, square cup forming and Yoshida buckling test and the

analysis results in order to validate the proposed energy approach. It was observed that the predictions of the modified energy method fit the experimental investigations well. According to the Yoshida buckling test, it was stated that higher material strength component and lower hardening exponent provide higher wrinkling limit. Moreover, according to the conical cup forming, the critical buckling stress for the curved sheet is related with the local curvature of the wrinkling region. Also, FEM simulations with different integration methods and element types were investigated in this study. According to the results, while no wrinkling were observed in the implicit method with four node shell elements (ABAQUS S4R), wrinkling appeared at very early stage in the explicit method with four node shell elements by using LS-DYNA. The disadvantage of the explicit model was very sensitive to simulation input parameters such as the element size, the punch velocity, etc. On the contrary, this sensitivity was not observed where the proposed energy method was implemented to the implicit FEM analysis. As a result, the modified energy approach provides reliable results for the prediction of the side-wall wrinkling.

Agrawal et al. [6] studied on axisymmetric deep drawing process. The minimum blank holding load needed to avoid the development of wrinkling in the flange area was determined in this study. To find the critical condition for the onset of wrinkling, the energy method was used. In this method, radial and circumferential stresses can be written in terms of blank holding force and then the expression of the work done by in-plane membrane forces can be obtained. The predictions of the model for the minimum blank holding force were in good agreement with experimental results. It was found that as normal anisotropy value decreases, the thickening of the flange area increases; therefore, the energy needed to bend the blank increases. Additionally, if initial thickness of the sheet metal increases, the number of developed wrinkles will decrease and the required minimum blank holding load will increase.

Kaftanoglu [7] studied flange wrinkling observed in axisymmetrical deep drawing by using the energy method. According to the study, there are two modes in the flange area, wrinkling and drawing. During the process, deformation of materials is in favour of which mode that requires least energy. In other words, if the energy requires for drawing is less than that for wrinkling, wrinkling would not occur. It was also indicated that as the number of wrinkles increases, the wrinkling energy

becomes higher. In addition to that, the required blank holding force for successful drawing were calculated theoretically. For verification, experiments were carried out by selecting mild steel, stainless steel, half-hard and hard aluminum as a material of round blanks in different sizes. The blank holding forces calculated theoretically were applied to the blanks and no wrinkling was observed in the experiments. So, the theoretical results agreed well with the empirical results in this study.

Shafaat et al. [8] studied about side-wall wrinkling of a galvanized steel sheet during the conical cup deep drawing processes by utilizing energy method. In this study, a new deflection function was proposed and compared with Wong and Cao's deflection function [4] in order to observe its performance. The effect of material anisotropy on the onset of wrinkling was obtained using Hosford and Hill's 48 yield criteria. According to the numerical results, effective stress based on the Hosford yield criterion was greater than that of Hill'48 yield criterion for all anisotropy conditions. Also it was investigated that enhancement of effective stress decreases the instantaneous moduli, critical wrinkling stress and consequently the critical cup height. These lead to contraction of yield locus. As a result, wrinkling occurs at smaller punch displacement in the deep drawing analysis by using Hosford yield criteria. Additionally, it was observed that the critical strain energy of wrinkling is affected by the deflection function . The strain energy based on the new deflection function was lower than that related to the Cao's deflection function. Since the required strain energy for wrinkling was provided at smaller punch displacement, the predicted results related to the new deflection function were better agreement with the experimental results. Moreover, when the application of anisotropy condition compared with the experimental investigations, numerical results shows similar behavior.

In Senior's study [9], the number of wrinkle was found by using energy method. In energy method, there are 3 energy terms. Those are the energy formed due to bending into a half wave segment of the flange (E_B), the energy formed due to the shortening of the flange circumferentially (E_H) and finally the energy formed due to the loading of the flange laterally (E_L). By adding (E_B) and (E_L) and then equating to (E_H), the number of flange wrinkle was found in this study. Also, the effect of the blank holding force on the number of wrinkle was researched.

Another method is general bifurcation theory in order to find out the onset of wrinkling.

Correia et al. [10] have worked on the onset of wrinkling in anisotropic metal sheets by using analytical approach and finite element simulations with ABAQUS/ Explicit. For analytical approach, wrinkling analyses were carried out using bifurcation theory for thin and shallow shells under bi-axial plane stress loading. Also, Ferron's yield criterion [11] was employed for both analytical and numerical approach. In this study, two different deep drawing simulations were examined. One of them was the conical cup deep drawing and the other is the deep drawing through a tractrix die. In the numerical simulation of conical cup deep drawing, 12 wrinkles were predicted while in analytical approach, the number of wrinkles was 10. Both of these results were found close to 11 wrinkles observed experimentally. In the deep drawing through a tractrix die, it was observed that when the blank diameter increases, the percentage of draw deformation decreases. Moreover,in analytical approach, it was reported that when the principal stress axes, the geometric axes of principal curvature and the principal orthotropic axes all coincide, the direction of the wrinkling is along one of the principal stress axes.

Chu and Xu [3] were examined the flange wrinkling observed in deep drawing process by using the general bifurcation theory for critical condition causing wrinkling. In order to calculate the critical drawing stress, the deformation theory of plasticity reported by Trientofyllidis and Needleman [12] was employed. The forecasts of the deformation theory for the onset of wrinkling were compared with the forecasts of the smooth yield surface flow theory of plasticity, the experimental values provided by Senior's study and the Senior's one dimensional theory [9]. According to the results, for the case of the drawing ratio bigger than or equal to 1.6, the predictions of both the deformation and flow theory in state of the critical drawing stress were the same. However, for the case of the drawing ratio smaller than 1.6, the predicted critical drawing stress in terms of the flow theory was larger than that calculated by the deformation theory. Also,the average hoop stresses related with both the deformation theory and flow theory were larger than the stresses predicted by Senior's one dimensional theory. According to the comparison of the wrinkle number between the deformation theory and Senior's theory, the deformation theory predicted more

wrinkle and correlated well with the experimental data. The main reason of this differences between the Senior's one dimensional theory and deformation theory is replacing the Young's modulus with the reduced modulus in the elastic stability equation is not enough to involve plasticity in buckling problems. Moreover, the effects of material anisotropy, drawing ratios and strain hardening on the onset of wrinkling were examined. The critical drawing stress increases with increasing drawing ratio, plastic anisotropy and work hardening index. Also it was investigated that plastic anisotropy has very little effect on the predictions of the wrinkle wave number.

In addition, in literature, there are different approaches from the energy method and bifurcation theory. Below are some examples that illustrate other methods.

The wrinkling phenomenon was analyzed by a simplified method in Weili et al. work [13]. This method was proposed so that complicated plastic bifurcation theory, an initial imperfection of the sheet and a wrinkling criterion may not be needed for wrinkling simulation.In the simplified method, direct node projection in the contact algorithm and blank holding gap in the blank holder treatment were taken into consideration. There are three different methods used in contact algorithms; these are the Lagrange multiplier method, the penalty function method and finally the direct node projection method. The direct node projection method was selected since it was simple and reliable. In their study,the deep drawing of a square cup, a hemispherical cup, a cylindrical cup and a real auto-body panel was simulated by applying the simplified method. The agreement between the analytical results and the empirical results were found to be satisfactory.

Nordlund et al. [14] proposed an algorithmic procedure to predict the onset and distribution of wrinkles at early stage of a sheet metal forming analysis. This procedure can be applied for all loading conditions and it is independent of the material model employed.In this procedure, the wrinkle indicator was introduced to compute the closeness to wrinkling. The value of indicator, based on the second order incremental work, is in the interval [-1,1]. In the study, it was implemented into an explicit finite element code, Dyna3d, and two different tests were done to show its performance. These tests were the Yoshida buckling test and the fluid forming test.

In both tests, it was observed that wrinkles were developed in regions where the value of wrinkle indicator was negative. And during deformation, the negative wrinkle indicator firstly seen in the outer boundary of area where wrinkling starts. It was also stated that the most negative values were detected at the inflexion points.

2.2 Studies about Implementations of Yield Criteria into Finite Element Software

This part includes past studies about implementations of different yield functions to deep drawing simulations via a finite element software and confirmation of the numerical results of related yield functions.

In Nowak et al. study [15], a newly-developed yield function which is continuation of Burzynski isotropic yield function [16], was implemented to ABAQUS/Explicit with a VUMAT subroutine. The square cup deep drawing process was studied. The proposed yield function is for the transversally isotropic materials under the state of plane stress. It was shown that the yield function gave reasonable results. However, comparing with the von Mises yield criteria, the yield function should be developed.

In Yoon et al. study [17], CPB06ex2 yield function was implemented to ABAQUS/Standard for materials with no tension/compression asymmetry. In order to validate the analysis results, for AA6111-T4 alloy, the finite element results and the experimental earing profile in Numisheet 2002 were compared. Moreover, AA5042-H2 alloy was employed in order to compare CPB06ex2 and Yld2000-2D yield function with experimental results. According to experimental results, the eight ears was observed at the final stage of the deep drawing process. CPB06ex2 can predict 8 ears and Yld2000-2D can predict only 4 ears. The reason of that is the CPB06ex2 yield function includes more anisotropy coefficients. Second purpose of the study is to investigate the effect of the evolution of anisotropy. In both yield criterion, anisotropy coefficients are not fixed. For CPB06ex2 yield criterion, the anisotropy coefficients corresponds to different level of plastic work were determined by using a UMAT subroutine. For Yld2000-2D yield criterion, the flow stresses in 0°, 45°and 90°, the biaxial flow stress, r values were found in experiment for different

value of plastic work and that values were used as an input data. In conclusion, the evolution of anisotropy does not affect the prediction of number of ears but it affects the prediction of cup height distribution.

Another study was done by Jia and Bai [18] on ductile fracture prediction by using anisotropic eMMC model. The MMC fracture model which is on the basis of the stress invariant was imported into the eMMC model which is on the basis of strain under the plane stress state. The Yld2000-2D yield criterion was assigned to the TRIP780 high strength steel and the CPB06ex2 yield criterion was assigned to the AZ31B-H24 magnesium alloy. For different loads, the finite element analyses were done in ABAQUS/Explicit via VUMAT subroutine and good agreement between experimental and analysis results was observed.

M. Vrh et al. [19] studied the ability of prediction of the BBC2008 plane stress yield criterion. For the purpose of validation of the constitutive model, AA5042-H2 and AA2090-T3 aluminum alloys were selected. The constitutive equations were integrated by using the NICE scheme in ABAQUS/Explicit via VUMAT subroutine. There are two alternative in BBC2008 yield function. One of them is the BBC2008 yield function with 8 anisotropic coefficient, the other is the yield function with 16 anisotropic coefficient. In order to compare the predictions of normalized uni-axial yield stress ratios and the planar distribution of r-coefficient for AA2090 aluminum alloy, experiment results, CPB06ex2 yield criterion, Yld2000-2d yield criterion, Yld2004-18p, BBC2008-16p and BBC2008-8p yield criterion have been utilized. The results show that the r-coefficient predictions of the BBC2008-16p is the closest to the experimental results comparing to other yield criteria. For predicting the planar distribution of the the uni-axial yield stress ratios, BBC2008-16p predicts better than the BBC2008-8p, as expected. BBC2008-16p version, CPB06ex2 and Yld2004-18p yield criterion predict the planar distribution of the uni-axial yield stress ratios similarly. According to the experiment, the material should yield 6 ears and only the BBC2008-16p can predict the correct number of ears. For the AA5042-H2 aluminum alloy, the comparison of the planar distribution of the r-coefficient and uni-axial yield stress ratios between the BBC2008-16p, the BBC2008-8p, the CPB06ex2 yield criterion and experimental results have been made. Again, the predictions of r-coefficients for BBC2008-16p yield criteria is better than the BBC2008-8p and the

CPB06ex2. For stress ratios, BBC2008-16p and CPB06ex2 have similar predictions. For the prediction of the number of ears,the BBC2008-16p can predict 8 ears however the BBC2008-8p can predict just 4 ears. Moreover, to prove the flexibility of the BBC2008 yield function, a highly anisotropic fictitious model was employed. This model can yield 12 ears according to the theory. In the paper, it is stated that the BBC2008-16p yield criterion is capable of predicting 12 ears in the cup deep drawing simulation.

Yoon et al. [20] implemented the Yld2004-18p yield criterion into a finite element code to show its performance about defining the anisotropic behaviour of materials. The cup drawing tests were simulated for an AA2090-T3 aluminum sheet sample by using LS-DYNA3D. In numerical simulations, a multi-stage return mapping procedure was used for stress increments. Also, experiments were conducted for verification. It was found that the experimental and simulated cup heights were in excellent agreements. Moreover, the Yld96 model results was added for comparison purpose. As stated in the study, the finite element code with Yld2004-18p was able to predict six ears while the Yld96 model [21] predicted only four ears. Additionally, an analytical approach was derived to calculate cup heights of materials. In this analytical approach, it is possible that using the r- values measured every 15°, initial blank geometry and cup geometry, the first approximation of the earing profile can be determined.

Moreira et al. [22] were performed a study on experimental and numerical results of the cylindrical cup deep drawing test. Ferron's anisotropic yield criterion [11] and Hill's quadratic yield criterion [23] were used for numerical simulations. The anisotropic yield criterion of Ferron was implemented into the ABAQUS/Explicit code by employing the radial return algorithm via a VUMAT subroutine. The coefficients of Ferron's function were determined according to the both experimental $\sigma(\alpha)$ and $R(\alpha)$ values. Then, predicted radial strain distributions and earing profiles of an IF steel and an tinplate steel were compared with experimental data. It was found that the earing profile for the IF steel related to Ferron's model adjusted to $\sigma(\alpha)$ was in improved agreement with experimental data than the earing profiles obtained from the other models.In addition, for the tinplate steel, both Ferron's model adjusted to $R(\alpha)$ and Hill's criterion predicted the radial strain values closer to experimental

values at 45°. However, at 0°and 90°, Hill's model underestimated the radial strains. According to the study, the reason of that was the differences in the shape of the yield surfaces of Hill's and Ferron's model. In conclusion, Ferron's yield criterion predicts strain distributions and earing profiles of materials more accurately comparing with Hill's yield criterion.

Tang et al. [24] were studied on the cylindrical cup drawing of AA2090-T3 aluminium alloy by considering Hill'48, Yld2000-2d and Drucker yield criteria with non-associated flow rule in order to predict earing profile. For stress integration, three different integration scheme were used, namely tangent cutting plane explicit method (TCPE), semi explicit method (SEMIE) and simple explicit method (SIMPE). These integration algorithms with yield functions were compared to evaluate their computation stability and computation times. Moreover, the predictions of related yield functions for earing profile were compared with results of experiment. It was found that while Drucker under non-associated flow rule got fast results compared with Hill'48 and Yld2000-2d, the most accurate results were calculated using non-associated plastic model for Yld2000-2d with tangent cutting plane explicit and semi-explicit algorithms.

2.3 Studies about the Effect of Various Parameters on Simulation of Cup Drawing Operations

In this part, past studies about the effect of different parameters on cup drawing simulations are involved. During design of tooling and optimization of process parameters, the information in this part is crucial.

Foudeh et al. [25] studied the effect of different parameters on wrinkling during square cup deep drawing process. These parameters are die and punch radii, the friction coefficient between the sheet metal and the die surfaces, blank holder gap, force of the blank holder and material of the sheet. In this study, 3 different aluminum alloys were selected for deep drawing process such as A6111-T4, AA5754-O and Al-1050. For simulations, ABAQUS/ Explicit was preferred.In accordance with the results, A6111-T4 is more inclined to wrinkle than other aluminum alloys. On the

other hand, the least blank holding force is required to prevent wrinkling for Al-1050 alloy. Also, it was observed from the experimental test, the blank holding force is needed to avoid wrinkling but too much force may lead to tearing. The increase in the friction coefficient value provides reduction in wrinkling; nevertheless,excessive increase in the friction coefficient may cause rupture in the sheet metal. In addition, the blank holder gap should be between 1 to 1.3 and the die radius should be between 5 to 7 times the blank thickness to avoid wrinkling. As well, too small punch radius may cause an increase in the stress in the sheet metal and excessively large punch radius may cause the insufficient contact surface between the sheet and punch. So it should be between 5 to 9 times the sheet thickness.

The effects of tool design parameters on the distribution of the thickness in sheet metal in deep drawing process in Zein et al. work [26]. ABAQUS /Explicit was selected as a finite element program. In order to validate the results, the comparison of thickness values with Colgan and Monaghan's [27] numerical and experimental analysis was done. For analysis, material property of steel was used. The experimental results imply that the blank holding force should be less than three tons and the punch radius should be more than three times the thickness of the blank in order to avoid increased thinning.Also, for the die shoulder radius, the recommended value is eight times the thickness of the sheet. In addition, both Zein and Nowak's work, the punch, die and blank holder were meshed with R3D4 elements while for the meshing of sheet metal, S4R element type was used.

CHAPTER 3

CONSTITUTIVE RELATIONS

3.1 Hardening Models

3.1.1 Isotropic Hardening

The yield surface in case of the isotropic hardening model enlarges uniformly without any movement in space. Figure 3.1 represents the change of yield surface with isotropic hardening [28].

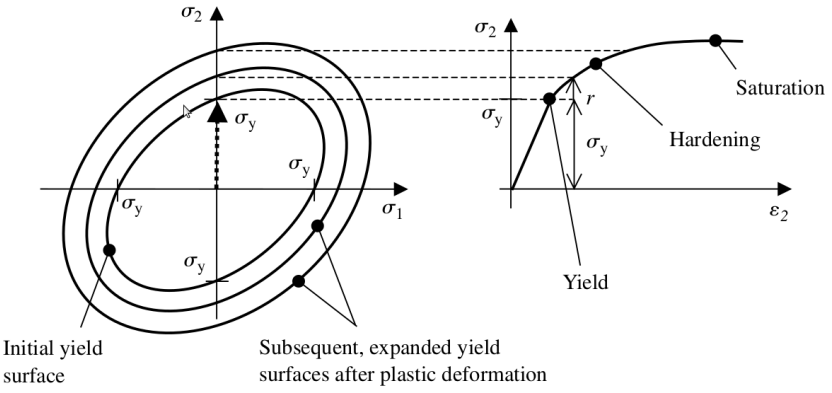

Figure 3.1: Isotropic Hardening

The yield function for the isotropic hardening can be written as [28],

$$f(\boldsymbol{\sigma}, \overline{\epsilon}^p) = \sigma_e(\boldsymbol{\sigma}) - \sigma_Y(\overline{\epsilon}^p) = 0 \tag{3.1}$$

where σ_Y is the current uni-axial yield strength that depends on effective plastic strain, $\overline{\epsilon}^p$. From the consistency condition,

$$f(\boldsymbol{\sigma} + d\boldsymbol{\sigma}, \overline{\epsilon}^p + d\overline{\epsilon}^p) = 0 \tag{3.2}$$

$$f(\boldsymbol{\sigma} + d\boldsymbol{\sigma}, \overline{\epsilon}^p + d\overline{\epsilon}^p) = f(\boldsymbol{\sigma}, \overline{\epsilon}^p) + \frac{\partial f}{\partial \boldsymbol{\sigma}} : d\boldsymbol{\sigma} + \frac{\partial f}{\partial \overline{\epsilon}^p} d\overline{\epsilon}^p = 0 \tag{3.3}$$

where the inner product is denoted by ":". Combining Equation (3.2) and Equation (3.3) gives,

$$\frac{\partial f}{\partial \boldsymbol{\sigma}} : d\boldsymbol{\sigma} + \frac{\partial f}{\partial \overline{\epsilon}^p} d\overline{\epsilon}^p = 0 \tag{3.4}$$

From the normality rule,

$$\frac{\partial f}{\partial \boldsymbol{\sigma}} : d\boldsymbol{\sigma} + \frac{\partial f}{\partial \overline{\epsilon}^p} d\lambda \left(\frac{2}{3} \frac{\partial f}{\partial \boldsymbol{\sigma}} : \frac{\partial f}{\partial \boldsymbol{\sigma}} \right)^{1/2} = 0 \tag{3.5}$$

Rearranging Equation (3.5), the plastic multiplier can be found from the following equation ;

$$d\lambda = \frac{-(\partial f / \partial \boldsymbol{\sigma}) : d\boldsymbol{\sigma}}{(\partial f / \partial \overline{\epsilon}^p) \Big[(2/3) \Big[(\partial f / \partial \boldsymbol{\sigma}) : (\partial f / \partial \boldsymbol{\sigma}) \Big] \Big]^{1/2}} \tag{3.6}$$

3.1.2 Kinematic Hardening

Kinematic hardening is inspired with the Bauschinger effect which is the decrease in the yield stress when a material is loaded in opposite direction after plastic deformation. In kinematic hardening, the shape and size of the yield surface do not change, but translates in the stress space. The yield surface can be expressed as

$$F = f(\boldsymbol{\sigma} - \boldsymbol{\alpha}) - K = 0 \tag{3.7}$$

where K represents a material constant that depends on the size of the yield surface and $\boldsymbol{\alpha}$ is often called as back stress. Figure 3.2 represents the change of yield surface with kinematic hardening [28].

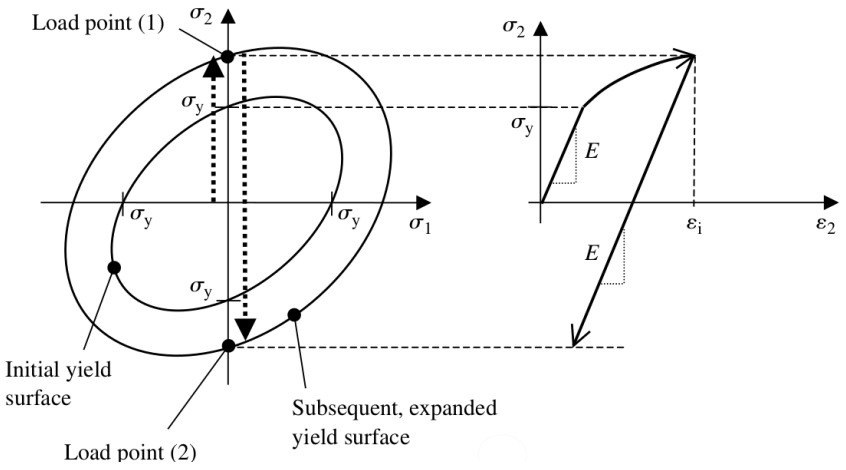

Figure 3.2: Kinematic Hardening

According to the linear kinematic model of Ziegler, the back stress can be written as

$$d\boldsymbol{\alpha} = (\boldsymbol{\sigma} - \boldsymbol{\alpha})\, d\mu \tag{3.8}$$

where $d\mu$ is a scalar constant. In order to find the plastic multiplier, $d\lambda$, df can be set equal to zero due to the consistency condition.

$$\frac{\partial f}{\partial \boldsymbol{\sigma}} : d\boldsymbol{\sigma} + \frac{\partial f}{\partial \boldsymbol{\alpha}} : (\boldsymbol{\sigma} - \boldsymbol{\alpha}) d\mu = 0 \tag{3.9}$$

then

$$\frac{\partial f}{\partial \boldsymbol{\sigma}} : d\boldsymbol{\sigma} = \frac{\partial f}{\partial \boldsymbol{\sigma}} : (\boldsymbol{\sigma} - \boldsymbol{\alpha}) d\mu = 0 \tag{3.10}$$

and $d\mu$ can be written as

$$d\mu = \frac{(\partial f / \partial \boldsymbol{\sigma}) : d\boldsymbol{\sigma}}{(\partial f / \partial \boldsymbol{\sigma}) : (\boldsymbol{\sigma} - \boldsymbol{\alpha})} \tag{3.11}$$

The back stress is

$$d\boldsymbol{\alpha} = \frac{(\boldsymbol{\sigma} - \boldsymbol{\alpha})[(\partial f / \partial \boldsymbol{\sigma}) : d\boldsymbol{\sigma}]}{(\partial f / \partial \boldsymbol{\sigma}) : (\boldsymbol{\sigma} - \boldsymbol{\alpha})} \tag{3.12}$$

The plastic multiplier, $d\lambda$, can be found the normality condition.

$$(\boldsymbol{n} : d\boldsymbol{\sigma})\boldsymbol{n} = K^p\, d\boldsymbol{\epsilon^p} \tag{3.13}$$

where K^p is the plastic modulus and $\boldsymbol{n}$ is the unit normal at the surface.Then

$$\frac{\frac{\partial f}{\partial \boldsymbol{\sigma}} : d\boldsymbol{\sigma}}{\left(\frac{\partial f}{\partial \boldsymbol{\sigma}} : \frac{\partial f}{\partial \boldsymbol{\sigma}}\right)^{\frac{1}{2}}} \; \frac{\frac{\partial f}{\partial \boldsymbol{\sigma}}}{\left(\frac{\partial f}{\partial \boldsymbol{\sigma}} : \frac{\partial f}{\partial \boldsymbol{\sigma}}\right)^{\frac{1}{2}}} = K^p\, d\boldsymbol{\epsilon^p} \tag{3.14}$$

$$d\boldsymbol{\epsilon^p} = \frac{d\boldsymbol{\sigma}}{K^p \left[\frac{\partial f}{\partial \boldsymbol{\sigma}} : \frac{\partial f}{\partial \boldsymbol{\sigma}}\right]} : \left[\frac{\partial f}{\partial \boldsymbol{\sigma}} \otimes \frac{\partial f}{\partial \boldsymbol{\sigma}}\right] \tag{3.15}$$

where the tensor product is denoted by $\otimes$. From the normality condition, the plastic multiplier is

$$d\lambda = \frac{1}{K^p} \frac{\frac{\partial f}{\partial \boldsymbol{\sigma}} : d\boldsymbol{\sigma}}{\frac{\partial f}{\partial \boldsymbol{\sigma}} : \frac{\partial f}{\partial \boldsymbol{\sigma}}} \tag{3.16}$$

3.1.3 Combined Isotropic and Kinematic Hardening

In combined hardening, the material hardens both isotropically and kinematically but the dominant hardening is kinematic hardening. Figure 3.3 represents the change of yield surface with combined hardening [28].

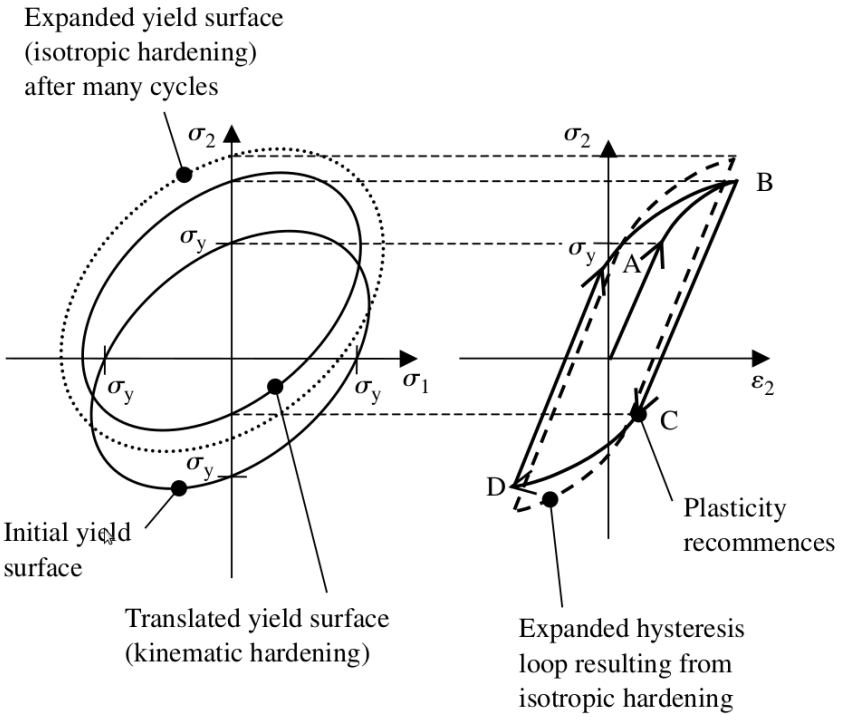

Figure 3.3: Combined Isotropic and Kinematic Hardening

In numerical analyses, the Chaboche-Zeigler combined model was used. According to the model, the back stress rate is

$$d\boldsymbol{\alpha} = C\frac{1}{\overline{\sigma}}(\boldsymbol{\sigma} - \boldsymbol{\alpha}) - \gamma\boldsymbol{\alpha}d\overline{\epsilon}^p \tag{3.17}$$

where

$$\overline{\sigma} = \sigma_Y + Q(1 - e^{-b\overline{\epsilon}^p}) \tag{3.18}$$

In Equation (3.17), C and γ are material constants related with the nonlinear kinematic hardening part. In Equation (3.18), b and Q are material parameters related with the isotropic part and σ_Y is the initial yield stress.

The equivalent plastic strain can be calculated as

$$d\overline{\epsilon}^p = \frac{\frac{df}{d\boldsymbol{\sigma}} : \boldsymbol{C} : d\boldsymbol{\epsilon}}{Qbe^{-b\overline{\epsilon}^p} + C - \gamma\frac{df}{d\boldsymbol{\sigma}} : \boldsymbol{C} : d\boldsymbol{\alpha} + \frac{df}{d\boldsymbol{\sigma}} : \boldsymbol{C} : \frac{df}{d\boldsymbol{\sigma}}} \tag{3.19}$$

where $\boldsymbol{C}$ is a fourth order tensor.

3.2 Yield Criteria

3.2.1 Von Mises Yield Criterion

For von Mises yield criterion, materials yield when the state of stresses provide the below condition

$$f = \overline{\sigma} - \sigma_Y = \sqrt{\frac{3}{2}\boldsymbol{\sigma}' : \boldsymbol{\sigma}'} - \sigma_Y \tag{3.20}$$

in which the deviatoric stress tensor is denoted as $\boldsymbol{\sigma}'$. The yield function can be written in terms of principal stress such as

$$f = \frac{1}{\sqrt{2}}\Big[(\sigma_1 - \sigma_2)^2 + (\sigma_2 - \sigma_3)^2 + (\sigma_3 - \sigma_1)^2\Big]^{1/2} - \sigma_Y \tag{3.21}$$

For plane stress condition,

$$f = \frac{1}{\sqrt{2}}\Big[(\sigma_1 - \sigma_2)^2 + \sigma_1^2 + \sigma_2^2\Big]^{1/2} - \sigma_Y \tag{3.22}$$

3.2.1.1 Von Mises Yield Criterion with Isotropic Hardening

For a material that yields according to isotropic hardening,

$$\frac{\partial f}{\partial \boldsymbol{\sigma}} : d\boldsymbol{\sigma} - \frac{\partial \sigma_Y}{\partial \overline{\epsilon}^p} d\overline{\epsilon}^p = 0 \tag{3.23}$$

And from Equation (3.20)

$$\frac{\partial f}{\partial \boldsymbol{\sigma}} = \frac{3}{2}\frac{\boldsymbol{\sigma'}}{\overline{\sigma}} \tag{3.24}$$

This gives

$$\frac{3}{2}\frac{\boldsymbol{\sigma'}}{\overline{\sigma}} : d\boldsymbol{\sigma} - \frac{\partial \sigma_Y}{\partial \overline{\epsilon}^p} d\overline{\epsilon}^p = 0 \tag{3.25}$$

Then,

$$d\overline{\epsilon}^p = \frac{\frac{3}{2}(\boldsymbol{\sigma'}/\overline{\sigma}) : d\boldsymbol{\sigma}}{(\partial \sigma_Y / \partial \overline{\epsilon}^p)} \tag{3.26}$$

From the general flow rule,

$$d\boldsymbol{\epsilon^p} = d\lambda \frac{\partial f}{\partial \boldsymbol{\sigma}} \tag{3.27}$$

and

$$d\overline{\epsilon}^p = \sqrt{\frac{2}{3} d\boldsymbol{\epsilon^p} : d\boldsymbol{\epsilon^p}} \tag{3.28}$$

Thus,

$$d\overline{\epsilon}^p = \sqrt{\frac{2}{3}\left(d\lambda \frac{\partial f}{\partial \boldsymbol{\sigma}}\right) : \left(d\lambda \frac{\partial f}{\partial \boldsymbol{\sigma}}\right)} = d\lambda \sqrt{\frac{3}{2}\frac{\boldsymbol{\sigma'}}{\overline{\sigma}} : \frac{\boldsymbol{\sigma'}}{\overline{\sigma}}} = d\lambda \sqrt{\frac{\frac{3}{2}\boldsymbol{\sigma'} : \boldsymbol{\sigma'}}{\overline{\sigma}^2}} = d\lambda \tag{3.29}$$

So the plastic multiplier can be written as

$$d\lambda = \frac{\frac{3}{2}(\boldsymbol{\sigma'}/\overline{\sigma}) : d\boldsymbol{\sigma}}{(\partial \sigma_Y / \partial \overline{\epsilon}^p)} \tag{3.30}$$

3.2.1.2 Von Mises Yield Criterion with Kinematic Hardening

The yield function using kinematic hardening according to von Mises criterion is

$$f = \left[\frac{3}{2}(\boldsymbol{\sigma'} - \boldsymbol{\alpha}) : (\boldsymbol{\sigma'} - \boldsymbol{\alpha})\right]^{1/2} - \sigma_Y \tag{3.31}$$

The normal of the yield surface is of the form

$$\frac{\partial f}{\partial \boldsymbol{\sigma}} = \frac{3}{2}\frac{\boldsymbol{\sigma'} - \boldsymbol{\alpha}}{\overline{\sigma}} \tag{3.32}$$

Then the plastic strain rate can be calculated as

$$d\boldsymbol{\epsilon^p} = d\lambda\left(\frac{3}{2}\frac{\boldsymbol{\sigma'} - \boldsymbol{\alpha}}{\overline{\sigma}}\right) \tag{3.33}$$

The equivalent plastic strain rate can be determined by using Equation (3.28). The back stress rate can be written as

$$d\boldsymbol{\alpha} = \frac{2}{3}H d\boldsymbol{\epsilon^p} \tag{3.34}$$

where H represents the slope of the yield stress-plastic strain curve.

3.2.1.3 Von Mises Yield Criterion with Combined Hardening

In combined hardening, the yield function includes the back stress as in kinematic hardening.

$$f = \left[\frac{3}{2}(\boldsymbol{\sigma'} - \boldsymbol{\alpha}) : (\boldsymbol{\sigma'} - \boldsymbol{\alpha})\right]^{1/2} - \sigma_Y \tag{3.35}$$

C and γ can be calculated by using the stress-strain curve acquired from the first half cyle of a uniaxial tension or compression test data [29]. The back stress can be calculated for each data point as

$$\alpha_i = \sigma_i - (\sigma_Y)_i \tag{3.36}$$

where $(\sigma_Y)_i$ represents the size of the yield surface. Also, the back stress evolution law for a half cycle is

$$\boldsymbol{\alpha} = \frac{C}{\gamma}(1 - e^{-\gamma\boldsymbol{\epsilon^p}}) \tag{3.37}$$

Combining Equation (3.36) and (3.37), C and γ can be found.

3.2.2 Hill's 48 Yield Criterion with Isotropic Hardening

Hill proposed a yield criterion for orthotropic materials [23] that can be defined as

$$\begin{aligned} 2f(\sigma_{ij}) = \quad & H(\sigma_{xx} - \sigma_{yy})^2 + F(\sigma_{yy} - \sigma_{zz})^2 + G(\sigma_{zz} - \sigma_{xx})^2 + 2L\sigma_{yz}^2 + \\ & 2M\sigma_{zx}^2 + 2N\sigma_{xy}^2 - 1 \end{aligned} \tag{3.38}$$

where F, G, H, L, M and N are defined as anisotropy material constants. In this criterion, Bauschinger effect and the effect of hydrostatic pressure on yielding are not taken into consideration. Also, the principal axes of anisotropy are selected as Cartesian reference axes. Assuming X, Y and Z are described as the tensile yield stresses in the principal anisotropic directions,

$$\frac{1}{X^2} = G + H \tag{3.39}$$

$$\frac{1}{Y^2} = H + F \tag{3.40}$$

$$\frac{1}{Z^2} = F + G \tag{3.41}$$

Then, the anisotropy constants are expressed as

$$F = \frac{1}{2}\left(\frac{1}{Z^2} + \frac{1}{Y^2} - \frac{1}{X^2}\right) \tag{3.42}$$

$$G = \frac{1}{2}\left(\frac{1}{Z^2} + \frac{1}{X^2} - \frac{1}{Y^2}\right) \tag{3.43}$$

$$H = \frac{1}{2}\left(\frac{1}{Y^2} + \frac{1}{X^2} - \frac{1}{Z^2}\right) \tag{3.44}$$

By denoting the shear yield stresses in yz, xz, xy planes by R, S and T, respectively, L, M, N can be calculated as

$$2L = \frac{1}{R^2}, \quad 2M = \frac{1}{S^2}, \quad 2N = \frac{1}{T^2} \tag{3.45}$$

When the associated flow rule is employed, the plastic strain increments become

$$\begin{aligned}
d\epsilon^p_{xx} &= d\gamma\big[H(\sigma_{xx}-\sigma_{yy})+G(\sigma_{xx}-\sigma_{zz})\big] \\
d\epsilon^p_{yy} &= d\gamma\big[F(\sigma_{yy}-\sigma_{zz})+H(\sigma_{yy}-\sigma_{xx})\big] \\
d\epsilon^p_{zz} &= d\gamma\big[G(\sigma_{zz}-\sigma_{xx})+F(\sigma_{zz}-\sigma_{yy})\big] \\
d\epsilon^p_{xy} &= d\gamma N\sigma_{xy} \\
d\epsilon^p_{yz} &= d\gamma L\sigma_{yz} \\
d\epsilon^p_{xz} &= d\gamma M\sigma_{xz}
\end{aligned} \tag{3.46}$$

The equivalent stress can be calculated from

$$\bar{\sigma} = \sqrt{\frac{3}{2}\left(\frac{\begin{array}{l}F(\sigma_{yy}-\sigma_{zz})^2+H(\sigma_{xx}-\sigma_{yy})^2+\quad G(\sigma_{zz}-\sigma_{xx})^2+2L\sigma^2_{yz} \\ \qquad\qquad\qquad\qquad\qquad\qquad +2M\sigma^2_{zx}+2N\sigma^2_{xy}\end{array}}{F+G+H}\right)} \tag{3.47}$$

For the plane stress case, the yield function gives

$$2f(\sigma_{ij}) = (G+H)\sigma^2_{xx} - 2H\sigma_{xx}\sigma_{yy} + (H+F)\sigma^2_{yy} + 2N\sigma^2_{xy} - 1 = 0 \tag{3.48}$$

The yield function can be rearranged in terms of Lankford parameters.

$$\sigma^2_{xx} - \frac{2r_0}{1+r_0}\sigma_{xx}\sigma_{yy} + \frac{r_0(1+r_{90})}{r_{90}(1+r_0)}\sigma^2_{yy} + \frac{r_0+r_{90}}{r_{90}(r_0+1)}(1+2r_{45})\sigma^2_{xy} = (\sigma_Y)^2 \tag{3.49}$$

where

$$\begin{aligned}
r_0 &= \frac{d\epsilon^p_{yy}}{d\epsilon^p_{zz}} = \frac{H}{G} \\
r_{90} &= \frac{d\epsilon^p_{xx}}{d\epsilon^p_{zz}} = \frac{H}{F} \\
r_{45} &= \frac{2N-(F+G)}{2(F+G)}
\end{aligned} \tag{3.50}$$

In above equation, σ_Y represents the yield stress in x direction.

3.2.3 CPB06ex2 Yield Criterion with Isotropic Hardening

Cazacu et al. [30] proposed an isotropic yield function in order to take into account of tension/ compression asymmetry, as shown below

$$\Phi(\sigma'_1, \sigma'_2, \sigma'_3, k, a) = (\mid \sigma'_1 - k\sigma'_1 \mid)^a + (\mid \sigma'_2 - k\sigma'_2 \mid)^a + (\mid \sigma'_3 - k\sigma'_3 \mid)^a \tag{3.51}$$

where σ'_i, i=1...3 are the principal values of the deviatoric stress tensor $\boldsymbol{\sigma'}$ while a describes the degree of the homogeneity and k is the parameter of strength differential that can be expressed as

$$k = \frac{1 - \left(\frac{2^a - 2(\sigma_T/\sigma_C)^a}{2(\sigma_T/\sigma_C)^a - 2}\right)^{\frac{1}{a}}}{1 + \left(\frac{2^a - 2(\sigma_T/\sigma_C)^a}{2(\sigma_T/\sigma_C)^a - 2}\right)^{\frac{1}{a}}} \tag{3.52}$$

where σ_T and σ_C is the uni-axial yield in tension and compression, respectively. Cazacu et al. [30] applied a fourth-order tensor $\boldsymbol{C}$ on the deviatoric stress tensor $\boldsymbol{\sigma'}$ to import anisotropic characteristic to the isotropic yield function. Hence, the CPB06 yield function can be written in the form:

$$F = \Phi(\Sigma_1, \Sigma_2, \Sigma_3, k, a) = (\mid \Sigma_1 \mid -k\Sigma_1)^a + (\mid \Sigma_2 \mid -k\Sigma_2)^a + (\mid \Sigma_3 \mid -k\Sigma_3)^a \tag{3.53}$$

with

$$\boldsymbol{\Sigma} = \boldsymbol{C} : \boldsymbol{\sigma'}$$

Then, Plunkett et al. [31] have demonstrated that if additional linear transformations are integrated into the CPB06 yield function, better representation of anisotropy can be observed. The following anisotropic yield function, called CPB06ex2, is defined as

$$\begin{aligned} F(\boldsymbol{\Sigma}, \boldsymbol{\Sigma'}, k, k', a) =& (\mid \Sigma_1 \mid -k\Sigma_1)^a + (\mid \Sigma_2 \mid -k\Sigma_2)^a + (\mid \Sigma_3 \mid -k\Sigma_3)^a + \\ & (\mid \Sigma'_1 \mid -k\Sigma'_1)^a + (\mid \Sigma'_2 \mid -k\Sigma'_2)^a + (\mid \Sigma'_3 \mid -k\Sigma'_3)^a \end{aligned} \tag{3.54}$$

For materials has same tension and compression yield strenght, the effective stress of the CPB06ex2 orthotropic yield function is of the form [17]

$$\overline{\sigma} = (\mid \Sigma_1 \mid^a + \mid \Sigma_2 \mid^a + \mid \Sigma_3 \mid^a + \mid \Sigma'_1 \mid^a + \mid \Sigma'_2 \mid^a + \mid \Sigma'_3 \mid^a)^{\frac{1}{a}} \tag{3.55}$$

where $(\Sigma_1, \Sigma_2, \Sigma_3)$ and $(\Sigma_1^{'}, \Sigma_2^{'}, \Sigma_3^{'})$ are the principal values of $\boldsymbol{\Sigma}$ and $\boldsymbol{\Sigma'}$, respectively. The transformed tensors are

$$\boldsymbol{\Sigma} = \boldsymbol{C} : \boldsymbol{\sigma'} \tag{3.56}$$

$$\boldsymbol{\Sigma'} = \boldsymbol{C'} : \boldsymbol{\sigma'} \tag{3.57}$$

where the fourth-order tensors $\boldsymbol{C}$ and $\boldsymbol{C'}$ are symmetric and orthotropic material parameters. For a three-dimensional state of stress, they can be represented by

$$\boldsymbol{C} = \begin{bmatrix} C_{11} & C_{12} & C_{13} & 0 & 0 & 0 \\ C_{12} & C_{22} & C_{23} & 0 & 0 & 0 \\ C_{13} & C_{23} & C_{33} & 0 & 0 & 0 \\ 0 & 0 & 0 & C_{44} & 0 & 0 \\ 0 & 0 & 0 & 0 & C_{55} & 0 \\ 0 & 0 & 0 & 0 & 0 & C_{66} \end{bmatrix} \tag{3.58}$$

$$\boldsymbol{C'} = \begin{bmatrix} C'_{11} & C'_{12} & C'_{13} & 0 & 0 & 0 \\ C'_{12} & C'_{22} & C'_{23} & 0 & 0 & 0 \\ C'_{13} & C'_{23} & C'_{33} & 0 & 0 & 0 \\ 0 & 0 & 0 & C'_{44} & 0 & 0 \\ 0 & 0 & 0 & 0 & C'_{55} & 0 \\ 0 & 0 & 0 & 0 & 0 & C'_{66} \end{bmatrix} \tag{3.59}$$

The parameters C_{ij} and $C_{ij}^{'}$ with $i, j = 1...3$ and the shear coefficients C_{66} and $C_{66}^{'}$ are associated with in-plane anisotropic properties while C_{44}, C'_{44}, C_{55}, C'_{55} are related with out-of-plane properties of the sheet. C_{11} and C'_{11} can be set as equal to one, without any loss in generality.

For plane stress, the components of the transformed tensor $\boldsymbol{\Sigma}$ are:

$$\begin{gathered} \Sigma_{xx} = \Phi_1 \, \sigma_{xx} + \Psi_1 \, \sigma_{yy}, \quad \Sigma_{yy} = \Phi_2 \, \sigma_{xx} + \Psi_2 \, \sigma_{yy} \\ \Sigma_{zz} = \Phi_3 \, \sigma_{xx} + \Psi_3 \, \sigma_{yy}, \quad \Sigma_{xy} = C_{66} \, \sigma_{xy} \end{gathered} \tag{3.60}$$

where

$$\begin{aligned}
\Phi_1 &= \tfrac{1}{3}(2C_{11} - C_{13} - C_{12}), \quad \Psi_1 = \tfrac{1}{3}(2C_{12} - C_{11} - C_{13}) \\
\Phi_2 &= \tfrac{1}{3}(2C_{12} - C_{22} - C_{23}), \quad \Psi_2 = \tfrac{1}{3}(2C_{22} - C_{12} - C_{23}) \\
\Phi_3 &= \tfrac{1}{3}(2C_{13} - C_{33} - C_{23}), \quad \Psi_3 = \tfrac{1}{3}(2\,C_{23} - C_{13} - C_{33})
\end{aligned} \tag{3.61}$$

In a similar way, the components of the $\mathbf{\Sigma'}$ can be defined by using $\Phi'_1, \Phi'_2, \Phi'_3$ and $\Psi'_1, \Psi'_2, \Psi'_3$ in terms of the coefficients C'_{ij}. For the both transformed tensors, the principal values are

$$\begin{aligned}
\Sigma_1 &= \tfrac{1}{2}\Big(\Sigma_{xx} + \Sigma_{yy} + \sqrt{(\Sigma_{xx} - \Sigma_{yy})^2 + 4\,\Sigma_{xy}^2}\Big) \\
\Sigma'_1 &= \tfrac{1}{2}\Big(\Sigma'_{xx} + \Sigma'_{yy} + \sqrt{(\Sigma'_{xx} - \Sigma'_{yy})^2 + 4\,\Sigma'^2_{xy}}\Big) \\
\Sigma_2 &= \tfrac{1}{2}\Big(\Sigma_{xx} + \Sigma_{yy} - \sqrt{(\Sigma_{xx} - \Sigma_{yy})^2 + 4\,\Sigma_{xy}^2}\Big) \\
\Sigma'_2 &= \tfrac{1}{2}\Big(\Sigma'_{xx} + \Sigma'_{yy} - \sqrt{(\Sigma'_{xx} - \Sigma'_{yy})^2 + 4\,\Sigma'^2_{xy}}\Big)
\end{aligned} \tag{3.62}$$

$$\Sigma_3 = \Sigma_{zz} \;\; and \;\; \Sigma'_3 = \Sigma'_{zz}$$

The anisotropy coefficients C_{ij} and C'_{ij} with $i, j = 1...3$ and C_{66}, C'_{66} can be found on the basis of the experimental normalized flow stress values, Lankford parameters, experimental bi-axial tension and experimental r_b. The yield stress in a direction at angle θ with the rolling direction x is determined by

$$\sigma_\theta = \sigma_Y^0 \left\{ \frac{\mid \Phi_1 \mid^a + \mid \Phi_2 \mid^a + \mid \Phi_3 \mid^a + \mid \Phi'_1 \mid^a + \mid \Phi'_2 \mid^a + \mid \Phi'_3 \mid^a}{\mid A_1 \mid^a + \mid A_2 \mid^a + \mid A_3 \mid^a + \mid A'_1 \mid^a + \mid A'_2 \mid^a + \mid A'_3 \mid^a} \right\}^{\frac{1}{a}} \tag{3.63}$$

where σ_Y^0 is the tensile yield stress in the rolling direction and

$$2A_1 = \left\{ \begin{array}{l} (\Phi_1 + \Phi_2)\ \cos^2\theta + (\Psi_1 + \Psi_2)\ \sin^2\theta + \\ \sqrt{((\Phi_1 - \Phi_2)cos^2\theta + (\Psi_1 - \Psi_2)\sin^2\theta)^2 + 4C_{66}^2 \sin^2\theta\cos^2\theta} \end{array} \right\}$$

$$2A_2 = \left\{ \begin{array}{l} (\Phi_1 + \Phi_2)\cos^2\theta + (\Psi_1 + \Psi_2)\sin^2\theta - \\ \sqrt{((\Phi_1 - \Phi_2)cos^2\theta + (\Psi_1 - \Psi_2)\sin^2\theta)^2 + 4C_{66}^2 \sin^2\theta\cos^2\theta} \end{array} \right\}$$

$$A_3 = \Phi_3\cos^2\theta + \Psi_3\sin^2\theta \tag{3.64}$$

with similar expression for $A_1^{'}$,$A_2^{'}$ and $A_3^{'}$. The bi-axial flow stress can be written as

$$\sigma_b = \sigma_Y^0 \left\{ \frac{|\Phi_1|^a + |\Phi_2|^a + |\Phi_3|^a + |\Phi_1^{'}|^a + |\Phi_2^{'}|^a + |\Phi_3^{'}|^a}{|\Phi_1+\Psi_1|^a + |\Phi_2+\Psi_2|^a + |\Phi_3+\Psi_3|^a + |\Phi_1^{'}+\Psi_1^{'}|^a + |\Phi_2^{'}+\Psi_2^{'}|^a + |\Phi_3^{'}+\Psi_3^{'}|^a} \right\}^{\frac{1}{a}} \tag{3.65}$$

The plastic potential is assumed to overlap with the yield functions. The width to thickness strain ratio, r_θ, under uni-axial tensile or compression loading in a direction at angle θ with the rolling direction in the xy plane is given by

$$r_\theta = -\frac{\sin^2\theta(\frac{\overline{\sigma}}{\sigma_{xx}}) - \sin(2\theta)(\frac{\overline{\sigma}}{\sigma_{xy}}) + \cos^2\theta(\frac{\overline{\sigma}}{\sigma_{yy}})}{(\frac{\overline{\sigma}}{\sigma_{xx}}) + (\frac{\overline{\sigma}}{\sigma_{yy}})} \tag{3.66}$$

where $\overline{\sigma}$ is given by Equation (3.55). The strain ratios in the rolling and transverse direction are

$$\begin{aligned} r_0 &= -\frac{\Lambda_1+\Lambda_1^{'}}{\Lambda_2+\Lambda_2^{'}} \\ r_{90} &= -\frac{\Lambda_3+\Lambda_3^{'}}{\Lambda_4+\Lambda_4^{'}} \end{aligned} \tag{3.67}$$

with

$$\begin{aligned} \Lambda_1 &= \Phi_1^{a-1}\Psi_1 + (-1)^a(\Phi_2^{a-1}\Psi_2 + \Phi_3^{a-1}\Psi_3) \\ \Lambda_2 &= \Phi_1^{a-1}(\Phi_1 + \Psi_1) + (-1)^a(\Phi_2^{a-1}\Psi_2 + \Phi_3^{a-1}\Psi_3 + \Phi_2^a + \Phi_3^a) \\ \Lambda_3 &= -\Psi_2^{a-1}\Phi_2 + (-1)^a(\Psi_1^{a-1}\Phi_1 + \Psi_3^{a-1}\Phi_3) \\ \Lambda_4 &= -\Psi_2^{a-1}(\Phi_2 + \Psi_2) + (-1)^a(\Psi_1^{a-1}\Phi_1 + \Psi_3^{a-1}\Phi_3 + \Psi_1^a + \Psi_3^a) \end{aligned} \tag{3.68}$$

In a similar manner, Λ'_1, Λ'_2, Λ'_3, Λ'_4 can be determined. The shear coefficients C_{66} and C'_{66} can be calculated from the theoretical expression of the pure shear yield stress. Hence

$$(\sigma_{xy})_Y = \frac{\sigma_Y^0}{2}\left\{\frac{\mid \Phi_1 \mid^a + \mid \Phi_2 \mid^a + \mid \Phi_3 \mid^a + \mid \Phi'_1 \mid^a + \mid \Phi'_2 \mid^a + \mid \Phi'_3 \mid^a}{\mid C_{66} \mid^a + \mid C'_{66} \mid^a}\right\}^{\frac{1}{a}} \tag{3.69}$$

Finally, minimization of the error function can provide the anisotropy coefficients C_{ij}, C'_{ij} with $i, j = 1...3$ and C_{66}, C'_{66}. The error function is

$$F = \sum_i^n \eta_i \left(1 - \frac{(\tilde{\sigma_\theta})_i^{th}}{(\tilde{\sigma_\theta})_i^{data}}\right)^2 + \sum_j^m \gamma_j \left(1 - \frac{r_j^{th}}{r_j^{data}}\right)^2 + w\left(1 - \frac{\sigma_b^{th}}{\sigma_b^{data}}\right)^2 \tag{3.70}$$

where n is the number of experimental directional flow stresses and m is the number of the experimental r-ratios, whilst η_i, γ_j and w are weight factors. Moreover, the superscripts in the above equation represent whether the value is experimental data or calculated from the yield function. For three dimensional stress states, the out-of-plane anisotropy coefficients C_{44}, C'_{44}, C_{55}, C'_{55} can be found from yield stress for simple shear in yz and xz planes and uni-axial tension at 45° between x and z, and between y and z. Thus

$$\begin{aligned}(\sigma_{yz})_Y &= \frac{\sigma_Y^0}{2}\left\{\frac{|\Phi_1|^a + |\Phi_2|^a + |\Phi_3|^a + |\Phi'_1|^a + |\Phi'_2|^a + |\Phi'_3|^a}{|C_{44}|^a + |C'_{44}|^a}\right\}^{\frac{1}{a}} \\ (\sigma_{xz})_Y &= \frac{\sigma_Y^0}{2}\left\{\frac{|\Phi_1|^a + |\Phi_2|^a + |\Phi_3|^a + |\Phi'_1|^a + |\Phi'_2|^a + |\Phi'_3|^a}{|C_{55}|^a + |C'_{55}|^a}\right\}^{\frac{1}{a}}\end{aligned} \tag{3.71}$$

In plane stress condition, the coefficients C_{44}, C'_{44}, C_{55}, C'_{55} are equal to zero [18].

3.2.4 BBC2008 Yield Criterion with Isotropic Hardening

The BBC2008 plane-stress yield criterion is proposed by Comsa and Banabic for highly orthotropic sheet metals [19]. The yield surface can be written in the form:

$$F(\sigma_{11}, \sigma_{22}, \sigma_{12} = \sigma_{21}, \sigma_Y) = \overline{\sigma}(\sigma_{11}, \sigma_{22}, \sigma_{12} = \sigma_{21}, \sigma_Y) - \sigma_Y(\overline{\epsilon^p}) = 0 \tag{3.72}$$

where σ_Y is the yield stress. The equivalent stress, $\overline{\sigma}$, is expressed as follows

$$\begin{aligned}
&\tfrac{\overline{\sigma}^{2k}}{w-1} = \textstyle\sum_{r=1}^{s} \Big\{ \quad w^{r-1}\Big\{\Big[L^r + M^r\Big]^{2k} + \Big[L^r - M^r\Big]^{2k}\Big\} \\
&\qquad\qquad +w^{s-r}\Big\{\Big[M^r + N^r\Big]^{2k} + \Big[M^r - N^r\Big]^{2k}\Big\}\Big\} \\
&L^r = l_1^r\sigma_{11} + l_2^r\sigma_{22} \\
&M^r = \sqrt{\Big[m_1^r\sigma_{11} - m_2^r\sigma_{22}\Big]^2 + \Big[m_3^r(\sigma_{12} + \sigma_{21})\Big]^2} \\
&N^r = \sqrt{\Big[n_1^r\sigma_{11} - n_2^r\sigma_{22}\Big]^2 + \Big[n_2^r(\sigma_{12} + \sigma_{21})\Big]^2} \\
&k, s \in N \setminus (0),\ w = (3/2)^{1/s} > 1, \\
&l_1^r,\ l_2^r,\ m_1^r,\ m_2^r,\ m_3^r,\ n_1^r,\ n_2^r,\ n_2^r \in R
\end{aligned} \tag{3.73}$$

where $k, l_1^r, l_2^r, m_1^r, m_2^r, m_3^r, n_1^r, n_2^r, n_2^r$ are material parameters. For BCC alloys, k is equal to 3 and for FCC alloys, k is equal to 4. Other quantities can be found by the minimization of an error function . The planar stress components are defined by the formula

$$\begin{aligned}
&\sigma_{11}\ |_\theta = \sigma_Y^\theta \cos^2\theta \\
&\sigma_{22}\ |_\theta = \sigma_Y^\theta \sin^2\theta \\
&\sigma_{12}\ |_\theta = \sigma_{21}\ |_\theta = \sigma_Y^\theta \cos\theta \sin\theta
\end{aligned} \tag{3.74}$$

where σ_Y^θ is the yield stress in the case of uni-axial traction along a direction that is denoted by the angle θ measured from the rolling direction . By using Equation (3.73) and Equation (3.74), the equivalent stress can be defined as follows

$$\overline{\sigma}\ |_\theta = \sigma_Y^\theta F_\theta \tag{3.75}$$

in which F_θ is

$$\begin{aligned}\frac{F_\theta^{2k}}{w-1} = \sum_{r=1}^{s} \Big\{ \quad & w^{r-1}\Big\{\Big[L_\theta^r + M_\theta^r\Big]^{2k} + \Big[L_\theta^r - M_\theta^r\Big]^{2k}\Big\} \\ & + w^{s-r}\Big\{\Big[M_\theta^r + N_\theta^r\Big]^{2k} + \Big[M_\theta^r - N_\theta^r\Big]^{2k}\Big\}\Big\}\end{aligned}$$

$$\begin{aligned}L_\theta^r &= l_1^r \cos^2\theta + l_2^r \sin^2\theta \\ M_\theta^r &= \sqrt{\Big[m_1^r \cos^2\theta - m_2^r \sin^2\theta\Big]^2 + \Big[m_3^r \sin 2\theta\Big]^2} \\ N_\theta^r &= \sqrt{\Big[n_1^r \cos^2\theta - n_2^r \sin^2\theta\Big]^2 + \Big[n_2^r \sin 2\theta\Big]^2}\end{aligned} \tag{3.76}$$

Then the normalized uni-axial yield stress can be calculated from Equation 3.77

$$y_\theta = \frac{\sigma_Y^\theta}{\sigma_Y} = \frac{1}{F_\theta} \tag{3.77}$$

The r-coefficient along a direction that is inclined by the angle θ from the rolling direction is

$$r_\theta = \frac{d\epsilon_{\theta+90}^p}{d\epsilon_{33}^p} \tag{3.78}$$

where $d\epsilon_{\theta+90}^p$ is the plastic strain rate along $\theta + 90$ direction and $d\epsilon_{33}^p$ is the plastic strain along thickness. After some manipulations,

$$r_\theta = \frac{F_\theta}{G_\theta} - 1 \tag{3.79}$$

where G_θ is given as

$$\begin{aligned}\frac{F_\theta^{2k-1} G_\theta}{w-1} = \sum_{r=1}^{s} \quad & \Big\{ w^{r-1}\Big[\hat{L}_\theta^r + \hat{M}_\theta^r\Big]\Big[L_\theta^r + M_\theta^r\Big]^{2k-1} \\ & + w^{r-1}\Big[\hat{L}_\theta^r - \hat{M}_\theta^r\Big]\Big[L_\theta^r - M_\theta^r\Big]^{2k-1} \\ & + w^{s-r}\Big[\hat{M}_\theta^r + \hat{N}_\theta^r\Big]\Big[M_\theta^r + N_\theta^r\Big]^{2k-1} \\ & + w^{s-r}\Big[\hat{M}_\theta^r - \hat{N}_\theta^r\Big]\Big[M_\theta^r - N_\theta^r\Big]^{2k-1}\Big\}\end{aligned} \tag{3.80}$$

in the above equation

$$\begin{aligned}\hat{L}_\theta^r &= l_1^r + l_2^r \\ \hat{M}_\theta^r &= \Big[m_1^r - m_2^r\Big]\Big[m_1^r \cos^2\theta - m_2^r \sin^2\theta\Big]/M_\theta^r \\ \hat{N}_\theta^r &= \Big[n_1^r - n_2^r\Big]\Big[n_1^r \cos^2\theta - n_2^r \sin^2\theta\Big]/N_\theta^r\end{aligned} \tag{3.81}$$

In the case of in-plane bi-axial traction, the planar stress components are

$$\sigma_{11} \mid_b = \sigma_Y^b, \;\; \sigma_{22} \mid_b = \sigma_Y^b, \;\; \sigma_{12} \mid_b = \sigma_{21} \mid_b = 0 \tag{3.82}$$

By replacing Equation (3.75), the associated equivalent stress

$$\bar{\sigma} \mid_b = F_b \sigma_Y^b \tag{3.83}$$

where F_b is

$$\begin{aligned} \frac{F_b^{2k}}{w-1} = \sum_{r=1}^{s} \Big\{ \;\; & w^{r-1} \Big\{ \Big[M_b^r + L_b^r \Big]^{2k} + \Big\{ \Big[L_b^r - M_b^r \Big]^{2k} \Big\} \\ & + w^{s-r} \Big\{ \Big[N_b^r + M_b^r \Big]^{2k} + \Big\{ \Big[M_b^r - N_b^r \Big]^{2k} \Big\} \Big\} \end{aligned} \tag{3.84}$$

with

$$L_b^r = l_1^r + l_2^r, M_b^r = m_1^r - m_2^r, N_b^r = n_1^r - n_2^r \tag{3.85}$$

The normalized bi-axial yield stress is

$$y_b = \frac{\sigma_Y^b}{\sigma_Y} = \frac{1}{F_b} \tag{3.86}$$

In the case of bi-axial traction, the r-coefficient is

$$r_b = \frac{d\epsilon_{22}^p}{d\epsilon_{11}^p} \tag{3.87}$$

After some manipulations, the r-coefficient becomes

$$r_b = \frac{F_b}{G_b} - 1 \tag{3.88}$$

where G_b is given as

$$\begin{aligned} \frac{F_b^{2k-1} G_b}{w-1} = \sum_{r=1}^{s} \Big\{ \;\; & w^{r-1} \Big[\hat{M}_b^r + \hat{L}_b^r \Big] \Big[M_b^r + L_b^r \Big]^{2k-1} \\ & + w^{r-1} \Big[\hat{L}_b^r - \hat{M}_b^r \Big] \Big[L_b^r - M_b^r \Big]^{2k-1} \\ & + w^{s-r} \Big[\hat{N}_b^r + \hat{M}_b^r \Big] \Big[N_b^r + M_b^r \Big]^{2k-1} \\ & + w^{s-r} \Big[\hat{M}_b^r - \hat{N}_b^r \Big] \Big[M_b^r - N_b^r \Big]^{2k-1} \Big\} \end{aligned} \tag{3.89}$$

here

$$\hat{L}_b^r = l_1^r, \;\; \hat{M}_b^r = m_1^r, \;\; \hat{N}_b^r = n_1^r \tag{3.90}$$

In order to find material parameters, authors proposed a method based on the minimization of the error function given as

$$\begin{aligned} & E \Big[l_1^r, l_2^r, m_1^r, m_2^r, m_3^r, n_1^r, n_2^r, n_3^r \mid r = 1, ..., s \Big] = \\ & \sum_{\theta_j} \Big[\frac{y_{\theta_j}^{(exp)}}{y_{\theta_j}} - 1 \Big]^2 + \sum_{\theta_j} \Big[r_{\theta_j}^{(exp)} - r_{\theta_j} \Big]^2 + \Big[\frac{y_b^{(exp)}}{y_b} - 1 \Big]^2 + \Big[r_b^{(exp)} - r_b \Big]^2 \end{aligned} \tag{3.91}$$

CHAPTER 4

FINITE ELEMENT ANALYSIS

Engineering problems can be handled with analytical or numerical methods. However, analytical solutions of some problems are very complex or not possible. For such problems, numerical methods can come into use.

Among other numerical methods, finite element method (FEM) has great importance to solve many engineering problems. In this method, a large solution domain is split into small and interconnected elements. Then it provides piecewise approximations to the governing equations using several variational methods [32].

ABAQUS/Explicit is selected as the finite element analysis code for the simulation of deep drawing operations in this study. It provides a wide range of user subroutines that allow to program to fit in user's special analysis requirements. In this thesis, VUMAT user material subroutines were employed to implement different constitutive models into the program. These constitutive models implemented were obtained by using BBC2008-8p, BBC2008-16p and CPB06ex2 yield criteria. Hill'48 yield criterion and von Mises yield criterion with combined, kinematic and isotropic hardening are already available in ABAQUS library. The VUMAT subroutines are Fortran codes that can be run through the use of Microsoft Visual Studio 2012 and Intel Fortran XE 2013 to ABAQUS/ Explicit. In the VUMAT subprograms, related constitutive models were combined with radial return mapping algorithm. Also, all finite element analyses that have been in the current study were on the basis of elasto-plastic material models.

4.1 Explicit Dynamic Analysis

The dynamic equilibrium equation can be given as

$$M\ddot{u}^{(j)} = F^{(j)} - R^{(j)} \tag{4.1}$$

In the above equation, the mass matrix is denoted as M, the forces obtained internally are denoted as R, the forces applied externally are denoted as F, $\ddot{u}$ is the acceleration and the superscripts mean the increment number. FEM software utilizes the rule of explicit central-difference time integration to calculate the displacements, velocities and accelerations for each increment [29]. The following equation represents the formula of explicit central-difference time integration

$$\dot{u}^{(j+1/2)} = \frac{\triangle t^{(j)} + \triangle t^{(j+1)}}{2}\ddot{u}^{(j)} + \dot{u}^{(j-1/2)} \tag{4.2}$$

$$u^{(j+1)} = \triangle t^{(j+1)}\dot{u}^{(j+1/2)} + u^{(j)} \tag{4.3}$$

Using the results of the previous increments, the values of the next increment can be calculated. During analysis, these increments are very small and for the stability, the following condition should be satisfied:

$$\triangle t \leq \frac{2}{\omega_{max}} \tag{4.4}$$

where ω_{max} is the highest frequency of the system. If damping is included, the condition of the stable time increment will become

$$\triangle t \leq \frac{2}{\omega_{max}}\left(\sqrt{1+\xi_{max}^2} - \xi_{max}\right) \tag{4.5}$$

where ξ_{max} is the critical damping fraction in the mode where the maximum frequency is acquired. ABAQUS/Explicit includes a small viscosity value for a damping effect to avoid high frequency oscillations. The stable time increment can be approximated as

$$\triangle t \approx \frac{L_{min}}{c_d} \tag{4.6}$$

where the minimum element size in the mesh of the part is denoted as L_{min} and c_d is the dilatational speed of wave formulated as

$$c_d = \sqrt{\frac{2\mu + \lambda}{\rho}} \tag{4.7}$$

where λ and μ are defined as Lame's first and second parameters and the material density is presented as ρ.

4.2 Radial Return Algorithm

The calculation of the stress state is done by using radial return algorithm at the stage of the development of VUMAT which is detailed as follows [11]. The yielding surface can be described as

$$F(\sigma_{ij}, \overline{\epsilon^p}) = \bar{\sigma} - \sigma_Y(\overline{\epsilon}^p) \tag{4.8}$$

where the effective stress and effective plastic strain is denoted as $\bar{\sigma}$ and $\overline{\epsilon}^p$, respectively. The increment of strain is divided into an elastic part and plastic part.

$$\triangle\epsilon_{ij} = \triangle\epsilon^e_{ij} + \triangle\epsilon^p_{ij} \tag{4.9}$$

The elastic stress-strain relationships is written in the incremental form as

$$\triangle\sigma_{ij} = C_{ijkl}\left(\triangle\epsilon_{kl} - \triangle\epsilon^p_{kl}\right) \tag{4.10}$$

where C_{ijkl} is defined as elasticity tensor. From the normality rule, the plastic strain rate is acquired as

$$\triangle\epsilon^p_{ij} = \triangle\lambda\frac{\partial F}{\partial\sigma_{ij}} \tag{4.11}$$

where plastic multiplier is denoted as $\triangle\lambda$. With the assumption of isotropic hardening,

$$\triangle\epsilon^p_{ij} = \triangle\overline{\epsilon}^p\frac{\partial F}{\partial\sigma_{ij}} \tag{4.12}$$

The plastic stress-strain relationship is of the form

$$\triangle\overline{\boldsymbol{\sigma}} = H(\boldsymbol{\sigma})\triangle\overline{\epsilon}^p \tag{4.13}$$

Radial return algorithm operates on the basis of an elastic forecaster and plastic corrector. First step of the increment is the calculation of the trial elastic stress by using following equation

$$(\sigma^{trial}_{ij})^{(n+1)} = \sigma^{(n)}_{ij} + \lambda tr(\triangle\epsilon)\delta_{ij} + 2\mu\triangle\epsilon_{ij} \tag{4.14}$$

where the subscripts represents the increment number. If the trial elastic stress is lower than the current yield stress, the elastic deformation occurs and the new state

of stress becomes equal to the trial stress. Otherwise, the new state of stress can be calculated with plastic corrector.

$$\sigma_{ij}^{(n+1)} = (\sigma_{ij}^{trial})^{(n+1)} - 2\mu \triangle \epsilon_{ij}^{p} \tag{4.15}$$

Many past researches about implementing of a new yield criteria to a software were done by using radial return algorithm [17, 22, 33, 34]. In the thesis, this algorithm was chosen to determine the new states of stress and strain values since it provides reasonable results according to the results of the past researches.

4.3 The Finite Element Model

In this study, the simulation of the cylindrical and square cup drawing operations are performed. In addition, the experimental results of the Benchmark 4 in Numisheet 2014 and the predictions of the constitutive models of this study were compared. For the verification of the codes, the predicted earing profile with the CPB06ex2 model and the experimental data reported by Yoon et al. [17] were compared with the predictions of the CPB06ex2 model used in the current study.

In all finite element analyses, the material properties of AA5042 aluminum alloy was employed for elasto-plastic material model. Due to the symmetries, the quarter of the cups were analyzed so the computational time was reduced apparently. In the numerical simulations of the square and cylindrical cup drawing operations, the friction model of Coulomb was used between die, punch, blank holder and sheet metal.

In FEM analyses, there are 3 types of elements for sheet metal forming simulations, namely, membrane element, continuum element and shell element. Membrane elements are preferred due to its simplicity and lower computation time for thin surfaces. However, bending stiffness is not included in membrane elements so it may not be suitable for the simulation of wrinkling which is a kind of buckling. Continuum elements can be used for the analysis of wrinkling; however, computation time is very large. Shell elements considers the effect of bending and computation time is comparably small [4]. For these reasons, the blank was modelled by four node shell

elements with reduced integration control (S4R) in this study. Also the drawn tools such as punch, die and blank holder were modelled as a rigid part for all cases.

4.3.1 Model for Verification

In the current study, for the verification of the CPB06ex2 code, the results of the cyclindrical cup drawing analysis and experimental results obtained by Yoon et al. [17] were employed. The tool dimensions are given in Table 4.1. Schematic view and the FE model are depicted in Figure 4.1 and 4.2, respectively. The blank holding force is equal to 10 kN. The Coulomb friction coefficient is 0.008 and the initial mesh number is specified as 600 in quarter of the sheet.

Table 4.1: Dimensions of the tools used for verification

Parameter	**t**	**r_d**	**r_p**	**d_b**	**d_d**	**d_p**
Dimension [mm]	0.274	2.28	2.28	76.07	46.74	45.72

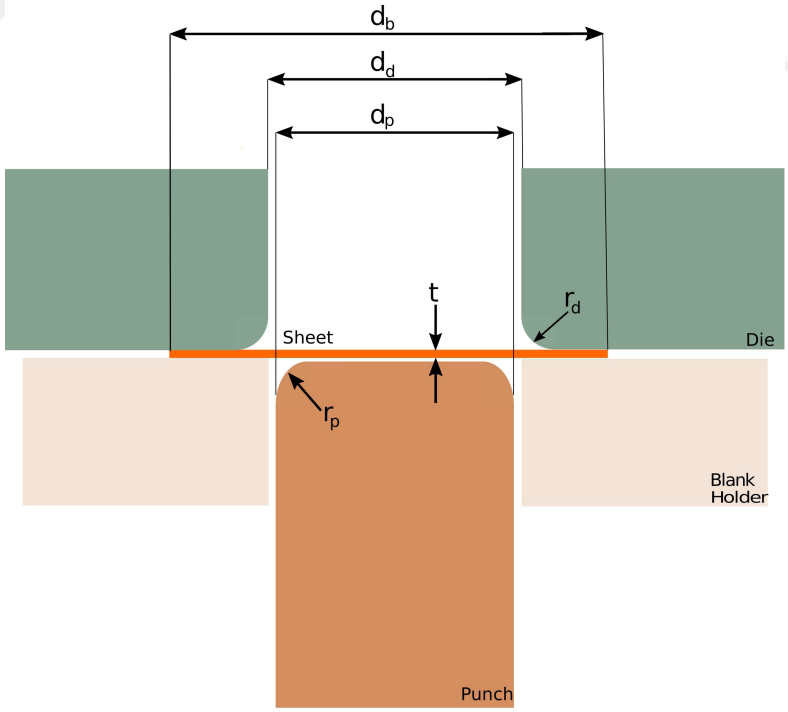

Figure 4.1: Schematic views of the tools and blank used for verification

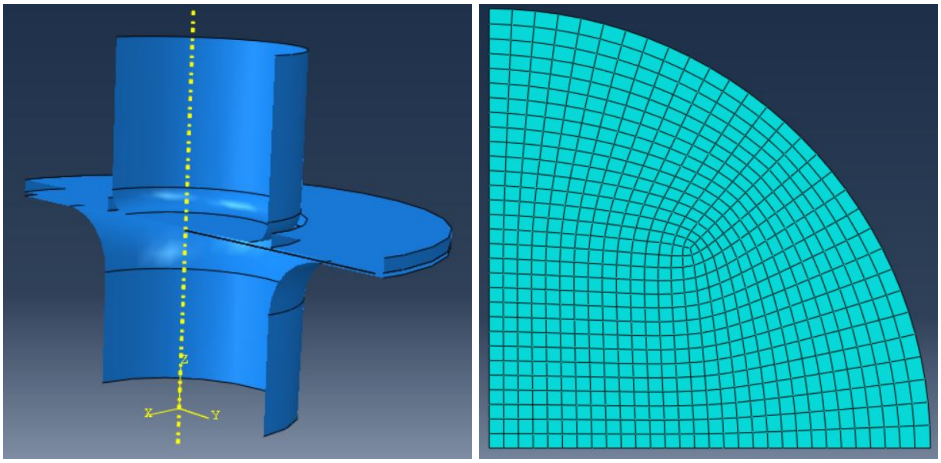

Figure 4.2: The FE model used for verification

4.3.2 Model for Side-Wall Wrinkling Analysis

In this thesis, the experimental data of the Numisheet 2014 Benchmark 4 reported by Neto et al.[5] were compared with the predictions of the constitutive models of the current study. Schematic views of the tools and blank are shown in Figure 4.3 [35]. In Table 4.2, dimensions of the drawing tools are given. The blank holding force is of magnitude 8.9 kN and the friction coefficient is set equal to 0.03. The whole sheet is pull into the die cavity. The coordinate system used for results is given in Figure 4.4 [35]. The FE model used in the numerical analysis is depicted in Figure 4.5. The initial mesh number is about 1800 in quarter of the sheet.

Table 4.2: Dimensions of the tools used in the Benchmark 4 of the Numisheet 2014 conference

Parameter	**T1**	**R1**	**R2**	**R3**	**H1**	**H2**	**D1**	**D2**	**D3**	**D4**	**D5**	**D6**
Dimension [mm]	0.2083	1.016	3.180	1.905	5.207	34.29	15.24	31.75	45.72	45.72	46.74	64.77

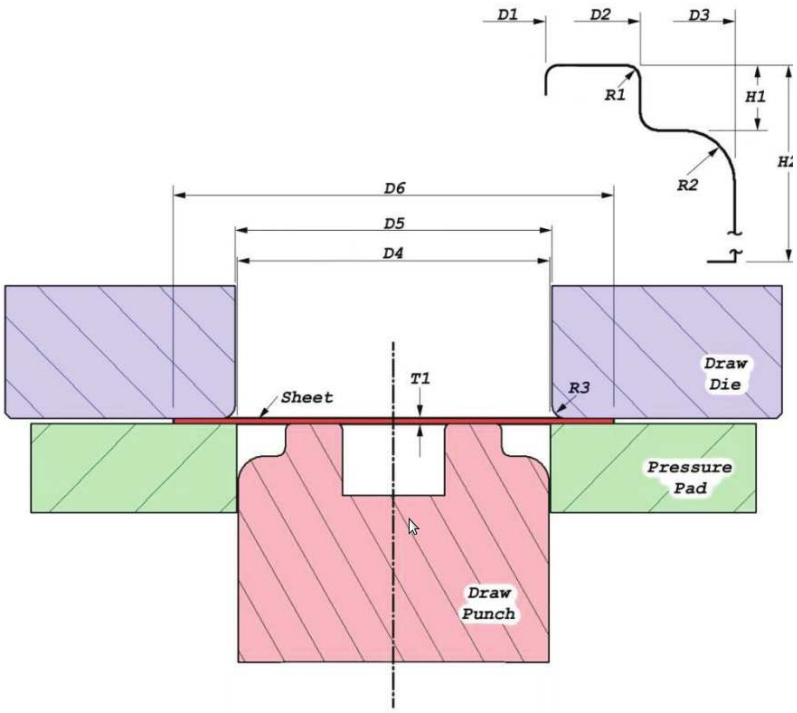

Figure 4.3: Schematic views of the tools and blank used in the Benchmark 4 of the Numisheet 2014 conference

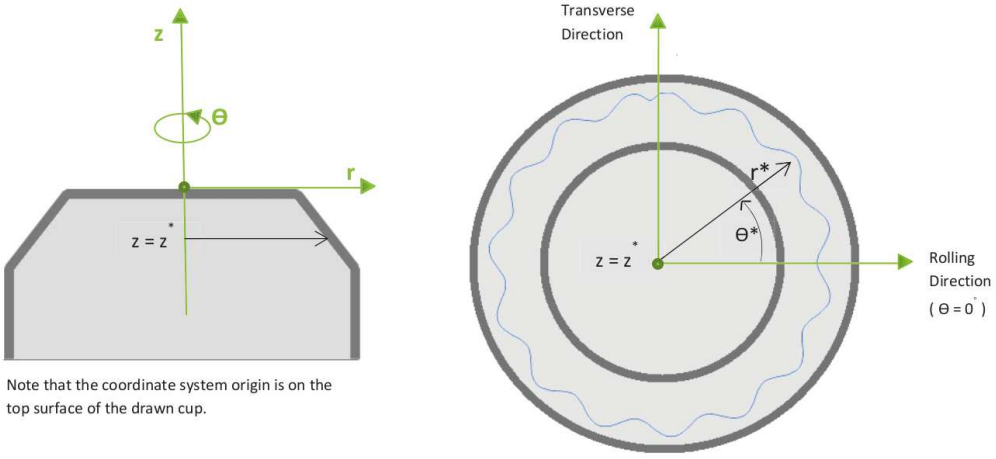

Figure 4.4: Coordinate system of the tools used in the Benchmark 4 of the Numisheet 2014 conference

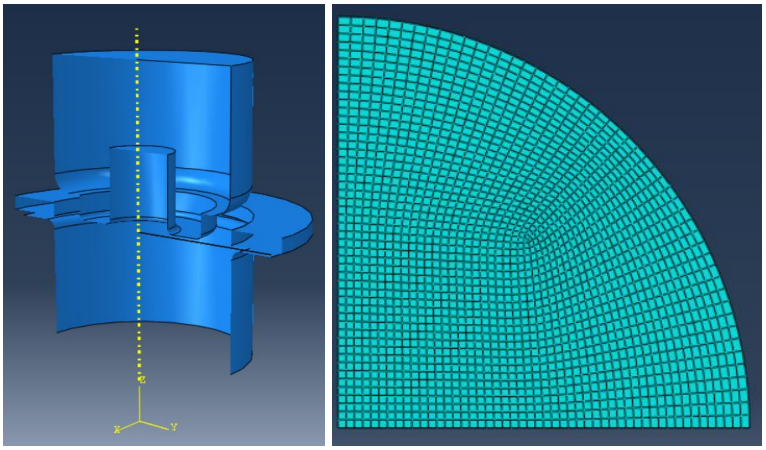

Figure 4.5: The FE model used in the Benchmark 4 of the Numisheet 2014 conference

4.3.3 Model for Flange Wrinkling Analysis in Cylindrical Cup Drawing

Schematic views of the tools and blank are shown in Figure 4.6. Dimensions of the drawn tools are given in Table 4.3. Initial mesh number is set equal to 1600 in quarter of the sheet. The value of the friction coefficient is set equal to 0.06. The FE model of the cylindrical cup drawing process is shown in Figure 4.7.

Table 4.3: Dimensions of the tools used in the cylindrical cup drawing

Parameter	**t**	**r_d**	**r_p**	**d_b**	**d_d**	**d_p**
Dimension [mm]	1	13.5	5	110	53	50

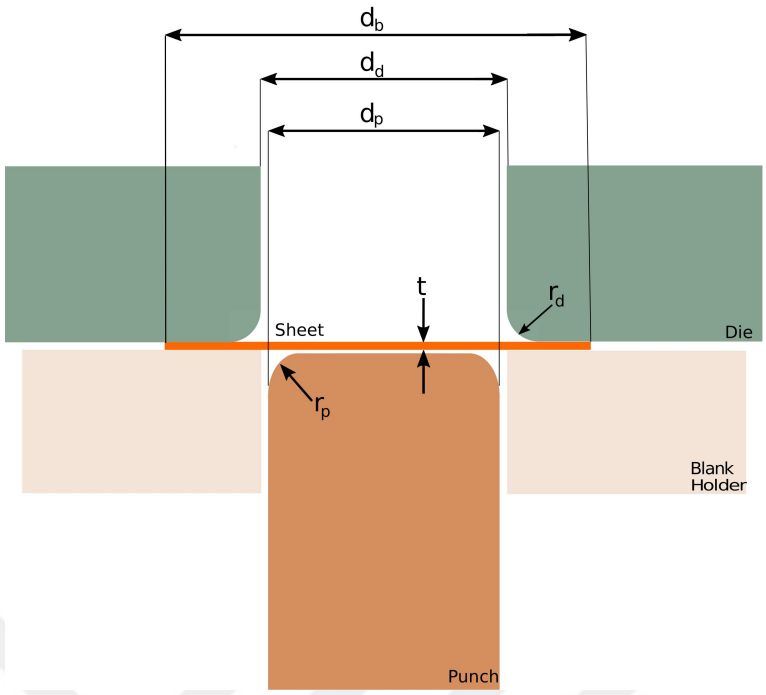

Figure 4.6: Schematic views of the tools and blank used in the cylindrical cup drawing

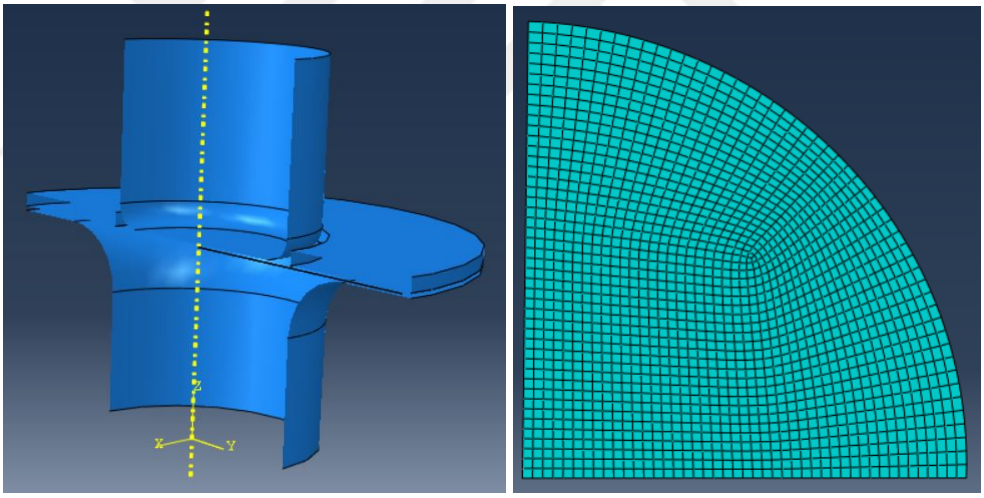

Figure 4.7: The FE model of the cylindirical cup drawing

4.3.4 Model for Flange Wrinkling Analysis in Square Cup Drawing

Schematic views of the tools and blank are presented in Figure 4.8. Initial element number is equal to 1600 in quarter of the sheet. The tool dimensions are provided in Table 4.4. The friction coefficient is equal to 0.06. The FE model of the square cup drawing process is presented in Figure 4.9.

Table 4.4: Dimensions of the drawing tool for the deep drawing process using square plate

Parameter	**t**	**r_d**	**r_p**	**d_b**	**d_d**	**d_p**
Dimension [mm]	1	4.5	4.5	80	42.5	40

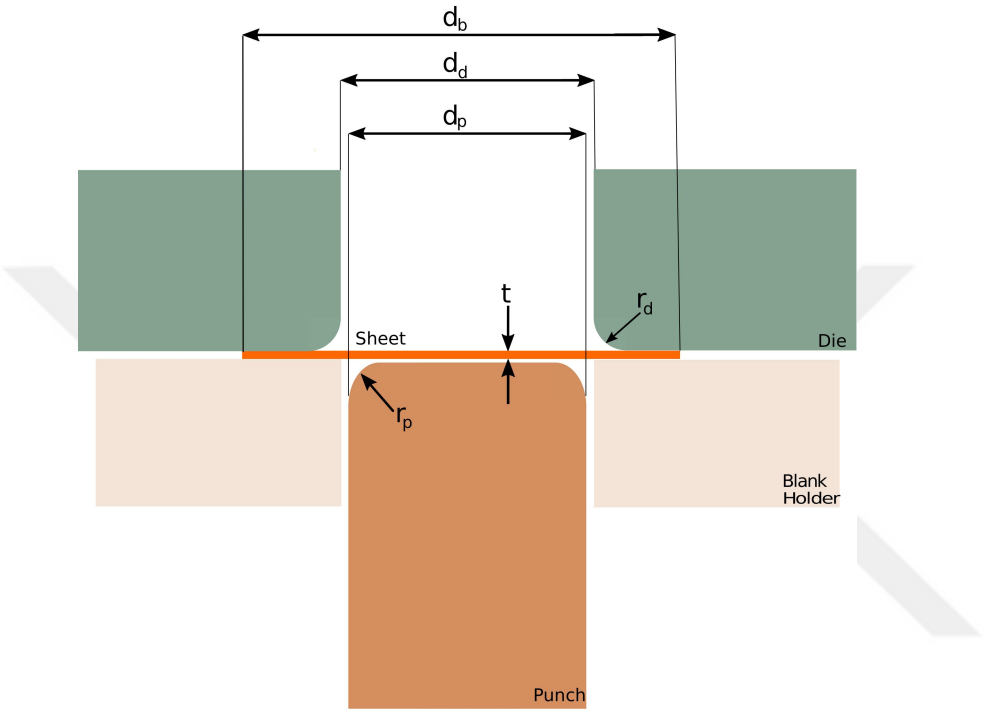

Figure 4.8: Schematic views of the tools and blank used in the square cup drawing

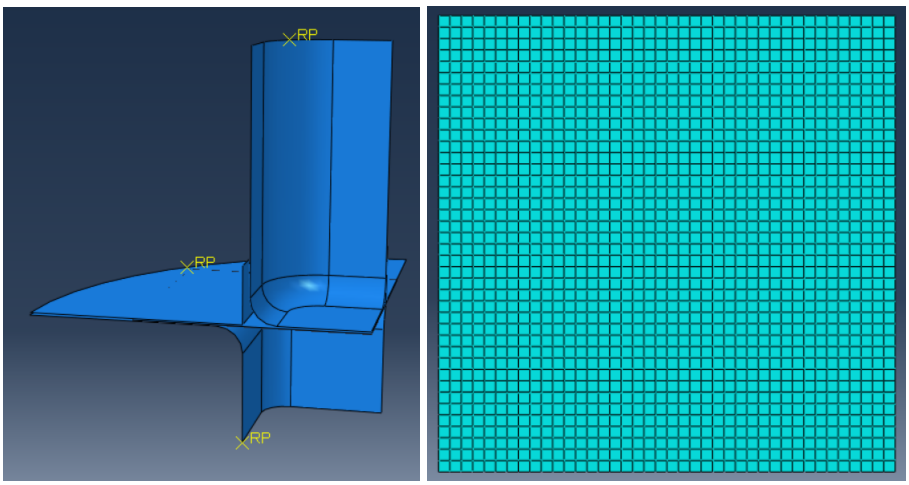

Figure 4.9: The FE model of the square cup drawing process

CHAPTER 5

RESULTS AND DISCUSSION

In this chapter, the verification of the developed models will be given and the numerical results of the cylindrical and square cup drawing analyses are provided by taking into account seven constitutive models formed by using von Mises with kinematic, isotropic and combined hardening, Hill'48 with isotropic hardening, BBC2008-8p with isotropic hardening, BBC2008-16p with isotropic hardening and CPB06ex2 with isotropic hardening. In addition, the comparison between the experimental data from Numisheet 2014 Benchmark 4 and the predictions of the constitutive models for wrinkling profile and punch load for different punch displacements are presented. For the validation of the code, the predicted earing profile using CPB06ex2 yield criterion and experimental findings reported by Yoon et al. [17] are compared with the prediction of the CPB06ex2 model used in this study. For all analyses, AA5042-H2 was used as the blank material. Table 5.1 shows mechanical properties of the material [35].

Table 5.1: Mechanical properties of AA5042-H2

Mechanical Properties	
Stress-strain curve	404.16-107.17 $e^{-18.416\overline{\epsilon^p}}$ MPa
Poisson's ratio	0.33
Young's modulus	68.9 GPa
r_0	0.354
r_{45}	1.069
r_{90}	1.396

For CPB06ex2 model, the anisotropy coefficients C_{ij},C'_{ij} with $i, j = 1...3$ and C_{66}, C'_{66} were found by minimizing the error function shown in Equation (3.70). Table 5.2 presents the anisotropy coefficients of CPB06ex2 for AA5042-H2 [17].

Table 5.2: Anisotropy coefficients of CPB06ex2 with increasing plastic work level

Plastic work per unit volume W_p [MPa]	**Anisotropy coefficients of CPB06ex2**					
	C_{12}	C_{13}	C_{22}	C_{23}	C_{33}	C_{66}
Initial Yielding	-0.0272	-0.6011	1.2870	0.6864	-0.2736	1.1514
	C'_{12}	C'_{13}	C'_{22}	C'_{23}	C'_{33}	C'_{66}
	-0.0897	0.0112	1.1322	-0.1092	-1.2009	1.3093
	C_{12}	C_{13}	C_{22}	C_{23}	C_{33}	C_{66}
W_p = 27.85	0.0001	-0.5513	1.1368	0.8049	0.0133	1.2630
	C'_{12}	C'_{13}	C'_{22}	C'_{23}	C'_{33}	C'_{66}
	0.2413	0.0351	1.5201	0.2806	-1.0053	-1.2713
	C_{12}	C_{13}	C_{22}	C_{23}	C_{33}	C_{66}
W_p = 35.52	0.00011	-0.5999	0.9926	0.8037	0.0867	1.2343
	C'_{12}	C'_{13}	C'_{22}	C'_{23}	C'_{33}	C'_{66}
	0.0684	-0.0790	1.3981	0.1279	-1.1592	-1.3359

For BBC2008-8p and BBC2008-16p constitutive models, material parameters can be found by minifying the error function given in Equation (3.91). The identified material parameters of the BBC2008-8p and BBC2008-16p can be seen in Table 5.3 and Table 5.4, respectively [19].

Table 5.3: Material parameters of BBC2008-8p for AA5042-H2

k	s	w	$l_1^{(1)}$	$l_2^{(1)}$	$m_1^{(1)}$	$m_2^{(1)}$	$m_3^{(1)}$
4	1	1.5	0.6473	0.3478	0.5540	0.5914	0.5813
$n_1^{(1)}$	$n_2^{(1)}$	$n_3^{(1)}$					
0.2796	0.5388	0.4866					

Table 5.4: Material parameters of BBC2008-16p for AA5042-H2

k	s	w	$l_1^{(1)}$	$l_2^{(1)}$	$m_1^{(1)}$	$m_2^{(1)}$	$m_3^{(1)}$
4	2	1.2247	0.3527	-0.7187	0	0	-0.8769
$n_1^{(1)}$	$n_2^{(1)}$	$n_3^{(1)}$	$l_1^{(2)}$	$l_2^{(2)}$	$m_1^{(2)}$	$m_2^{(2)}$	$m_3^{(2)}$
-0.4479	-0.0714	-0.2061	0.7275	0.3431	-0.5720	-0.6217	0.5675
$n_1^{(2)}$	$n_2^{(2)}$	$n_3^{(2)}$					
-0.2992	-0.6359	0					

5.1 Verification of the FE Model

Experimental findings and the earing profile predicted by using the CPB06ex2 yield criteria reported in the study of Yoon et al. [17] are compared with the predictions of the CPB06ex2 model developed in this thesis. Figure 5.1 shows the agreement between the predictions of the developed CPB06ex2 model of the thesis, experimental values and the results of the CPB06ex2 model of the study of Yoon et al. are found to be satisfactory.

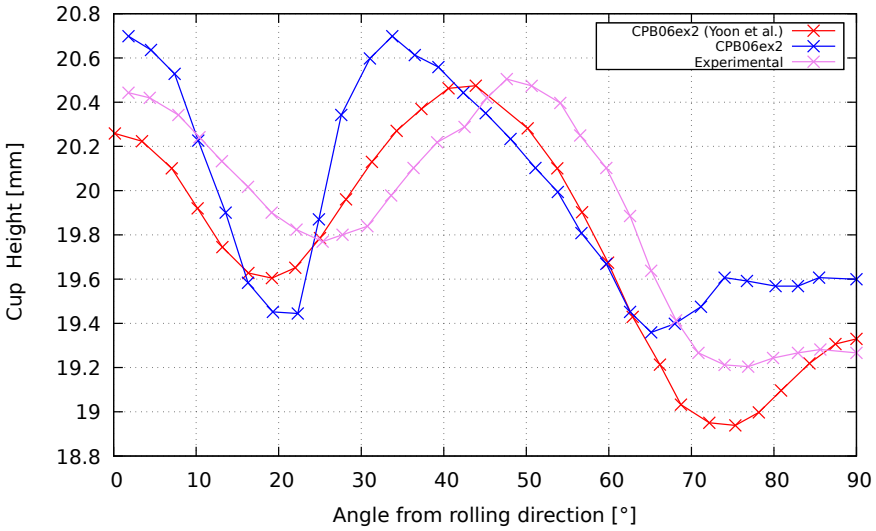

Figure 5.1: Earing profiles of completely drawn cup

5.2 Side-Wall Wrinkling Analysis

The comparison between predicted punch force variation by the developed models at several punch displacements and experimental data is shown in Figure 5.2. All experimental data of Numisheet 2014 Benchmark 4 have been obtained from the study of Neto et al. [5]. The simulation results show that the predicted punch force variation for CPB06ex2, von Mises with isotropic, kinematic and combined hardening are in good agreement with experiments. Especially, CPB06ex2 yield criterion gives the closest results to experimental data. However, BBC2008-8p and BB2008-16p underestimates the punch force.

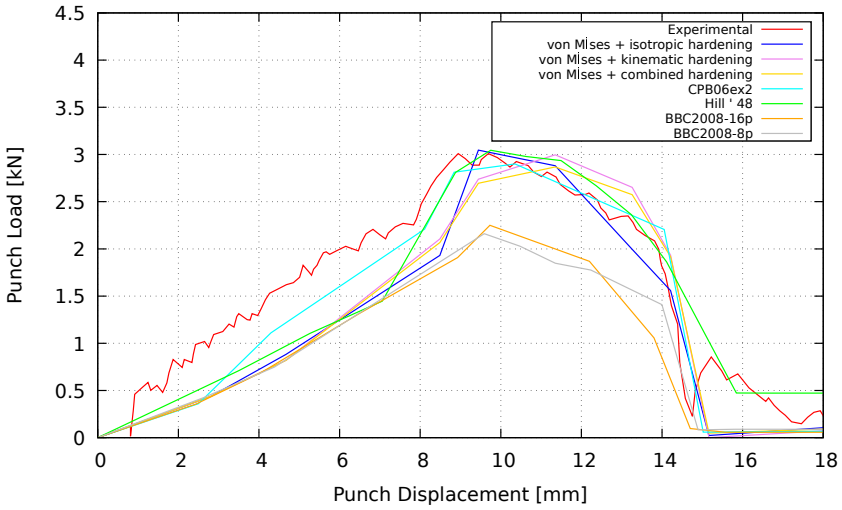

Figure 5.2: Punch load variation at different punch displacement during the drawing process

The wrinkling profile is investigated in two different cross sections perpendicular to the drawn cup axis at 3.5 mm and 5.5 mm in the negative z direction. In order to draw the cup completely, 20 mm punch displacement is given. The wrinkling profile is measured from the outer surface of the completely drawn cup. In experiments, 13 wrinkles were observed in both cross-sections. The numerical results present that while CPB06ex2 and Hill'48 predict 14 wrinkles, other constitutive models predict 12 wrinkles. Since the finite element models involves symmetry, even number of wrinkles are predicted in full models also. In experiments, it is believed that experimental errors such as eccentricity may result variation in wrinkle number. Therefore, it is observed that the agreement between the estimates of the constitutive models for the number of wrinkle and the experimental investigations are found to be satisfactory.

Furthermore, the comparison of the predicted wrinkling profile using related constitutive models and experimental results is given below. According to Figures 5.3-5.15, in the plane $z = -3.5mm$, the experimental results are in good agreement with the models, except the von Mises with kinematic hardening model. The most accurate prediction is obtained using CPB06ex2 yield criterion. However, the BBC2008-8p and BBC20008-16p models are better in predicting the wrinkling profile at the regions correspond to the transverse and rolling directions of the sheet metal.

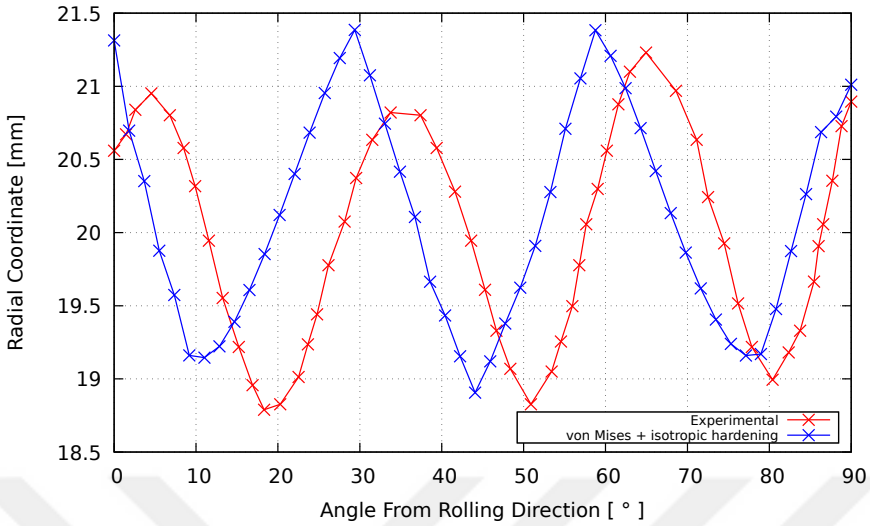

Figure 5.3: Wrinkling profile in the plane $z = -3.5mm$ obtained from the von Mises with isotropic hardening model

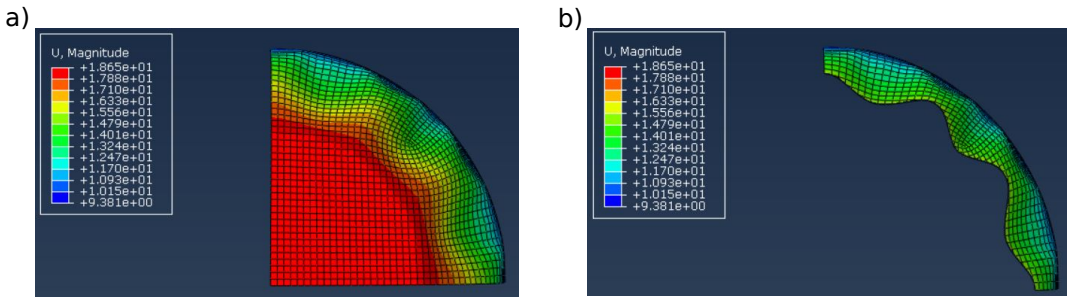

Figure 5.4: (a) The completely drawn cup using the von Mises with isotropic hardening model (b) The drawn cup in the plane $z = -3.5mm$ using the von Mises with isotropic hardening model

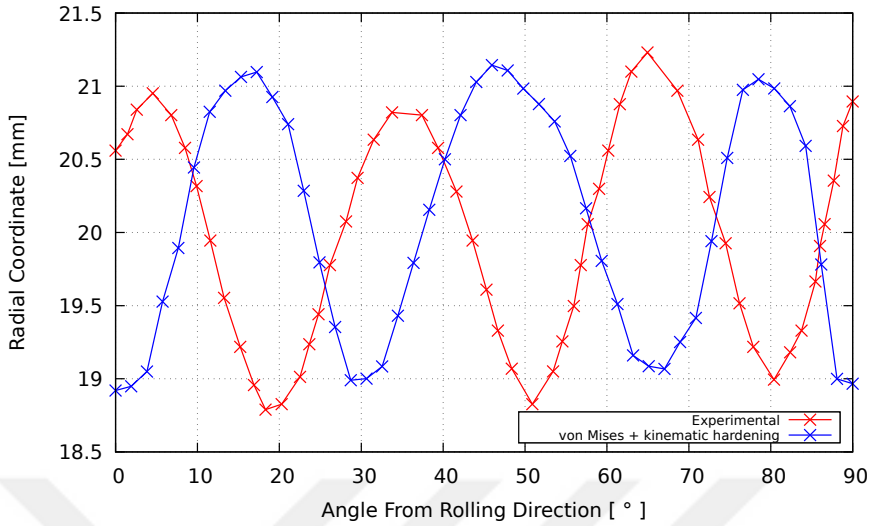

Figure 5.5: Wrinkling profile in the plane $z = -3.5mm$ obtained from the von Mises with kinematic hardening model

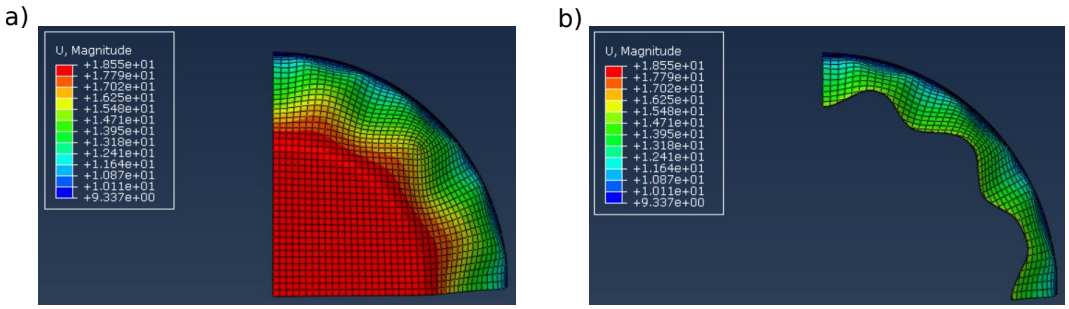

Figure 5.6: (a) The completely drawn cup using the von Mises with kinematic hardening model (b) The drawn cup in the plane $z = -3.5mm$ using the von Mises with kinematic hardening model

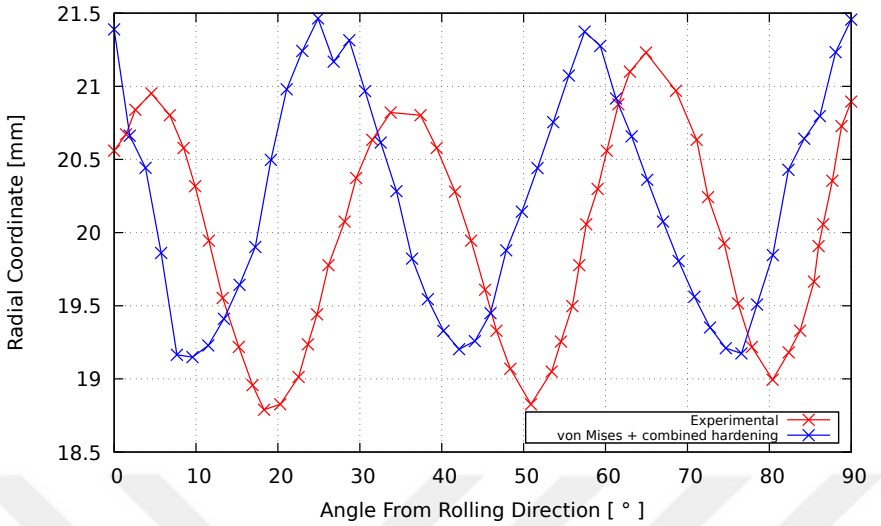

Figure 5.7: Wrinkling profile in the plane $z = -3.5mm$ obtained from the von Mises with combined hardening model

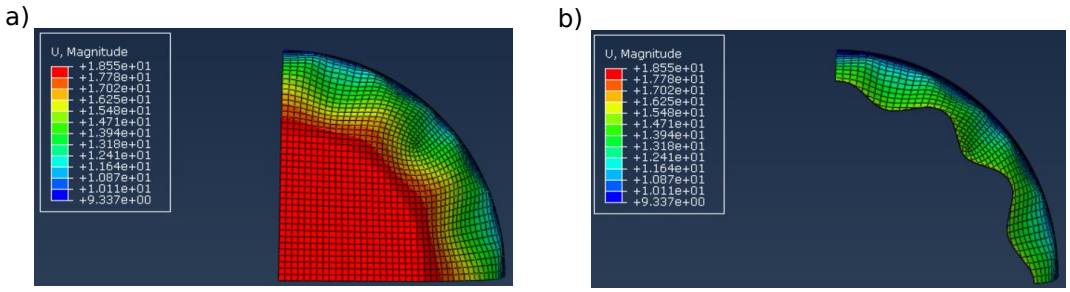

Figure 5.8: (a) The completely drawn cup using the von Mises with combined hardening model (b) The drawn cup in the plane $z = -3.5mm$ using the von Mises with combined hardening model

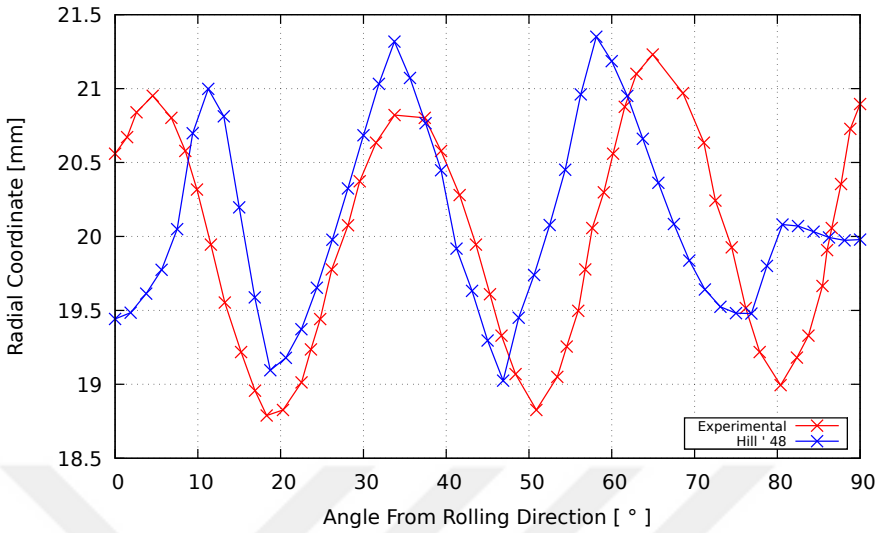

Figure 5.9: Wrinkling profile in the plane $z = -3.5mm$ obtained from the Hill'48 model

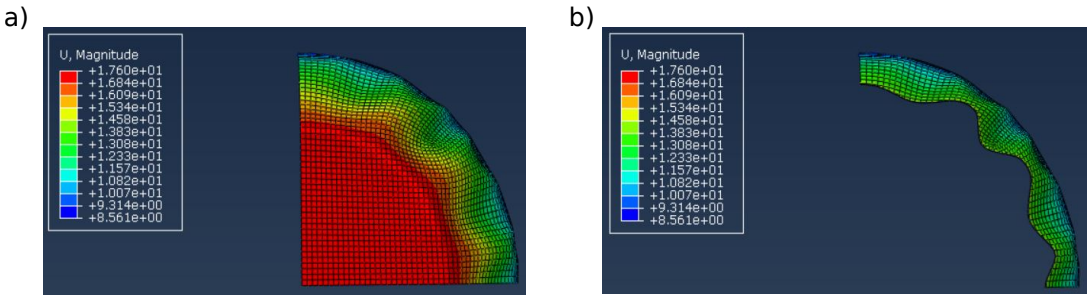

Figure 5.10: (a) The completely drawn cup using the Hill'48 model (b) The drawn cup in the plane $z = -3.5mm$ using the Hill'48 model

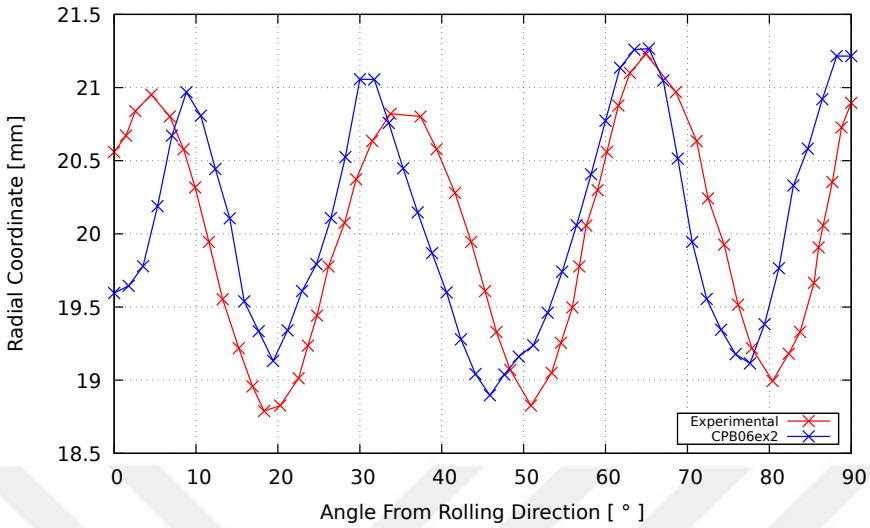

Figure 5.11: Wrinkling profile in the plane $z = -3.5mm$ obtained from the CPB06ex2 model

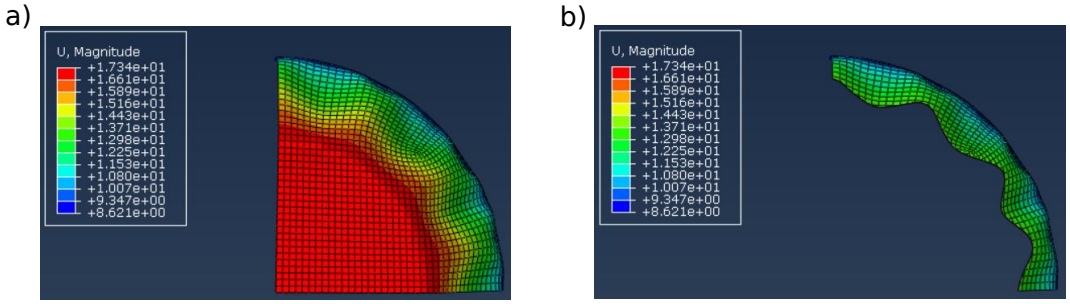

Figure 5.12: (a) The completely drawn cup using the CPB06ex2 model (b) The drawn cup in the plane $z = -3.5mm$ using the CPB06ex2 model

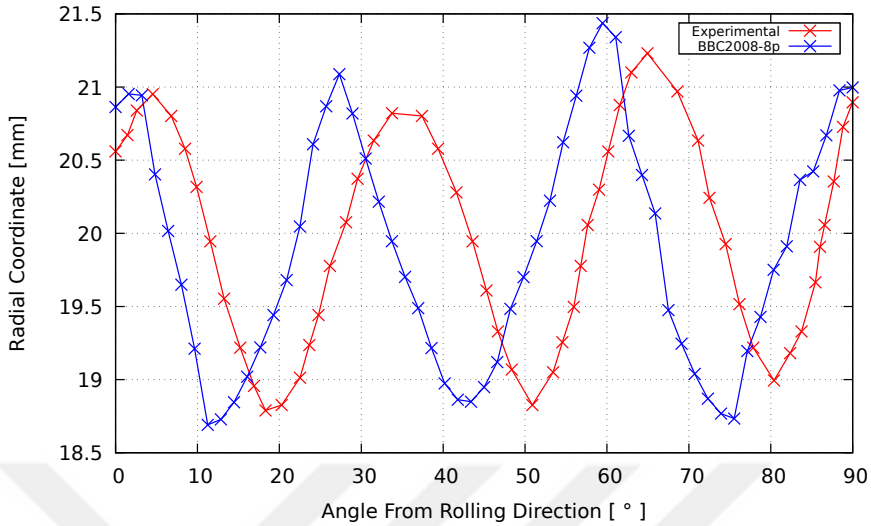

Figure 5.13: Wrinkling profile in the plane $z = -3.5mm$ obtained from the BBC2008-8p model

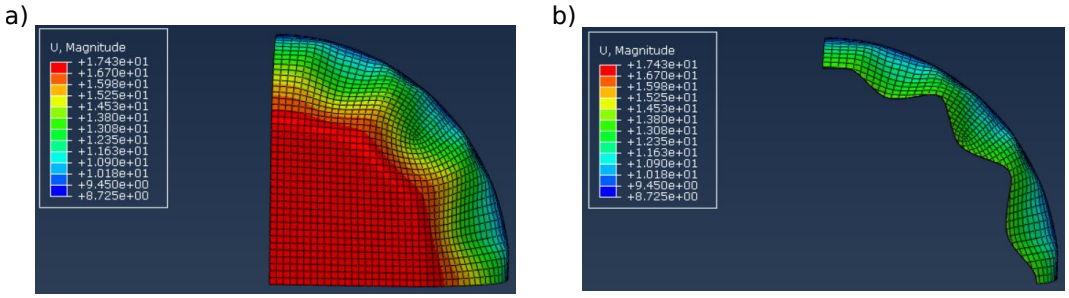

Figure 5.14: (a) The completely drawn cup using the BBC2008-8p model (b) The drawn cup in the plane $z = -3.5mm$ using the BBC2008-8p model

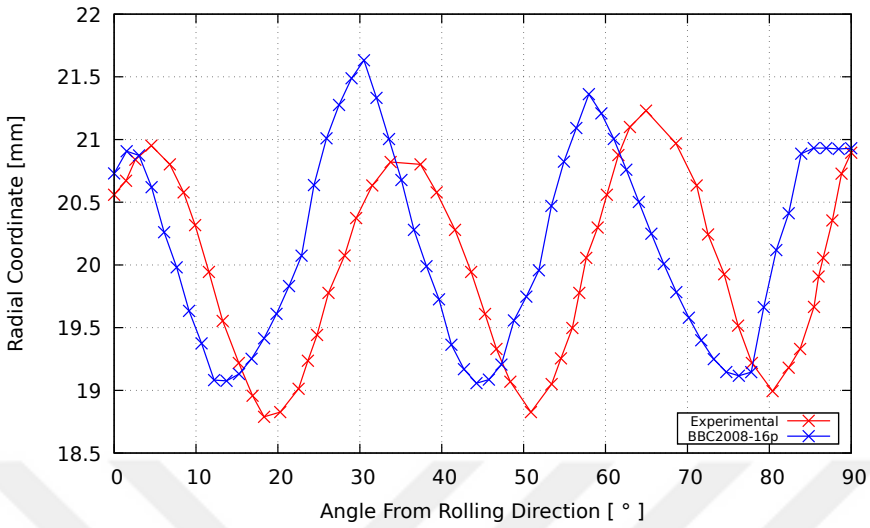

Figure 5.15: Wrinkling profile in the plane $z = -3.5mm$ obtained from the BBC2008-16p model

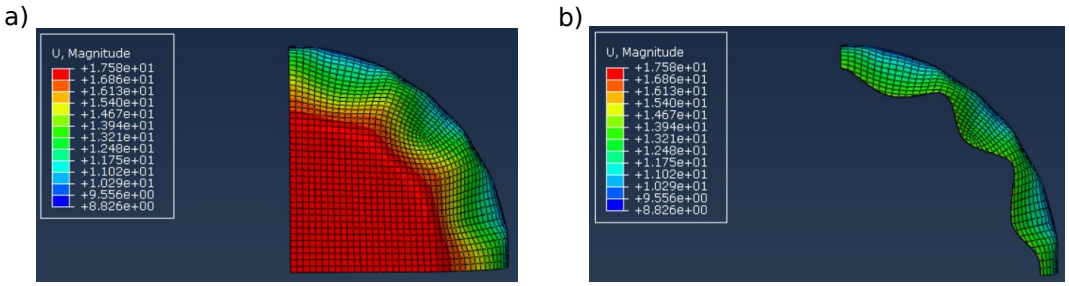

Figure 5.16: (a) The completely drawn cup using the BBC2008-16p model (b) The drawn cup in the plane $z = -3.5mm$ using the BBC2008-16p model

In the plane $z = -5.5mm$, it can be seen from Figures 5.17-5.29 that there are considerably deviations between the experimental data and the numerical results. The predicted amplitude of wrinkling is higher than the experimental one. The coefficient of friction value can be one the cause of dissimilarity between the experimental and numerical results. The recommended friction coefficient is 0.03 but the friction coefficient may vary as the punch moves. The contact pressure, the surface roughness of tools and sheet and the lubrication conditions can affect the value of friction coefficient.

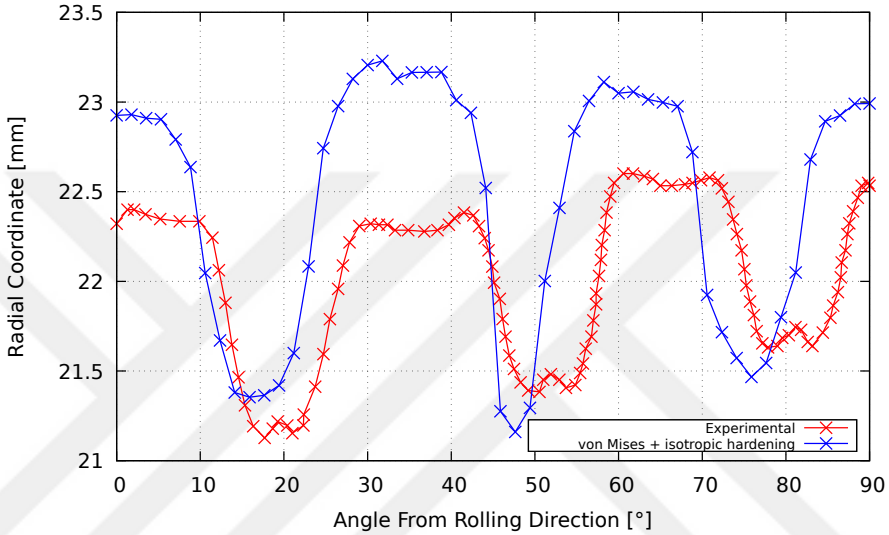

Figure 5.17: Wrinkling profile in the plane $z = -5.5mm$ obtained from the von Mises with isotropic hardening model

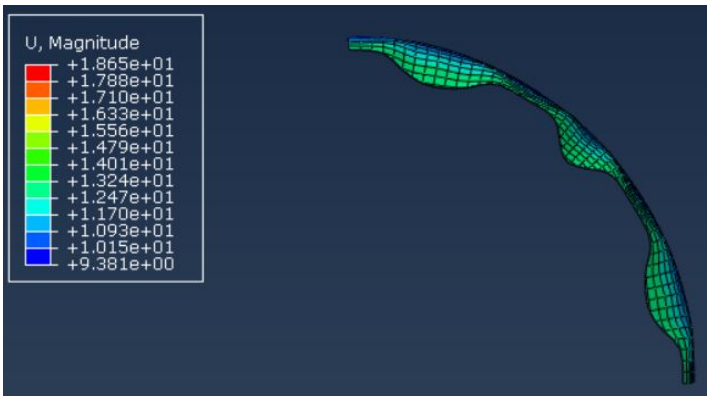

Figure 5.18: The drawn cup in the plane $z = -5.5mm$ using the von Mises with isotropic hardening model

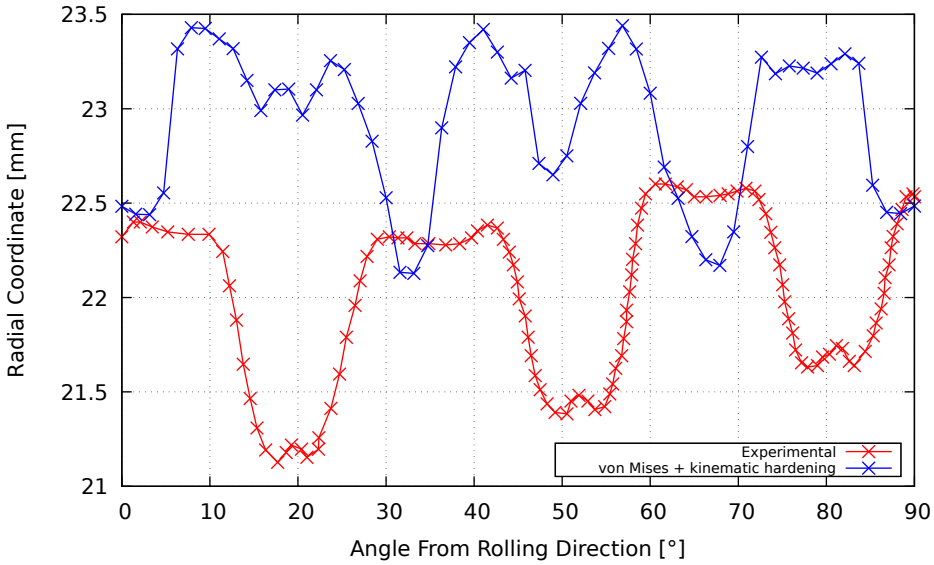

Figure 5.19: Wrinkling profile in the plane $z = -5.5mm$ obtained from the von Mises with kinematic hardening model

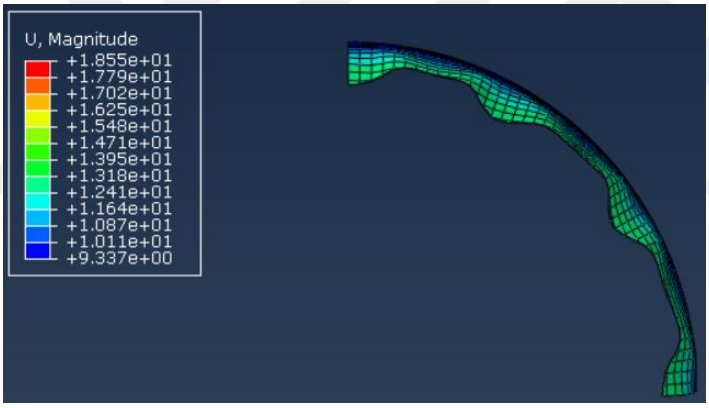

Figure 5.20: The drawn cup in the plane $z = -5.5mm$ using the von Mises with kinematic hardening model

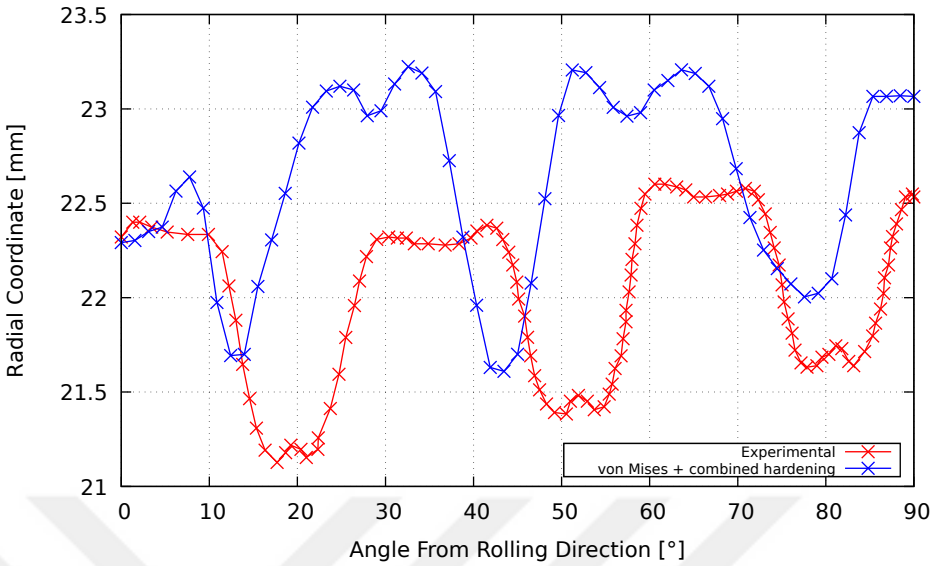

Figure 5.21: Wrinkling profiled in the plane $z = -5.5mm$ obtained from the von Mises with combined hardening model

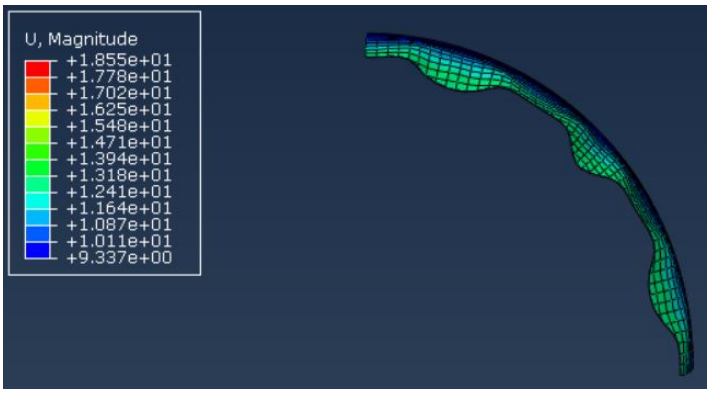

Figure 5.22: The drawn cup in the plane $z = -5.5mm$ using the von Mises with combined hardening model

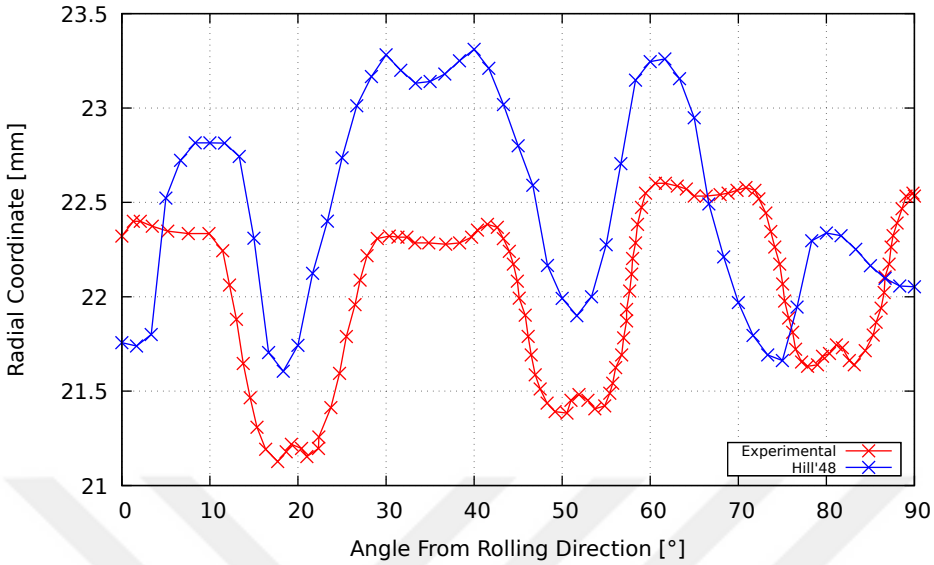

Figure 5.23: Wrinkling profile in the plane $z = -5.5mm$ obtained from the Hill'48 model

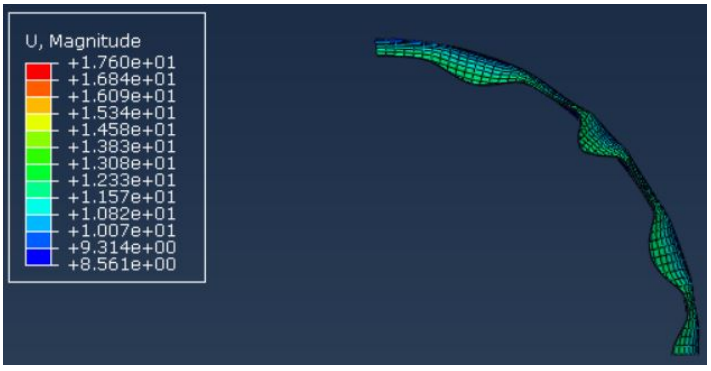

Figure 5.24: The drawn cup in the plane $z = -5.5mm$ using the Hill'48 model

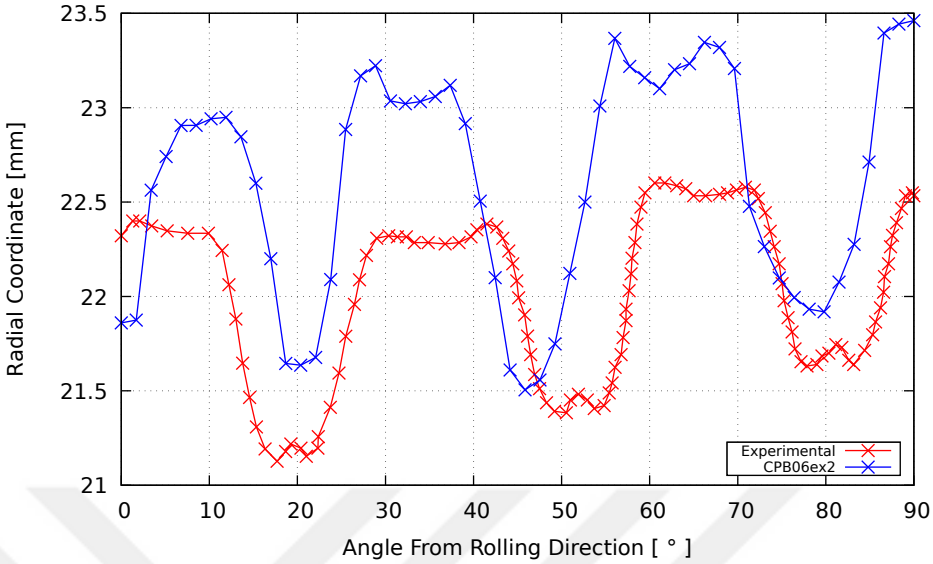

Figure 5.25: Wrinkling profile in the plane $z = -5.5mm$ obtained from the CPB06ex2 model

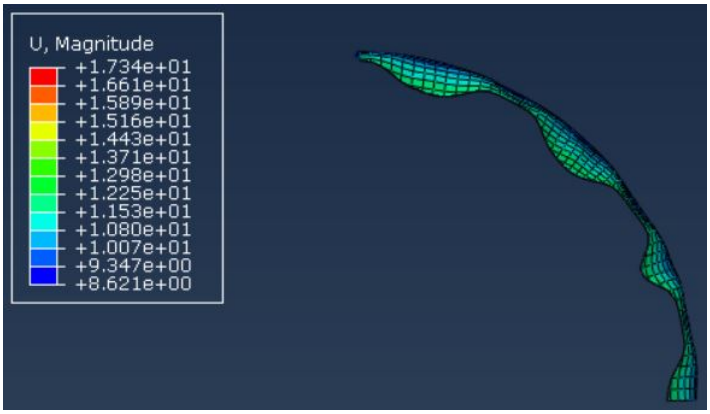

Figure 5.26: The drawn cup in the plane $z = -5.5mm$ using the CPB06ex2 model

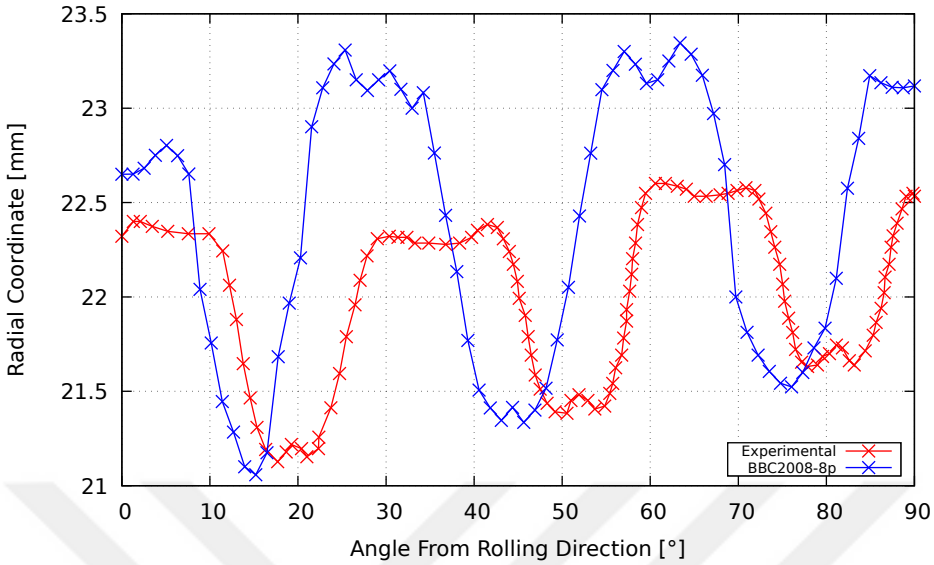

Figure 5.27: Wrinkling profile in the plane $z = -5.5mm$ obtained from the BBC2008-8p model

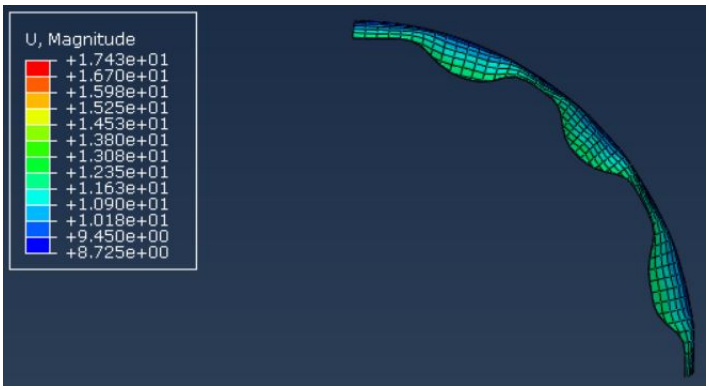

Figure 5.28: The drawn cup in the plane $z = -5.5mm$ using the BBC2008-8p model

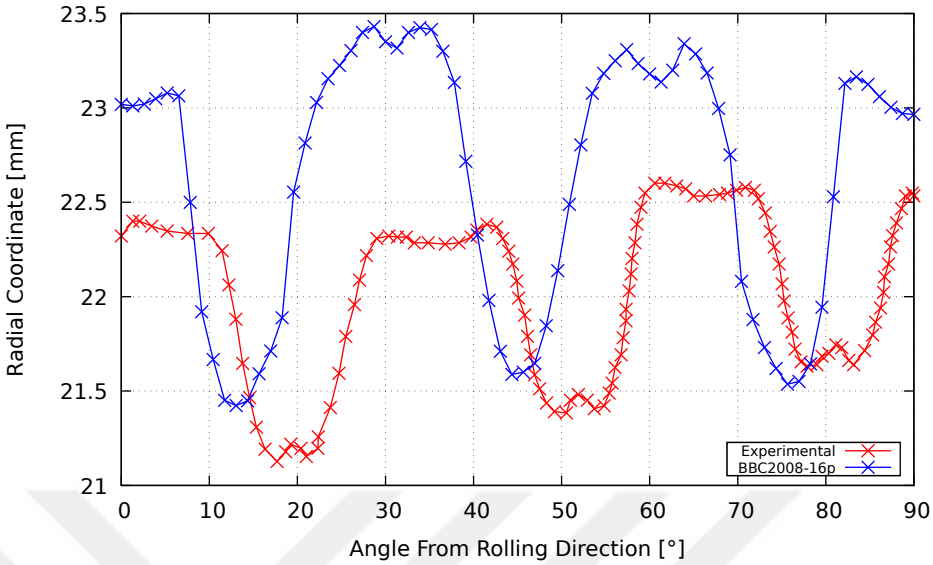

Figure 5.29: Wrinkling profile in the plane $z = -5.5mm$ obtained from the BBC2008-16p model

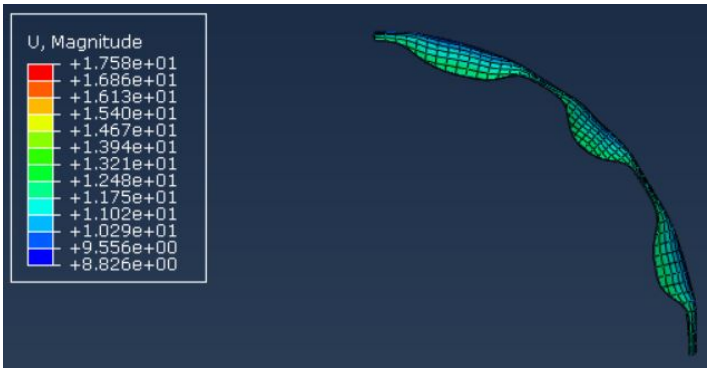

Figure 5.30: The drawn cup in the plane $z = -5.5mm$ using the BBC2008-16p model

According to the results, the von Mises with kinematic hardening model can not predict the side-wall wrinkling profile in the plane $z = -5.5mm$. However, the CPB06ex2 model shows the most similar trend with the experimental results comparing to other constitutive models.

5.3 Flange Wrinkling Analysis in Cylindrical Cup Drawing

Figures 5.31, 5.32 and 5.33 show the evolution of wrinkle heights in cylindrical cup drawing process at 15 mm, 20 mm and 25 mm punch displacement, respectively. The wrinkling amplitude of the von Mises with isotropic, kinematic and combined hardening, BBC2008-8p and BBC2008-16p models are generally consistent with each other. However, the Hill'48 and CPB06ex2 models predict higher than the other constitutive models considering same punch displacement and blank holding force. Figure 5.34 shows the maximum cup forming heights without occurence of wrinkling at various blank holding force in cylindrical cup drawing. Considering the same forming height, the yield criterion CPB06ex2 calculates the greatest blank holding force.

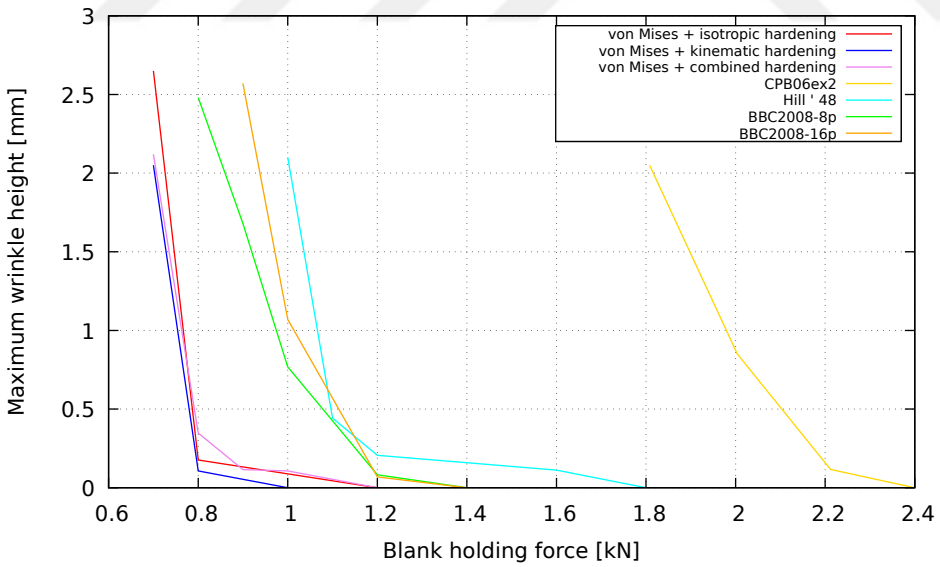

Figure 5.31: Evolution of wrinkle heights with different blank holding force at 15 mm punch travel in cylindrical cup drawing

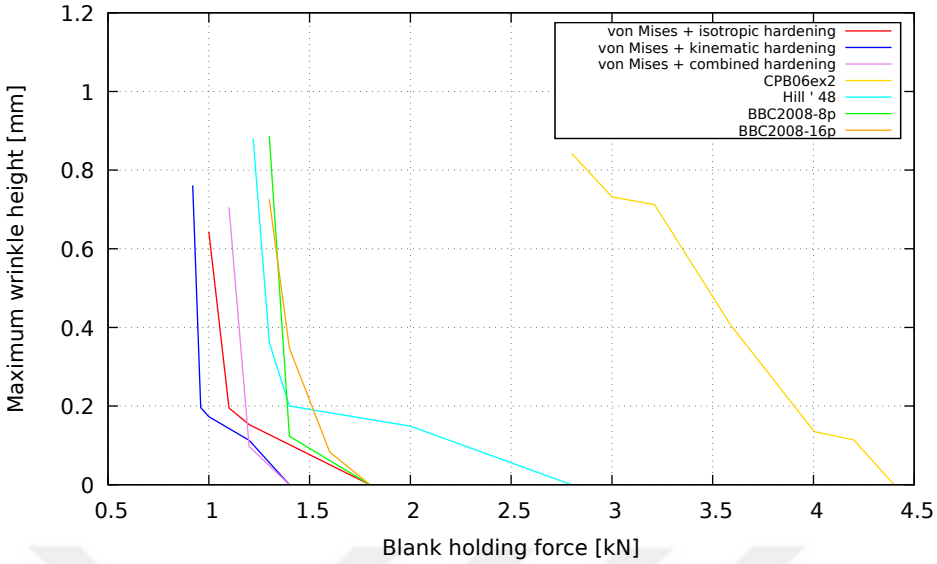

Figure 5.32: Evolution of wrinkle heights with different blank holding force at 20 mm punch travel in cylindrical cup drawing

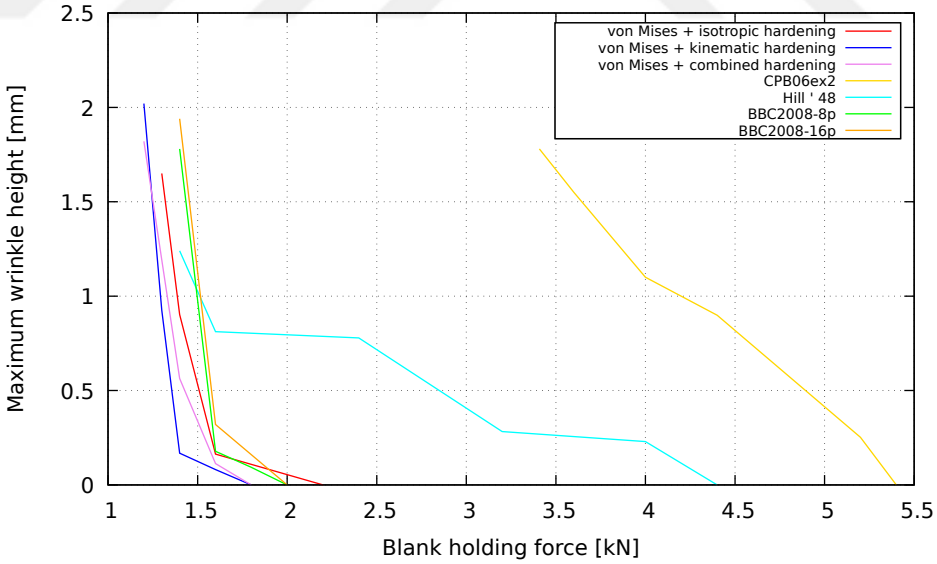

Figure 5.33: Evolution of wrinkle heights with different blank holding force at 25 mm punch travel in cylindrical cup drawing

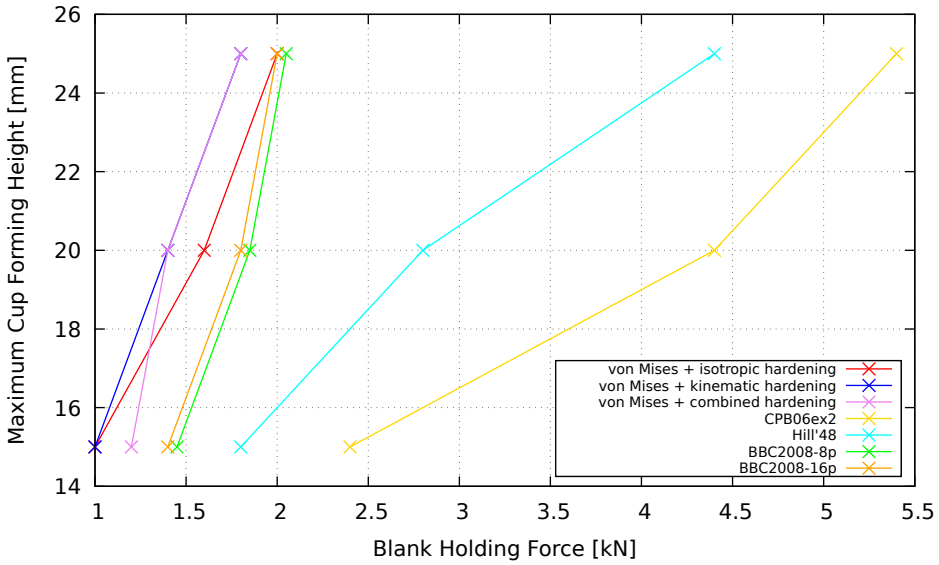

Figure 5.34: Maximum cup forming height variation at several blank holding force in cylindrical cup forming

Figures 5.35-5.42 show some sample drawn cups and their wrinkling profiles using the related constitutive models in the cylindrical cup drawing analyses. Measurements are done from the bottom of the drawn cup.

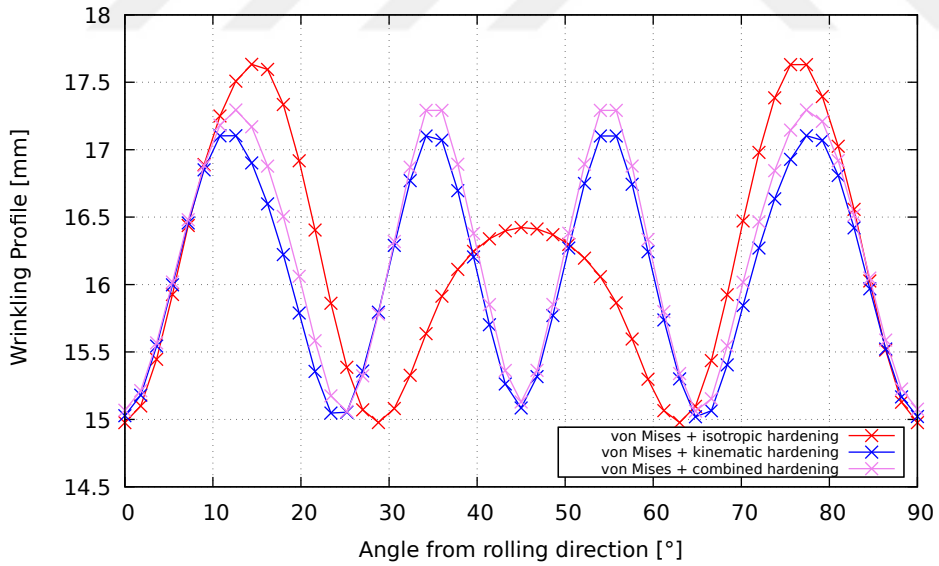

Figure 5.35: Wrinkling profile with 0.7 kN blank holding force at 15 mm punch travel using the von Mises yield criteria with the isotropic, kinematic and combined hardening models in cylindrical cup drawing

a)

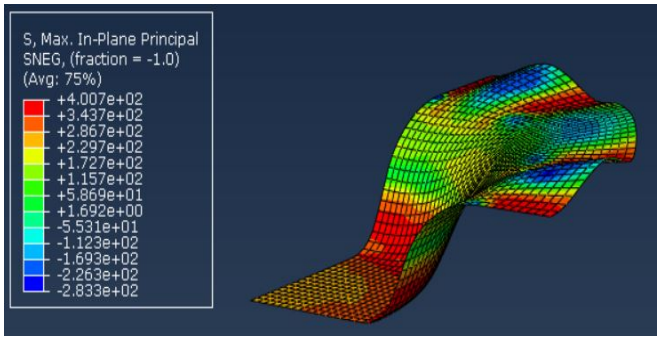

b)

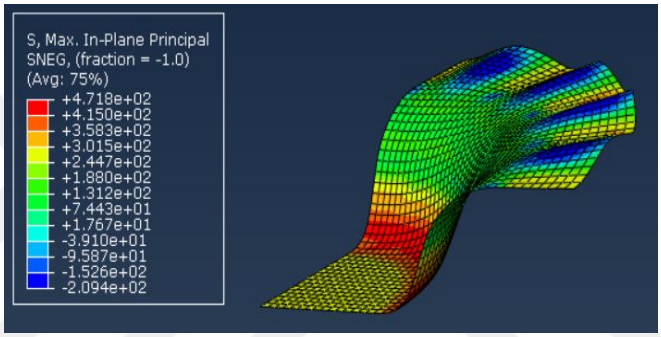

c)

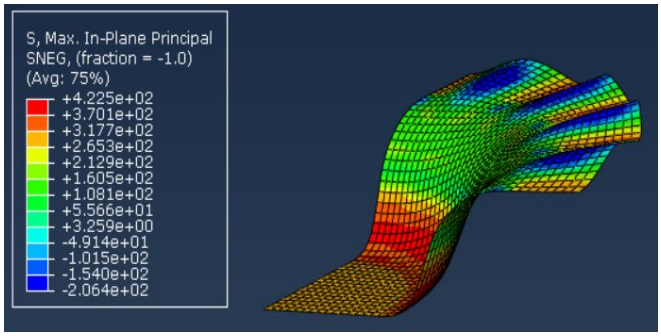

Figure 5.36: In cylindrical cup drawing, the drawn cup with 0.7 kN blank holding force at 15 mm punch travel using the von Mises yield criteria with (a) the isotropic hardening model (b) the kinematic hardening model (c) the combined hardening model

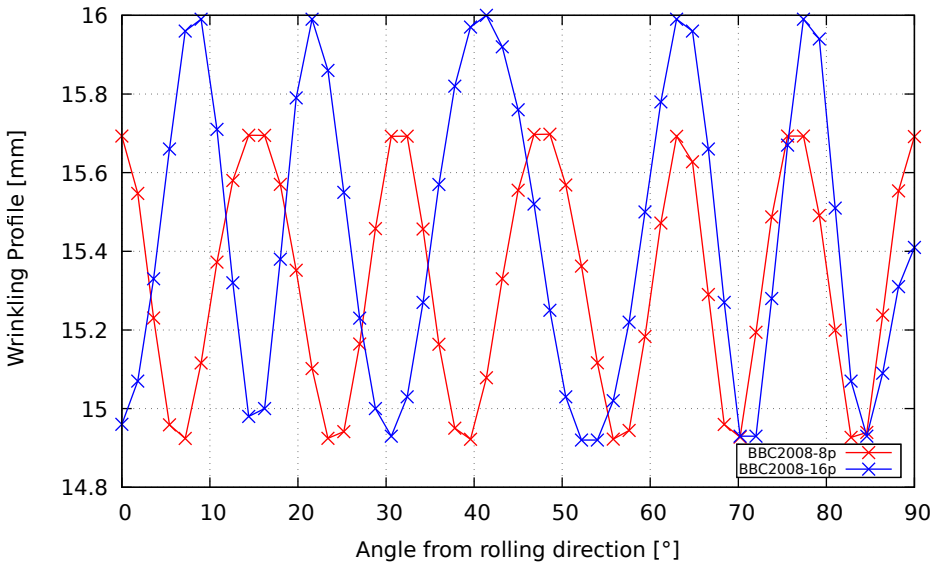

Figure 5.37: Wrinkling profile with 1.0 kN blank holding force at 15 mm punch travel using the BBC2008-8p, BBC2008-16p models in cylindrical cup drawing

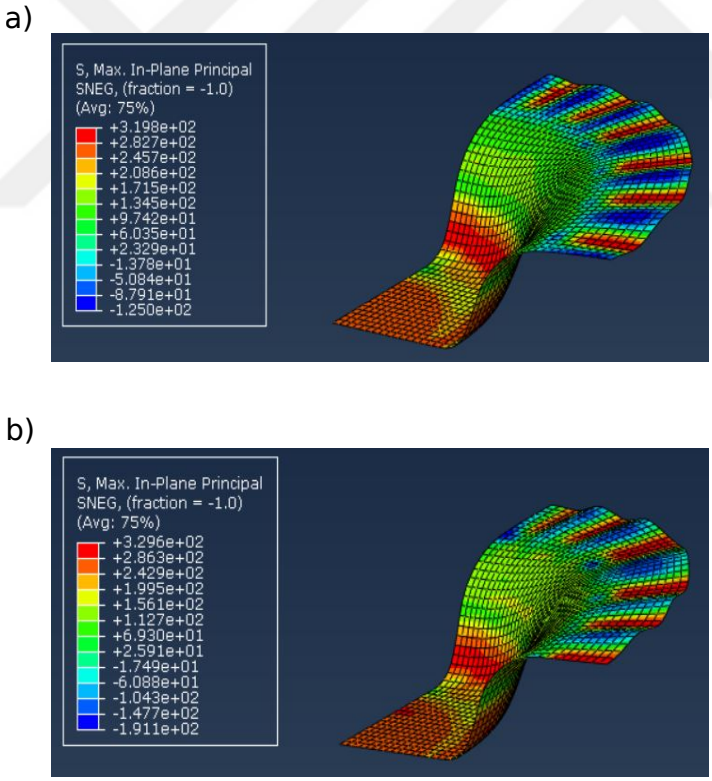

Figure 5.38: In cylindrical cup drawing, the drawn cup with 1.0 kN blank holding force at 15 mm punch travel using (a) the BBC2008-8p model (b) the BBC2008-16p model

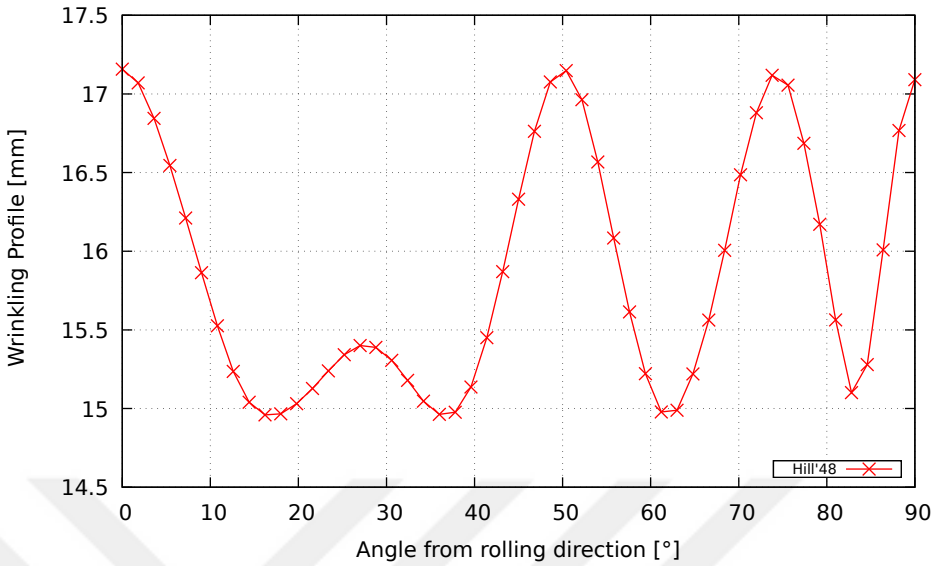

Figure 5.39: Wrinkling profile with 1.0 kN blank holding force at 15 mm punch travel using the Hill'48 model in cylindrical cup drawing

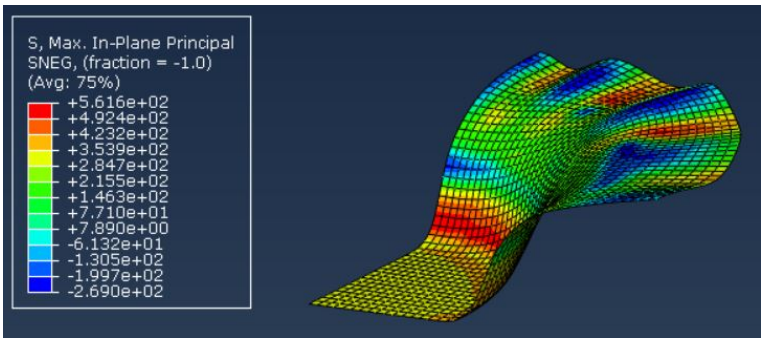

Figure 5.40: In cylindrical cup drawing, the drawn cup with 1.0 kN blank holding force at 15 mm punch travel using the Hill'48 model

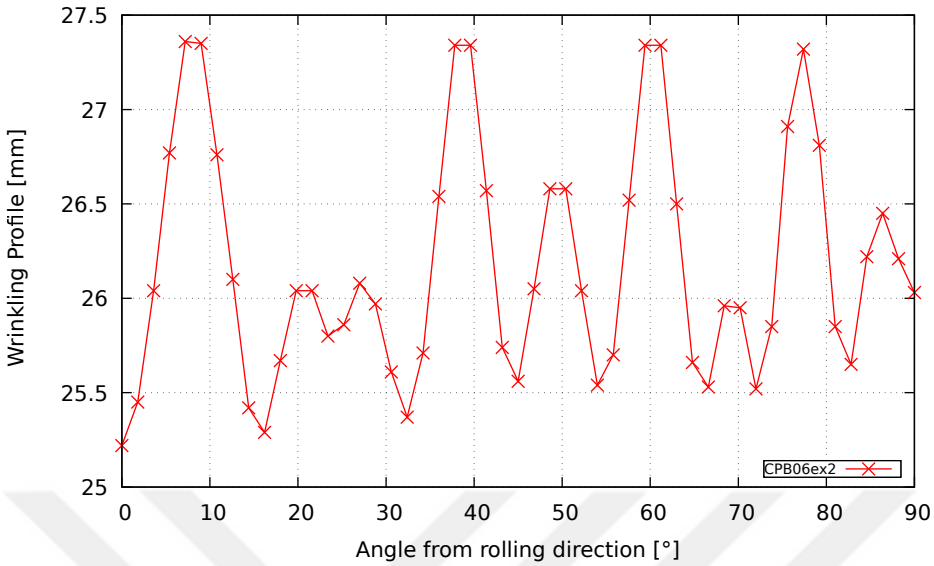

Figure 5.41: Wrinkling profile with 3.4 kN blank holding force at 25 mm punch travel using the CPB06ex2 model in cylindrical cup drawing

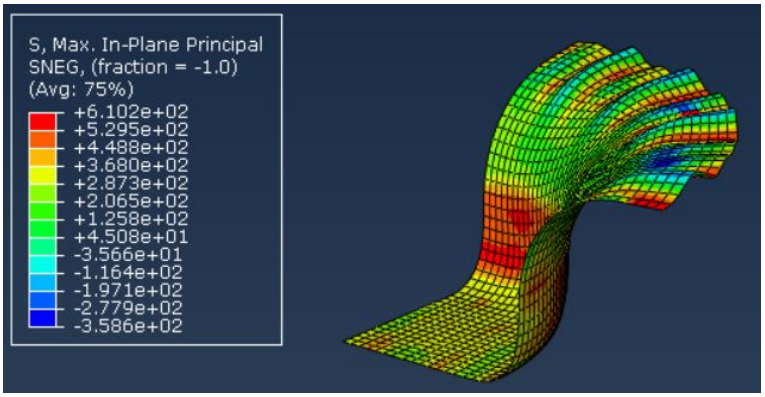

Figure 5.42: In cylindrical cup drawing, the drawn cup with 3.4 kN blank holding force at 25 mm punch travel using the CPB06ex2 model

Moreover, the flange wrinkling profiles with 0.7 kN blank holding force at 15 mm punch travel are presented in Figure 5.43 in order to compare the predictions of the developed models.

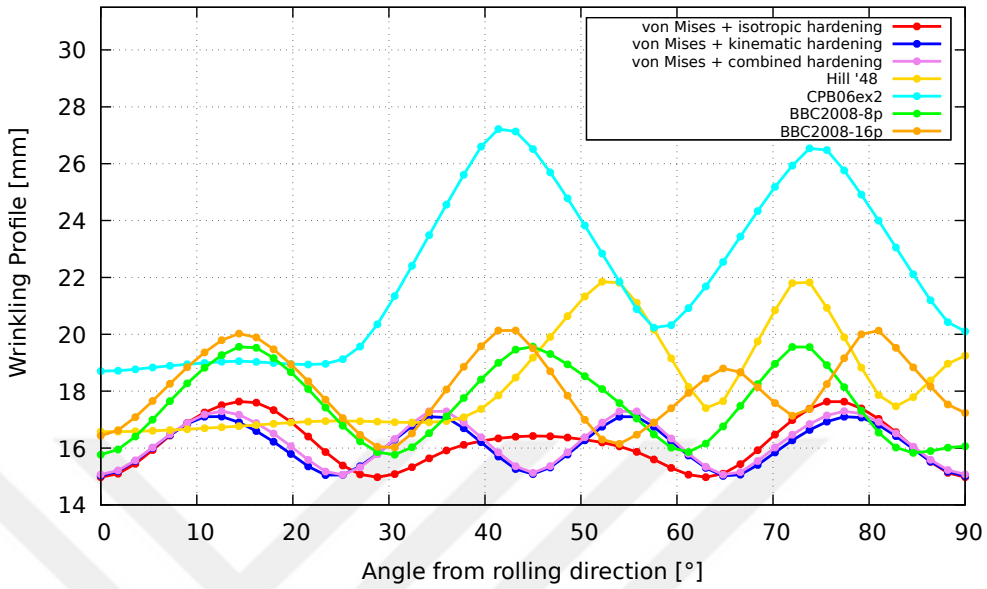

Figure 5.43: Wrinkling profile with 0.7 kN blank holding force at 15 mm punch travel

According to the Figures 5.44- 5.46, while the von Mises with kinematic and combined hardening models predict four wrinkles, the von Mises with isotropic hardening model predicts three wrinkles considering the same punch travel and blank holding force. The predictions of the Hill'48 and CPB06ex2 models show similar trend. Wrinkle is not observed at the regions correspond to the rolling direction of the sheet metal according to the the Hill'48 and CPB06ex2 models. The reason of these predictions can be high anisotropic behavior of the material. Moreover, the predictions of the BBC2008-8p and BBC2008-16p models for the number of wrinkle are different from each other.

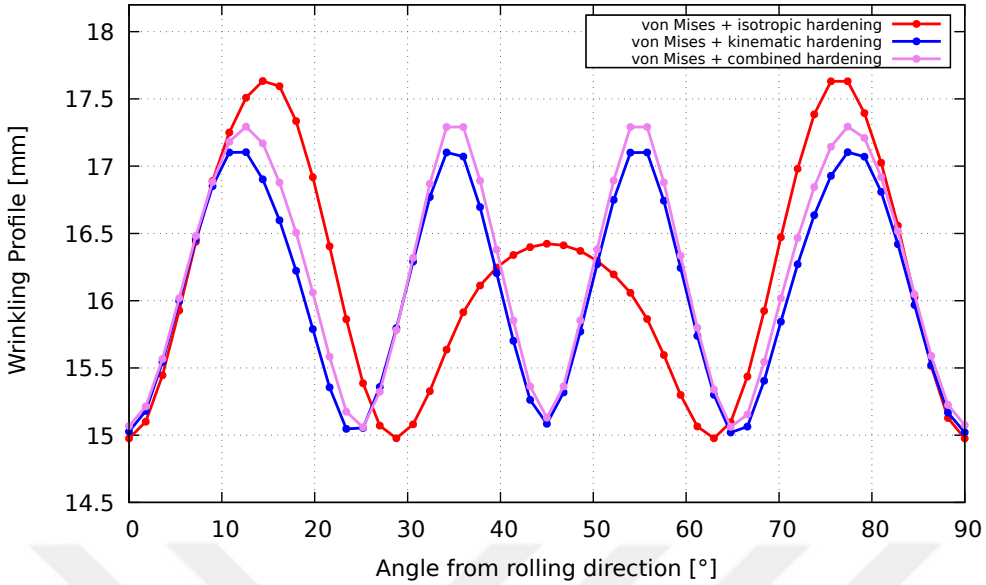

Figure 5.44: Wrinkling profile with 0.7 kN blank holding force at 15 mm punch travel by using the von Mises with isotropic, kinematic and combined hardening models

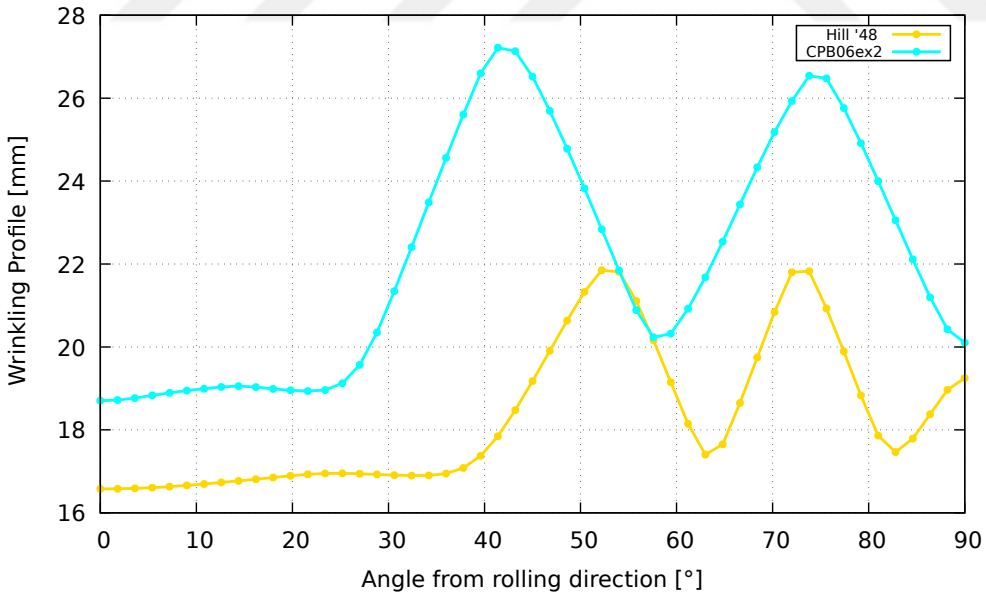

Figure 5.45: Wrinkling profile with 0.7 kN blank holding force at 15 mm punch travel by using the Hill'48 and CPB06ex2 models

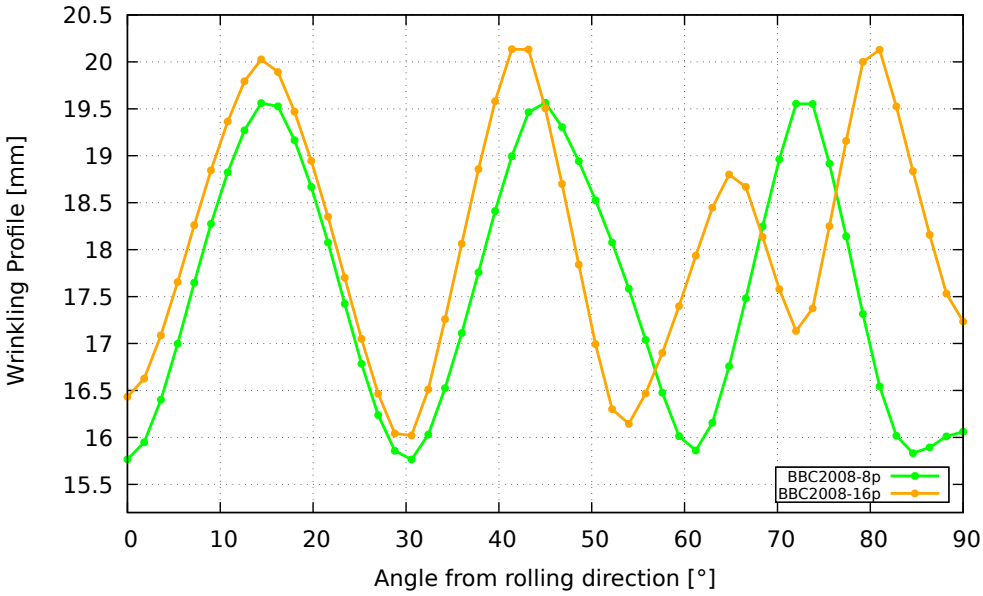

Figure 5.46: Wrinkling profile with 0.7 kN blank holding force at 15 mm punch travel by using the BBC2008-8p and BBC2008-16p models

5.4 Flange Wrinkling Analysis in Square Cup Drawing

In Figures 5.47, 5.48 and 5.49, the predicted wrinkle heights of the aluminum sheet are given for various blank holding forces at three different punch displacements considering the seven constitutive models. The maximum cup forming heights without occurence of wrinkling at different blank holding force are presented in Figure 5.50. It can be observed that the model of CPB06ex2 estimates the required blank holding forces to prevent wrinkling comparably higher. In the von Mises with isotropic, kinematic and combined hardening models, there are an abrupt change in the wrinkle heights for small variation of blank holding force at all punch displacements. Similar trends are observed mostly for the BBC2008-8p and BBC2008-16p models. Moreover, the predictions of the Hill'48 model for the blank holding force required for successful cup drawing are close to the predictions of the CPB06ex2 model.

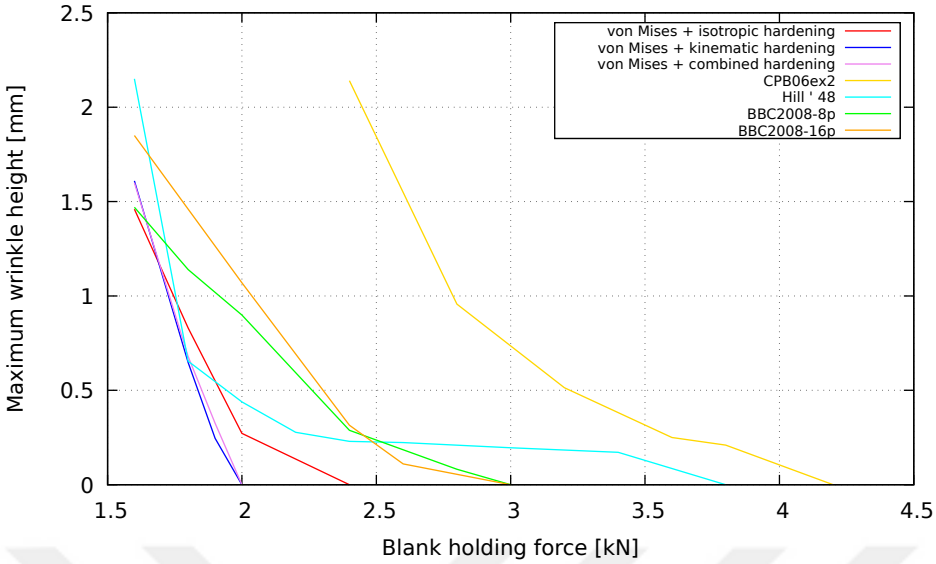

Figure 5.47: Evolution of wrinkle heights with different blank holding force at 10 mm punch travel in square cup drawing

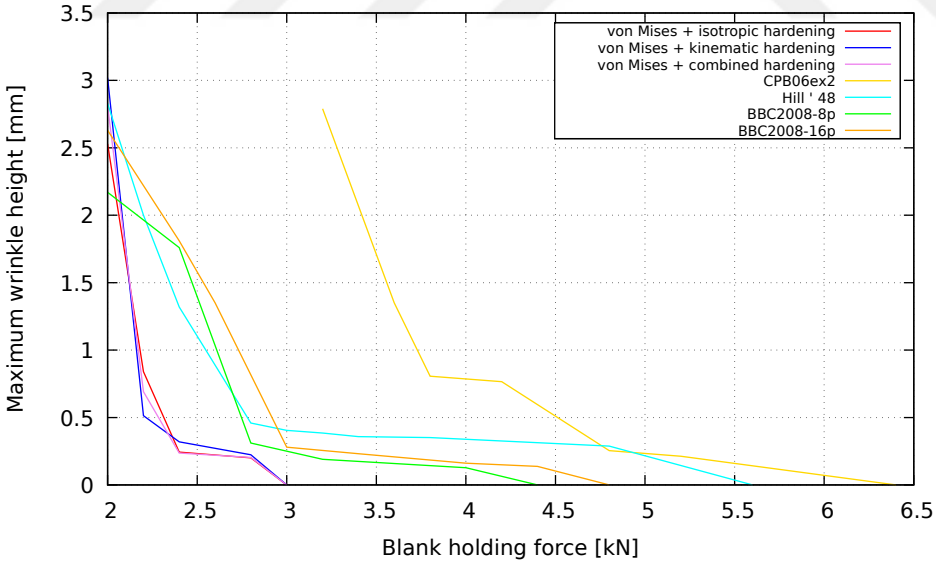

Figure 5.48: Evolution of wrinkle heights with different blank holding force at 15 mm punch travel in square cup drawing

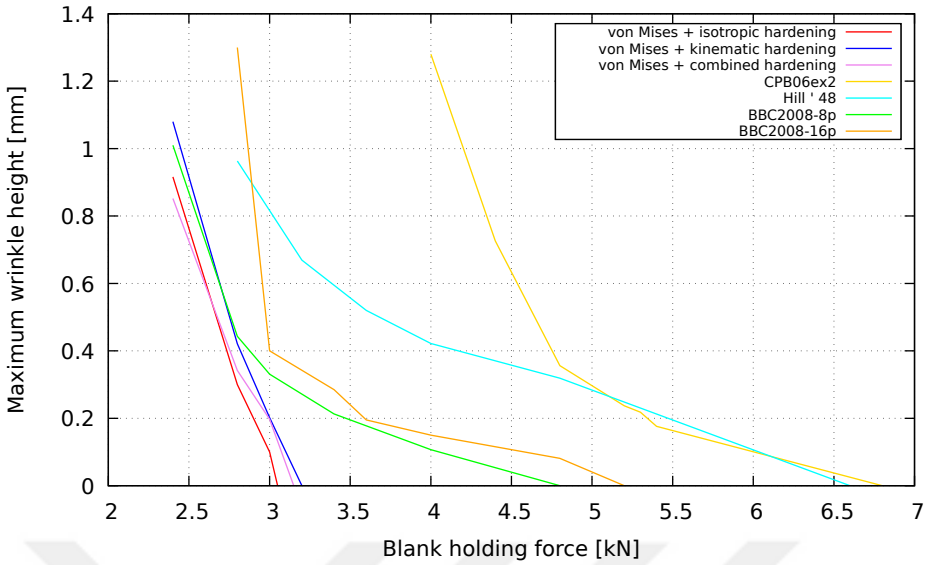

Figure 5.49: Evolution of wrinkle heights with different blank holding force at 20 mm punch travel in square cup drawing

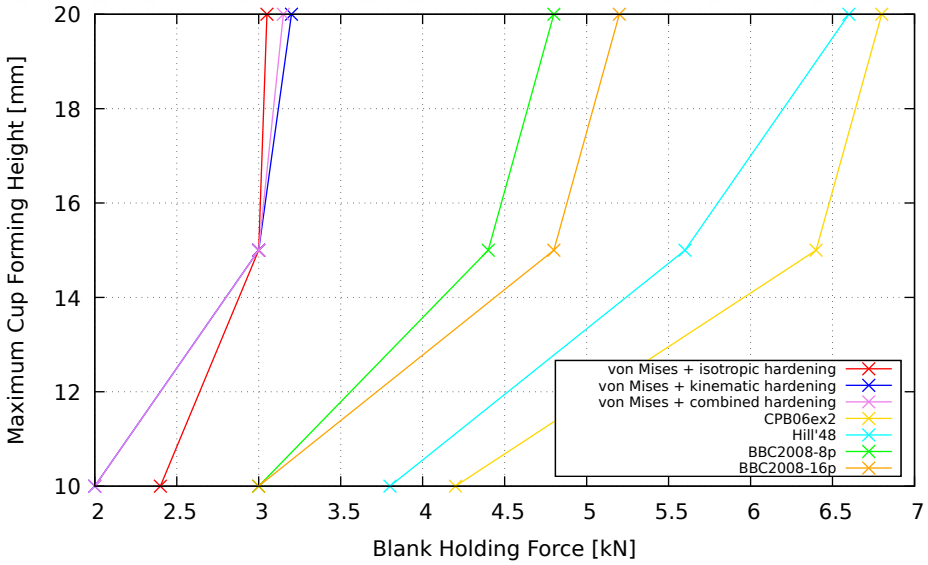

Figure 5.50: Maximum cup forming height variation at several blank holding force in square cup drawing

In Figures 5.51-5.56,the sample drawn cups and their wrinkling profiles are shown by using the related constitutive models in the square cup drawing analyses.

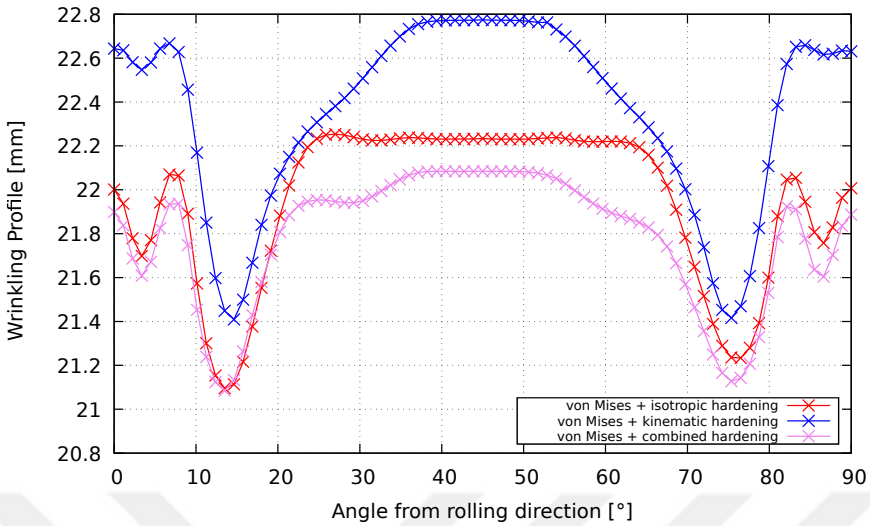

Figure 5.51: Wrinkling profile with 2.4 kN blank holding force at 20 mm punch travel using the von Mises yield criteria with the isotropic, kinematic and combined hardening models in square cup drawing

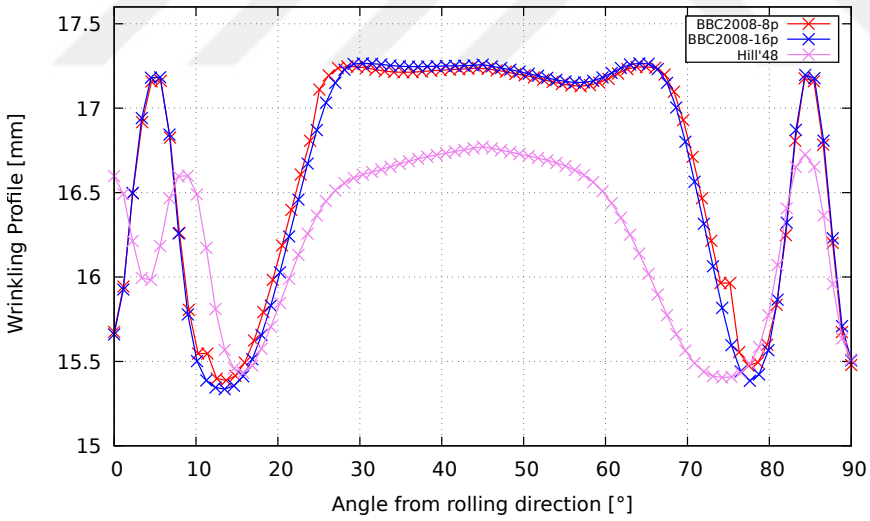

Figure 5.52: Wrinkling profile with 2.4 kN blank holding force at 15 mm punch travel using the Hill'48, BBC2008-8p and BBC2008-16p models in square cup drawing

a)

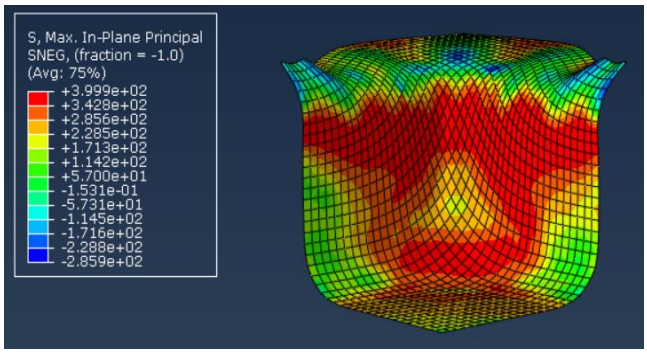

b)

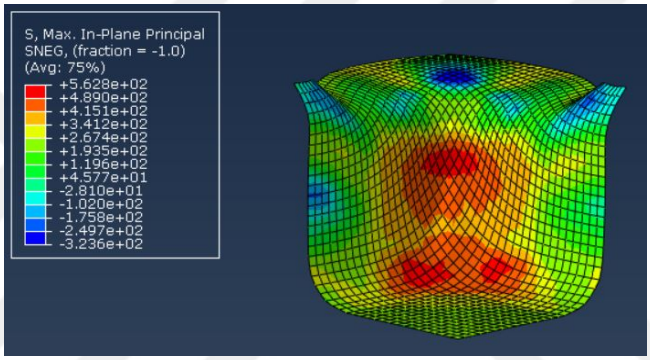

c)

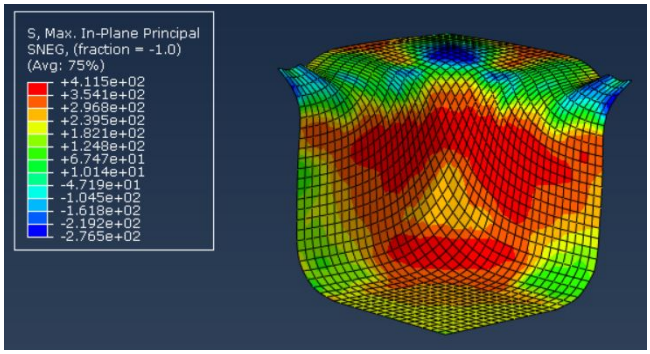

Figure 5.53: In square cup drawing, the drawn cup with 2.4 kN blank holding force at 20 mm punch travel using the von Mises yield criteria with (a) the isotropic hardening model (b) the kinematic hardening model (c) the combined hardening model

a)

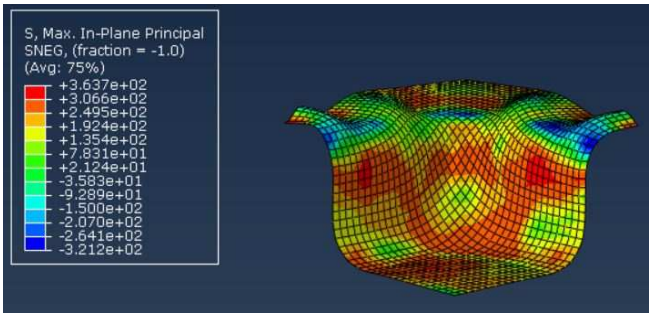

b)

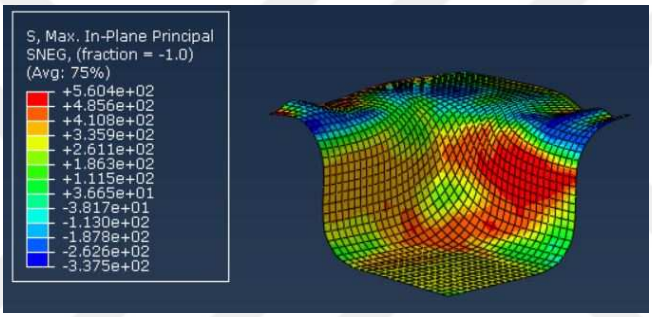

c)

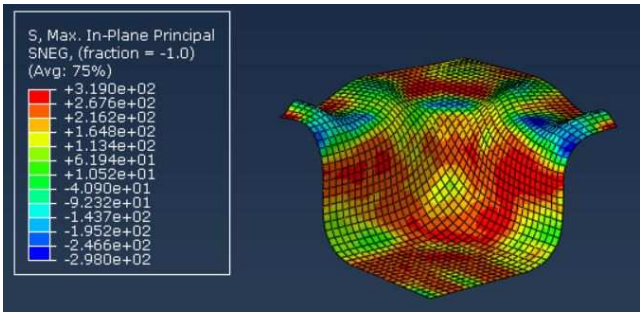

Figure 5.54: In square cup drawing, the drawn cup with 2.4 kN blank holding force at 15 mm punch travel using (a) the Hill'48 model (b) the BBC2008-8p model (c) the BBC2008-16p model

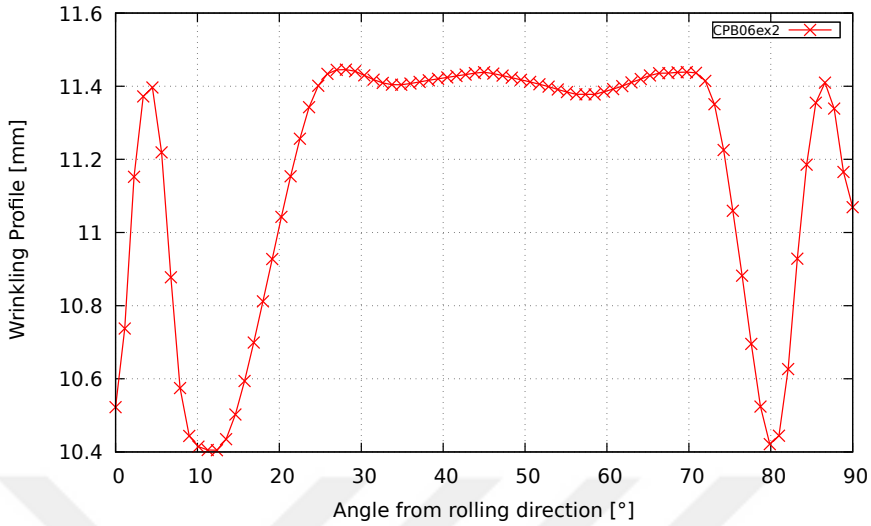

Figure 5.55: Wrinkling profile with 2.8 kN blank holding force at 10 mm punch travel using the CPB06ex2 model in square cup drawing

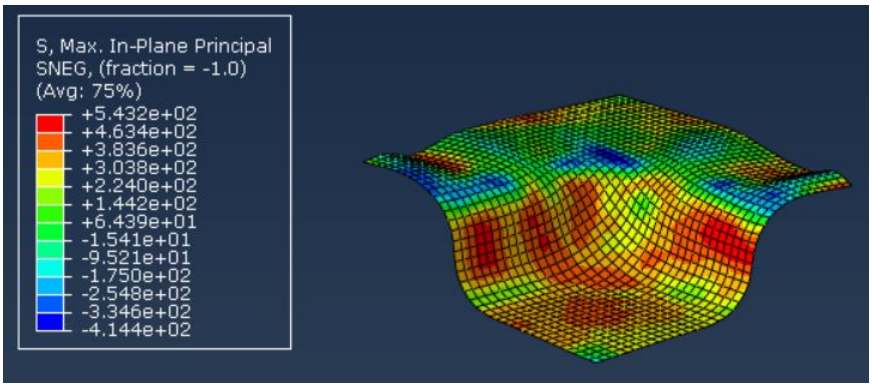

Figure 5.56: In square cup drawing, the drawn cup with 2.8 kN blank holding force at 10 mm punch travel using the CPB06ex2 model

Moreover, the flange wrinkling profiles with 2.4 kN blank holding force at 20 mm punch travel in the square cup drawing are presented in Figure 5.57 in order to compare the predictions of the developed models.

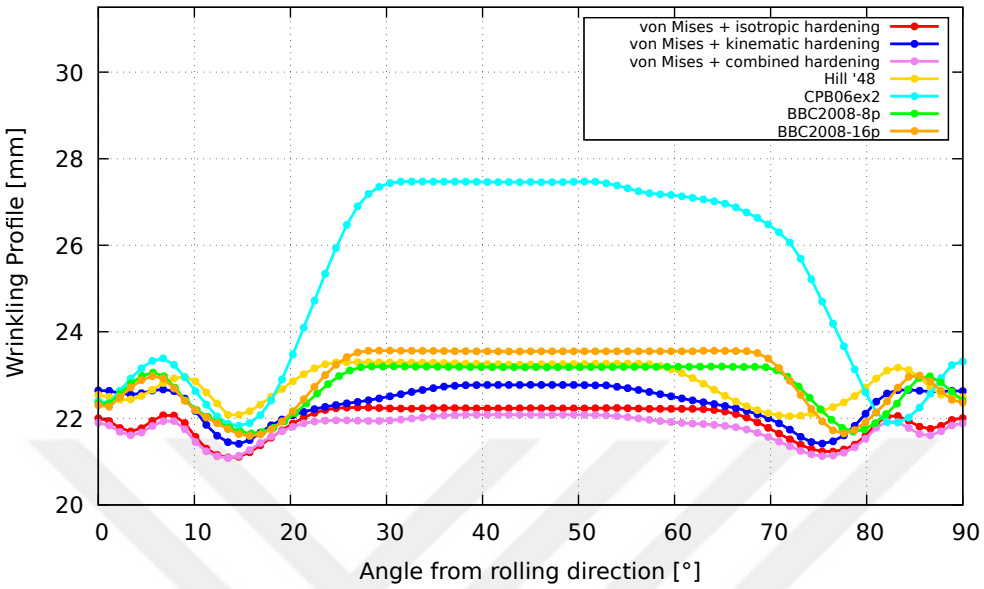

Figure 5.57: Wrinkling profile with 2.4 kN blank holding force at 20 mm punch travel

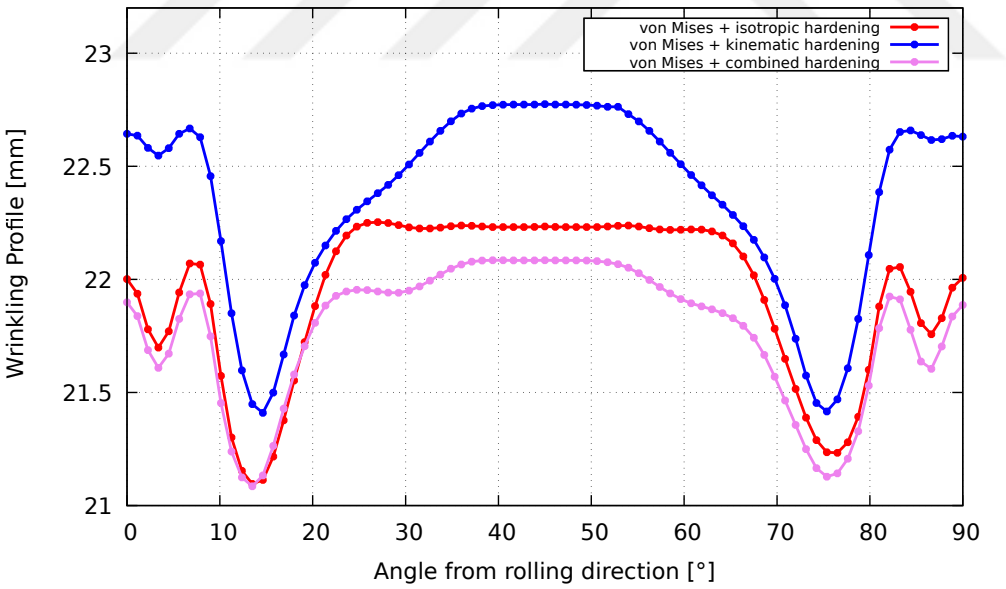

Figure 5.58: Wrinkling profile with 0.7 kN blank holding force at 15 mm punch travel by using the von Mises with isotropic, kinematic and combined hardening models

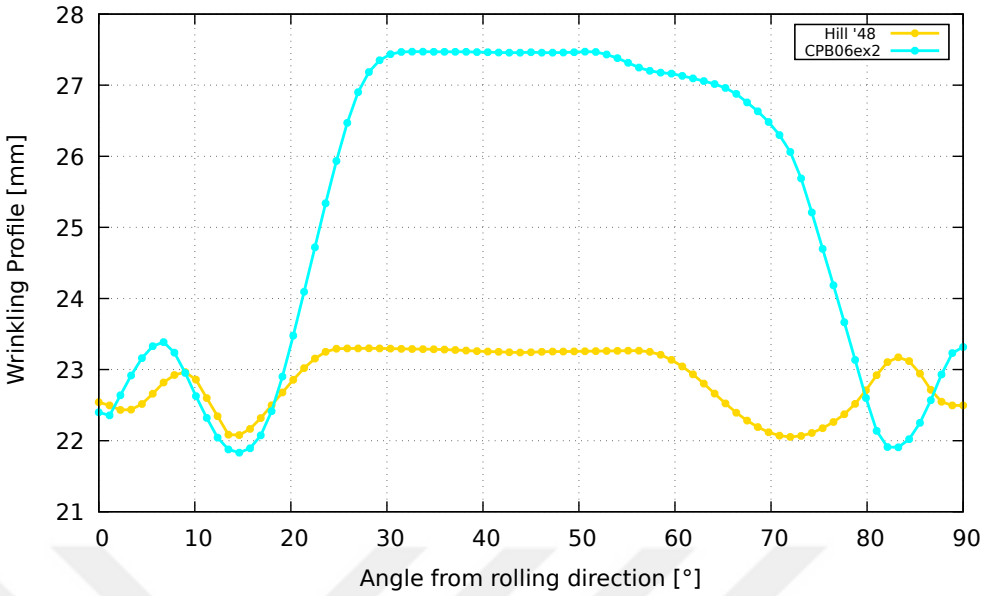

Figure 5.59: Wrinkling profile with 0.7 kN blank holding force at 15 mm punch travel by using the Hill'48 and CPB06ex2 models

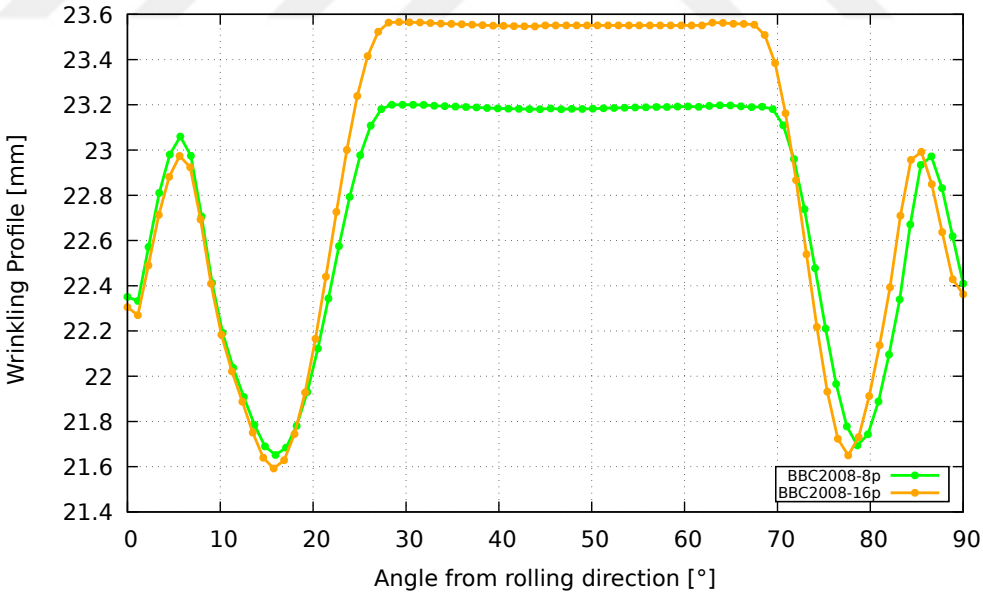

Figure 5.60: Wrinkling profile with 0.7 kN blank holding force at 15 mm punch travel by using the BBC2008-8p and BBC2008-16p models

According to the Figures 5.58- 5.60, the predictions of the von Mises with isotropic, kinematic and combined hardening models for the number of wrinkles are similar to each other. The results obtained by using the BBC2008-8p and BBC2008-16p models are in good agreement. Additionally, while the predictions of the Hill'48 and CPB06ex2 models for the flange wrinkling profile are similar in cylindrical cup drawing, there are some difference between the predictions of these two models in square cup drawing.

CHAPTER 6

CONCLUSIONS AND FUTURE WORKS

6.1 Conclusions

In this study, the capability of the constitutive models formed by the von Mises yield criterion with isotropic, kinematic and combined hardening and CPB06ex2, BBC2008-8p, BBC2008-16p and Hill'48 yield criteria with isotropic hardening on the simulation of wrinkling is investigated. The CPB06ex2, BBC2008-8p and BBC2008-16p yield criteria are implemented to ABAQUS through the user subroutine VUMAT. In order to validate the developed code for the CPB06ex2 model and the numerical results of the side-wall wrinkling analysis, the results from literature are employed. Also, the deep drawing process using cylindrical and square plates are analyzed to find out the effect of blank holding force on wrinkling. Following conclusions have been achieved from this study:

1. The diagram of the the punch force variation at different punch displacement shows that, for the completely drawn cup, the results of the CPB06ex2 model and the empirical data coincides excellently. The results of the von Mises yield criterion with isotropic hardening, kinematic hardening, combined hardening and Hill'48 models and experiment are also shown to be in good agreement. However, the punch force variation is underestimated by the BBC2008-8p and BBC2008-16p models.

2. The comparison of the experimental and numerical side-wall wrinkling profile is made for two cross sections at 3.5 mm and 5.5 mm from the cup bottom. At 3.5 mm, the predicted radial coordinates of the constitutive models are compatible with the experimental investigations, except the von Mises with

kinematic hardening model. In the transverse and rolling direction of the sheet metal, the predictions of the two versions of the BBC2008 model, the BBC2008-8p and BBC2008-16p, give similar results comparing with the experimental data. The CPB06ex2 model gives the most accurate results comparing to the other models excluding the regions near the rolling direction.

3. For the side-wall wrinkling profile at 5.5 mm, there are appreciable deviations between experimental wrinkle amplitude and numerical results. Additionally, the diagrams show that the kinematic hardening model is found to be unsuccessful in forecasting of wrinkling profile.

4. In experiments of the side-wall wrinkling, 13 wrinkles were observed. The agreement between the predictions of wrinkle number for the related constitutive models and experiment is found to be satisfactory.

5. The effect of blank holding force on wrinkling in cylindrical cup drawing was studied at 15 mm, 20 mm and 25 mm punch travel. In accordance with the numerical results, the predictions of CPB06ex2 for the wrinkling height are found significantly greater comparing with the other models in the case of the same blank holding force applied for all punch travels. The von Mises yield criterion with isotropic hardening, kinematic hardening, combined hardening and BBC2008-8p and BBC2008-16p criteria generally give the similar results.

6. The effect of blank holding force on wrinkling in square cup drawing was examined at 10 mm, 15mm and 20 mm punch travel. According to the simulation results, in view of the same punch travel conditions, the predicted blank holding force so as to prevent wrinkling has the highest value for the case of the CPB06ex2 and Hill'48 models. The results of the von Mises with isotropic hardening, kinematic hardening and combined hardening models show similar behaviour. The two versions of the BBC2008 yield criterion give also the similar results for the change of wrinkling amplitude under different blank holding force at all punch travels. Comparing the BBC2008 and von Mises yield criteria, the BBC2008 yield criterion predicts greater blank holding force for the same cup height. Additionally, it can be seen that the required blank holding force to avoid the wrinkling occurrence in square cup drawing is found

to be higher than that in cylindrical cup drawing considering the cases of the same punch travel.

7. For the earing profile, the predictions of the CPB06ex2 model developed in the current study and the experimental data show similar trend.

6.2 Future Works

As a future work, different stress integration algorithms can be implemented in order to check their consistency with experimental findings. Also, experiments for the square and cylindrical cup drawing processes can be conducted using AA5042-H2 aluminum alloy in order to find which constitutive model can represent how the blank holding force affects the wrinkling occurence more accurately.

REFERENCES

[1] E. Ghassemali, X. Song, M. Zarinejad, A. Danno, and M. Tan, *Bulk Metal Forming Processes in Manufacturing*. 09 2014.

[2] H. E. Theis, *Handbook of Metalforming Processes*. CRC Press, 1999.

[3] E. Chu and Y. Xu, "An elastoplastic analysis of flange wrinkling in deep drawing process," *International Journal of Mechanical Sciences*, vol. 43, pp. 1421–1440, 06 2001.

[4] X. Wang and J. Cao, "On the prediction of side-wall wrinkling in sheet metal forming processes," *International Journal of Mechanical Sciences*, vol. 42, no. 12, pp. 2369–2394, 2000.

[5] D. Neto, M. Oliveira, R. Dick, P. Barros, J. Alves, and L. Menezes, "Numerical and experimental analysis of wrinkling during the cup drawing of an aa5042 aluminium alloy," *International Journal of Material Forming*, vol. 10, no. 1, pp. 125–138, 2017.

[6] A. Agrawal, N. V. Reddy, and P. Dixit, "Determination of optimum process parameters for wrinkle free products in deep drawing process," *Journal of Materials Processing Technology*, vol. 191, no. 1-3, pp. 51–54, 2007.

[7] B. Kaftanoglu, "Plastic analysis of flange wrinkling in axisymmetrical deep-drawing," in *Proceedings of the Twenty-First International Machine Tool Design and Research Conference*, pp. 21–28, Springer, 1981.

[8] M. A. Shafaat, M. Abbasi, and M. Ketabchi, "Investigation into wall wrinkling in deep drawing process of conical cups," *Journal of Materials Processing Technology*, vol. 211, no. 11, pp. 1783–1795, 2011.

[9] B. W. Senior, "Flange wrinkling in deep-drawing operations," *Journal of the Mechanics and Physics of Solids*, vol. 4, no. 4, pp. 235–246, 1956.

[10] J. D. M. Correia and G. Ferron, "Wrinkling of anisotropic metal sheets under deep-drawing: analytical and numerical study," *Journal of Materials Processing Technology*, vol. 155, pp. 1604–1610, 2004.

[11] G. Ferron, R. Makkouk, and J. Morreale, "A parametric description of orthotropic plasticity in metal sheets," *International Journal of Plasticity*, vol. 10, no. 5, pp. 431–449, 1994.

[12] N. Triantafyllidis and A. Needleman, "An analysis of wrinkling in the swift cup test," *Journal of Engineering Materials and Technology*, vol. 102, no. 3, pp. 241–248, 1980.

[13] X. Weili, W. Huibao, Y. Yuying, and Z. Wang, "A simplified method of wrinkling simulation," *Journal of Materials Processing Technology*, vol. 121, no. 1, pp. 19–22, 2002.

[14] P. Nordlund and B. Häggblad, "Prediction of wrinkle tendencies in explicit sheet metal-forming simulations," *International journal for numerical methods in engineering*, vol. 40, no. 22, pp. 4079–4095, 1997.

[15] Z. Nowak, M. Nowak, and R. Pęcherski, "A plane stress elastic-plastic analysis of sheet metal cup deep drawing processes," *Shell structures: Theory and Applications*, vol. 3, p. 129, 2013.

[16] W. Burzynski, "Über die anstrengungshypothesen," *Schweizerische Bauzeitung*, vol. 94, no. 21, pp. 259–262, 1929.

[17] J.-H. Yoon, O. Cazacu, J. W. Yoon, and R. E. Dick, "Earing predictions for strongly textured aluminum sheets," *International Journal of Mechanical Sciences*, vol. 52, no. 12, pp. 1563–1578, 2010.

[18] Y. Jia and Y. Bai, "Ductile fracture prediction for metal sheets using all-strain-based anisotropic emmc model," *International Journal of Mechanical Sciences*, vol. 115, pp. 516–531, 2016.

[19] M. Vrh, M. Halilovič, B. Starman, B. Štok, D.-S. Comsa, and D. Banabic, "Capability of the bbc2008 yield criterion in predicting the earing profile in cup deep drawing simulations," *European Journal of Mechanics-A/Solids*, vol. 45, pp. 59–74, 2014.

[20] J. W. Yoon, F. Barlat, R. Dick, and M. Karabin, "Prediction of six or eight ears in a drawn cup based on a new anisotropic yield function," *International Journal of Plasticity*, vol. 22, no. 1, pp. 174–193, 2006.

[21] F. Barlat, Y. Maeda, K. Chung, M. Yanagawa, J. Brem, Y. Hayashida, D. Lege, K. Matsui, S. Murtha, S. Hattori, *et al.*, "Yield function development for aluminum alloy sheets," *Journal of the Mechanics and Physics of Solids*, vol. 45, no. 11-12, pp. 1727–1763, 1997.

[22] L. Moreira, G. Ferron, and G. Ferran, "Experimental and numerical analysis of the cup drawing test for orthotropic metal sheets," *Journal of materials processing technology*, vol. 108, no. 1, pp. 78–86, 2000.

[23] R. Hill, "A theory of the yielding and plastic flow of anisotropic metals," *Proceedings of the Royal Society of London. Series A. Mathematical and Physical Sciences*, vol. 193, no. 1033, pp. 281–297, 1948.

[24] B. Tang, F. Wu, Z. Wang, and S. Zhang, "Study on non-associated plasticity with various forward euler stress integration algorithms and its prediction of earing in cylindrical cup drawing," *International Journal of Mechanical Sciences*, vol. 157, pp. 384–402, 2019.

[25] M. R. Foudeh, S. Daneshmand, and H. I. Demirci, "Investigating aluminium sheet wrinkling during the deep drawing process," *Transactions of FAMENA*, vol. 37, no. 4, pp. 43–54, 2014.

[26] H. Zein, M. El-Sherbiny, M. Abd-Rabou, and M. El Shazly, "Effect of die design parameters on thinning of sheet metal in the deep drawing process," *American Journal of Mechanical Engineering*, vol. 1, no. 2, pp. 20–29, 2013.

[27] M. Colgan and J. Monaghan, "Deep drawing process: analysis and experiment," *Journal of materials processing technology*, vol. 132, no. 1-3, pp. 35–41, 2003.

[28] F. Dunne and N. Petrinic, *Introduction to computational plasticity*. Oxford University Press on Demand, 2005.

[29] D. Systèmes, "Abaqus 6.10: Analysis user's manual," *Providence, RI: Dassault Systèmes Simulia Corp*, 2010.

[30] O. Cazacu, B. Plunkett, and F. Barlat, "Orthotropic yield criterion for hexagonal closed packed metals," *International Journal of Plasticity*, vol. 22, no. 7, pp. 1171–1194, 2006.

[31] B. Plunkett, O. Cazacu, and F. Barlat, "Orthotropic yield criteria for description of the anisotropy in tension and compression of sheet metals," *International Journal of Plasticity*, vol. 24, no. 5, pp. 847–866, 2008.

[32] K. H. Huebner, E. Thornton, and E. Byrom, "The finite element method for engineers john wiley & sons," *New York*, 1982.

[33] K. Lange, M. Herrmann, P. Keck, and M. Wilhelm, "Application of an elasto-plastic finite-element code to the simulation of metal forming processes," *Journal of Materials Processing Technology*, vol. 27, no. 1-3, pp. 239–261, 1991.

[34] P. Vacher, R. Arrieux, and L. Tabourot, "Analysis of a criterion of deep drawing operation capability for thin orthotropic sheets," *Journal of Materials Processing Technology*, vol. 78, no. 1-3, pp. 190–197, 1998.

[35] R. Dick, R. Cardoso, M. Paulino, and J. W. Yoon, "Benchmark 4-wrinkling during cup drawing," in *AIP Conference Proceedings*, vol. 1567, pp. 262–327, AIP, 2013.